Department of Meteorology

University of Reading

The Development of a Fast Chemical Scheme for General Circulation Models

Chris Taylor

A thesis submitted for the degree of Doctor of Philosophy

March 23, 2003

Declaration

I con£rm that this is my own work and the use of all material from other sources has been properly and fully acknowledged.

Abstract

The modelling of stratospheric ozone and its response to climate change requires the use of coupled chemistry climate models. This thesis details the development of a fast chemical scheme, FASTOC, suitable for inclusion in general circulation models (GCMs). A number of other coupled chemistry GCMs have been developed over recent years. These have chemical schemes which can be categorised as simple parameterisations or complex schemes. The FASTOC model captures the advantages of both types of model. It is fast enough to perform long integrations, yet capable of capturing the many non-linear interactions in the stratospheric chemical system.

Firstly, a new version of a chemical box model is presented. It is updated to improve its ef£ciency and make it suitable for global calculations. This model is compared to a similar, but independent, model and found to give a good simulation of stratospheric chemistry.

Secondly, the box model is used to initialise the chemical parameterisation, FASTOC. This new model uses the Fully Equivalent Operational Model technique of Shorter *et al.* (1999), and represents a considerable advance on their model. FASTOC is compared to the box model and is found to be stable and give accurate results.

Some idealised experiments are presented, looking at perturbations to the present day atmosphere and to that in 2200. Perturbations to NO_x and temperature are found to be the most important after chlorine. It is concluded that the recovery of the ozone layer will depend strongly on future anthropogenic emissions.

Finally, FASTOC is coupled to the Reading Intermediate General Circulation Model. A timeslice experiment of 1979 conditions shows that the model is stable and simulates a very realistic atmosphere. Comparisons with observations and other models con£rm that the three dimensional structure of the model atmosphere is very good. Further experiments of 2060 conditions justify the conclusion of chapter 4. Furthermore, it is found that the recovery of the ozone layer may depend on latitude and time of year. Tropical regions may experience further depletion caused by NO_x, while high latitudes may see a super-recovery.

Acknowledgements

First and foremost, I would like to express my extreme gratitude to my supervisor, Keith Shine. It has been a pleasure to work with Keith, especially when we were both struggling to understand what was going on! His understanding and enjoyment of science have been the best guides I could have possibly asked for.

Thanks also to Michel Bourqui. Without his hard work much of the £nal chapter of this thesis would not have been possible. I can honestly say that the time working with Michel was the most enjoyable of the last three years. I also need to thank the rest of the radiation group, past and present, for welcoming a chemist and nodding politely during his ramblings about O_x, NO_x and other such mysteries.

I am indebted to John Austin for many interesting and helpful discussions throughout the course of my work. Thanks also to Glenn Carver for allowing me to use his chemical box model and for his interest and encouragement.

A huge thank you to all those who kept me going throughout my time in Reading. Thank you to Brenda, Marc, Dan, Helen J, Anna, Stuart, Christine, Andrew, Cyril, Barbara, Helen D, Tim M, Tim W, Laila, Jolene and all those who ever hit or kicked a ball, walked or skied the mountains, sailed a boat or just had coffee with me. Of all these people the greatest thanks go to those who worked, struggled and laughed with me from the start. Elspeth, James, Hilary and Ian. Without them I would never had made it.

Thanks also to my Mum and Dad, and to Mike and Steve, for your support and encouragement, even when you wondered what on Earth I was doing.

Finally, thank you to Siân, whose love, support, friendship and cups of tea have kept me going throughout.

Especially the tea.

Gonna change my way of thinking,
Make myself a different set of rules.
Gonna put my good foot forward,
And stop being in¤uenced by fools.

Bob Dylan
from “Gonna Change My Mind”

Contents

CHAPTER ONE

Introduction

1.1 Stratospheric Ozone

Ozone, although present in only trace amounts in the stratosphere, is vital to the survival of life on Earth and plays a crucial role in atmospheric chemistry, radiation and dynamics. The reason for this lies in its physical properties. It is the only atmospheric species that absorbs strongly in the UV-B region of the electromagnetic spectrum. This absorption protects the surface from this high energy radiation. Studies have shown that exposure to UV-B can have detrimental effects on the health of plants and animals (Quaite *et al.*, 1992; Williamson *et al.*, 2001; Xiong and Day, 2001). In addition, the temperature structure of the stratosphere is a direct result of the heating caused by absorption of solar and terrestrial radiation by ozone (see, for example, Wayne, 2000).

In the last few decades, man has demonstrated the potential to pollute the atmosphere on a global scale. The emission of halogenated compounds into the atmosphere has led to a global decline in stratospheric ozone (WMO, 1999) and the formation of the Antarctic "ozone hole" (Farman *et al.*, 1985). This could have serious effects, both by increasing the dose of UV-B at the surface and by in¤uencing the general circulation of the atmosphere. The study of anthropogenic and natural perturbations to stratospheric ozone is, therefore, of utmost importance. Understanding the complex chemical-radiative-dynamical system involved requires both observational work and the development of sophisticated computer models.

Several coupled-chemistry general circulation models have been developed over recent years (see section 1.4.1). These have either been complex chemistry models which are expensive to run, or simple parameterisations which are not physically based. It has not been possible, using a physically based model, to examine a range of possible futures and the variability of the chemistry-climate system. This thesis describes the development of a fast, physically based,

chemical scheme that is capable of performing such experiments.

This chapter provides an introduction to the science of stratospheric ozone, chemistry-climate interactions and issues in the modelling of those processes.

1.2 Stratospheric Chemistry and Dynamics

In order to understand the science of ozone depletion and the impact of chemistry-climate interactions on stratospheric ozone, it is necessary to understand the processes which control its concentration and distribution. Good accounts of the science of stratospheric ozone can be found in Brasseur *et al.* (1999), Wayne (2000), Dessler (2000), and other texts. A useful review on the subject of ozone depletion was recently published by Solomon (1999) and further information can be found in the WMO (1999) and SORG (1999) reports.

1.2.1 Some Concepts in Atmospheric Chemistry

This section will brie¤y outline some useful concepts that will be used in the following discussion of stratospheric chemistry.*

Lifetime

The thermodynamics of a process are studied in order to determine whether it will occur spontaneously. This does not, however, reveal the speed of that process. In atmospheric chemistry, where the timescale of a process may be years or a fraction of a second, the kinetics of the system is the primary consideration.

Consider the theoretical unimolecular reaction

$$A \rightarrow B. \tag{1.1}$$

The rate of this reaction is

$$-\frac{d[A]}{dt} = \frac{d[B]}{dt} = k[A] \tag{1.2}$$

*A glossary of notation and acronyms is given at the end of this thesis.

where k is the rate constant for the reaction. The local chemical lifetime (or timescale or e-folding time) of A, τ, is the time in which the concentration of A falls to $\frac{1}{e}$ of the original concentration,

$$[A]_\tau = \frac{1}{e}[A]_0. \tag{1.3}$$

Integrating equation 1.2 between $t = 0$ and $t = \tau$, and substituting equation 1.3 gives

$$\tau = \frac{1}{k}. \tag{1.4}$$

This can be used to determine the controlling processes in the atmosphere. Short timescale processes will dominate those with longer timescales. In many studies it is assumed that processes with short timescales are in local equilibrium or *photochemical steady state*.

Partitioning

The concept of *partitioning* concerns which form atoms of a particular element are found in. Species can be categorised on the basis of their reactivity as *active* or *reservoir* species.

Active species are the reactive, short-lived species that take part in ozone destroying catalytic cycles. They may, however, have many reactions that do not involve ozone. Reservoir species are longer-lived and do not actively destroy ozone. As the name suggests, they are the pool from which active species are formed.

A third useful category is *source gas*. These are stable species, emitted at the surface, that are not oxidised by the tropospheric hydroxyl radical OH, or photolysed by the longer wavelength solar radiation that reaches the troposphere. They are slowly transported into the stratosphere where they are photolysed by short-wave ultra-violet light, or oxidised by the excited oxygen atom, $O(^1D)$.

1.2.2 Ozone Photochemistry

The £rst successful attempt to describe the photochemistry of ozone in the stratosphere was made by Chapman (1930). He proposed the following reactions:

$$O_2 + h\nu \rightarrow 2O \tag{1.5}$$

$$2(O + O_2 \overset{M}{\rightarrow} O_3) \tag{1.6}$$

$$O_3 + h\nu \rightarrow O + O_2 \tag{1.7}$$

$$O + O_3 \rightarrow 2O_2 \tag{1.8}$$

$$O + O \overset{M}{\rightarrow} O_2 \tag{1.9}$$

where $h\nu$ represents a photon and M signi£es that collision with a third body is required to stabilise the excited intermediate molecule. Reaction 1.9 is now known to be unimportant due to the very low abundance of atomic oxygen in the stratosphere.

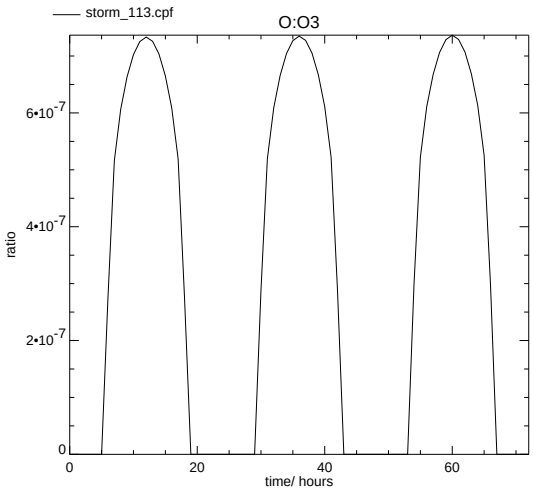

Figure 1.1: *3 days of STORM chemical box model output at one hour intervals at 22km, 45° north, showing the ratio of* O *to* O_3. *This ratio is of the order of* 10^{-6} *at noon. STORM is described in chapter 2*

The fast rates of reaction 1.6 and reaction 1.7 mean that the lifetime of ozone in the stratosphere is around 10^3 seconds and that of O is only 10^{-3} seconds. Reaction 1.7 is the major loss mechanism for O_3 but most O rapidly reacts with O_2 to reform O_3 via reaction 1.6. While the cycling between O and O_3 is rapid, conversion to O_2 by reaction 1.8 is slow, so the sum of O and O_3 is roughly constant. This leads to the useful concept of *odd oxygen*, or O_x . O_x is de£ned as the sum of O and O_3, and has a lifetime of days to years in the stratosphere. It is important to note

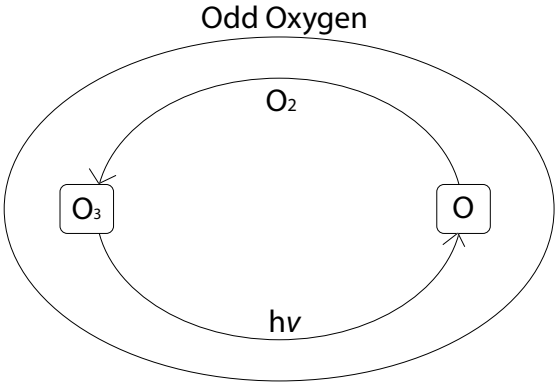

Figure 1.2: *Odd oxygen consists of ozone and atomic oxygen. The two species are rapidly interconverted, but the sum of the two changes much more slowly.*

that nearly all stratospheric O_x is in the form of O_3 as reaction 1.6 is much faster than reaction 1.7 (see £gure 1.1). This means that the concentration of odd oxygen is approximately equal to that of ozone and, although the lifetime of each ozone molecule is relatively short, the total amount of ozone can only change on timescales equal to the lifetime of O_x. This is illustrated in £gure 1.2.

Most atomic oxygen is found in the ground state, $O(^3P)$. If, however, the photon in reaction 1.7 is of a wavelength less than about 300 nm then the electronically excited $O(^1D)$ may be formed. This high energy species is more reactive than is $O(^3P)$.

Although the Chapman reactions explain much of the behaviour of stratospheric ozone, models using this oxygen-only chemistry overestimate the amount of stratospheric ozone (Wayne, 2000). Additional loss processes exist in the form of catalytic cycles. Many of these take the form proposed by Stolarski and Cicerone (1974):

Cycle 1:

$$X + O_3 \rightarrow XO + O_2 \tag{1.10}$$

$$XO + O \rightarrow X + O_2 \tag{1.11}$$

$$net : \mathbf{O_3 + O \rightarrow 2O_2}$$

where X can be Cl, Br, NO or OH.

This type of cycle is effective in the upper stratosphere, where atomic oxygen is relatively abundant. In the lower stratosphere cycles that do not involve this species are more ef£cient (Wayne, 2000). For example:

Cycle 2:

$$OH + O_3 \rightarrow HO_2 + O_2 \tag{1.12}$$

$$HO_2 + O_3 \rightarrow OH + O_2 + O_2 \tag{1.13}$$

$$net : \mathbf{O_3 + O_3 \rightarrow O_2 + O_2 + O_2}$$

or

Cycle 3:

$$HO_2 + ZO \rightarrow HOZ + O_2 \tag{1.14}$$

$$HOZ + h\nu \rightarrow OH + Z \tag{1.15}$$

$$Z + O_3 \rightarrow ZO + O_2 \tag{1.16}$$

$$OH + O_3 \rightarrow HO_2 + O_2 \tag{1.17}$$

$$net : \mathbf{O_3 + O_3 \rightarrow O_2 + O_2 + O_2}$$

where Z may be Cl or Br.

1.2.3 Other Chemical Families

A number of chemical species play important roles in the catalytic destruction of ozone, including species of nitrogen, hydrogen, chlorine and bromine.

Nitrogen Chemistry

The main source gas for nitrogen dioxide in the stratosphere is N_2O, which has both biogenic and anthropogenic sources (Finlayson-Pitts and Pitts Jr., 2000). It can be oxidised by $O(^1D)$ to form NO,

$$N_2O + O(^1D) \rightarrow 2NO, \tag{1.18}$$

or inert N_2,

$$N_2O + O(^1D) \rightarrow N_2 + O_2. \tag{1.19}$$

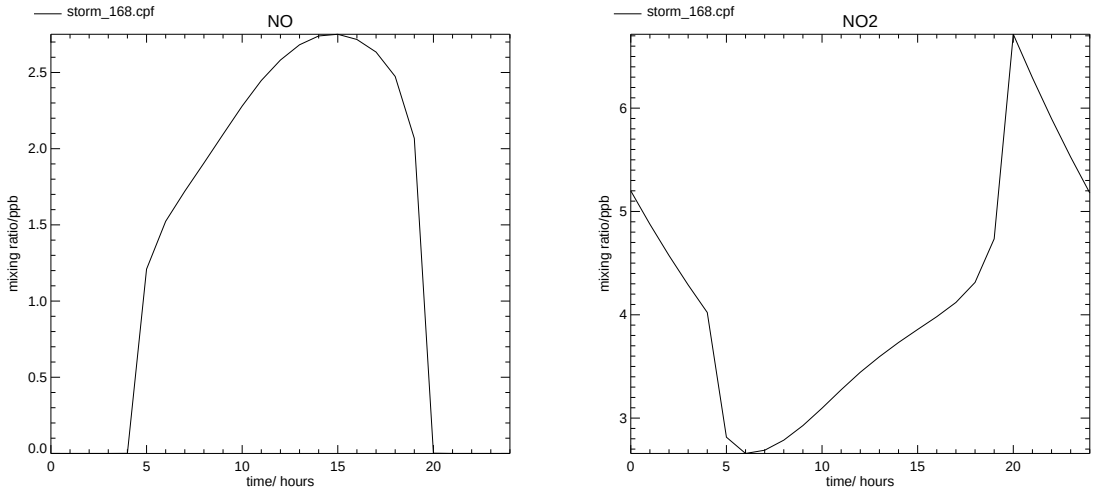

(a) NO (b) NO_2

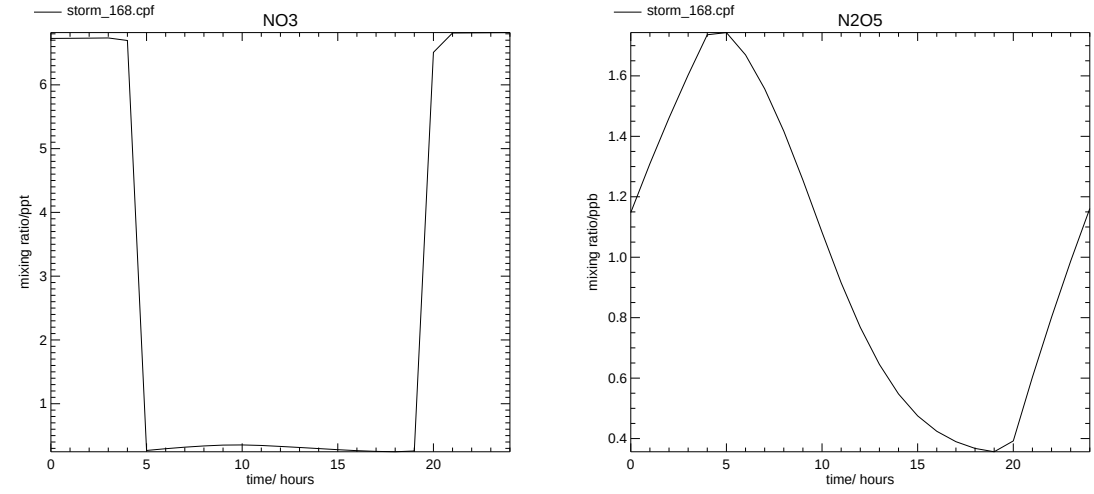

(c) NO_3 (d) N_2O_5

Figure 1.3: *The diurnal cycles of four short lived nitrogen species are shown. The data come from the STORM chemical box model, run for one day beginning at midnight for 40°N at 24km. STORM is described fully in chapter 2*

The nitrogen released by destruction of N_2O is known as NO_y or *odd nitrogen*. NO_y consists of all atmospheric nitrogen that is not in the form of N_2 or N_2O.

NO, NO_2 and NO_3 are all active species and are known collectively as NO_x. NO, formed mainly by reactions 1.20 and 1.21, is present only during the day (see £gure 1.3(a)), while NO_3, formed by reaction 1.22 and 1.23, is photolysed rapidly so is present only at night (see £gure 1.3(c)). NO_2 is formed during the day by reactions 1.22, 1.23 and 1.24 (see £gure 1.3(b)). At night it is converted into N_2O_5 via the equilibrium 1.23.

$$NO_2 + h\nu \rightarrow NO + O \tag{1.20}$$

$$NO_2 + O \rightarrow NO + O_2 \tag{1.21}$$

$$N_2O_5 + h\nu \rightarrow NO_2 + NO_3 \tag{1.22}$$

$$N_2O_5 \overset{M}{\rightleftharpoons} NO_2 + NO_3 \tag{1.23}$$

$$NO + O_3 \rightarrow NO_2 + O_2 \tag{1.24}$$

The NO_x catalytic cycles are very important in controlling O_x, particularly cycle 4.

Cycle 4:

$$NO + O_3 \rightarrow NO_2 + O_2 \tag{1.25}$$

$$NO_2 + O \rightarrow NO + O_2 \tag{1.26}$$

$$net : \mathbf{O_3} + \mathbf{O} \rightarrow \mathbf{O_2} + \mathbf{O_2}.$$

N_2O_5 is only a short term reservoir for nitrogen as it is photolysed quite readily by reaction 1.22. The most important nitrogen reservoir, nitric acid (HNO_3), couples the chemistry of nitrogen and that of hydrogen. It is formed by reaction 1.27

$$NO_2 + OH \overset{M}{\rightarrow} HNO_3 \tag{1.27}$$

and by several heterogeneous reactions on the surface of aerosols or polar stratospheric clouds (see section 1.2.4). NO_x is released from HNO_3 by photolysis or oxidation by OH. A second reservoir that couples nitrogen and hydrogen chemistry is HNO_4. This species plays only a limited role in nitrogen partitioning due to its low abundance, but it can have a signi£cant role in the hydrogen budget under certain conditions (Donaldson *et al.*, 2000).

Hydrogen Chemistry

The main stratospheric sources of hydrogen species are the oxidation of water vapour, methane and molecular hydrogen by $O(^1D)$. See reaction 1.28, for example.

$$H_2O + O(^1D) \rightarrow 2OH. \tag{1.28}$$

H, OH and HO_2 form the HO_x, or *odd hydrogen* family. They have very short lifetimes and exist only during the day (see £gure 1.4). The HO_x species do not have any signi£cant reservoirs,

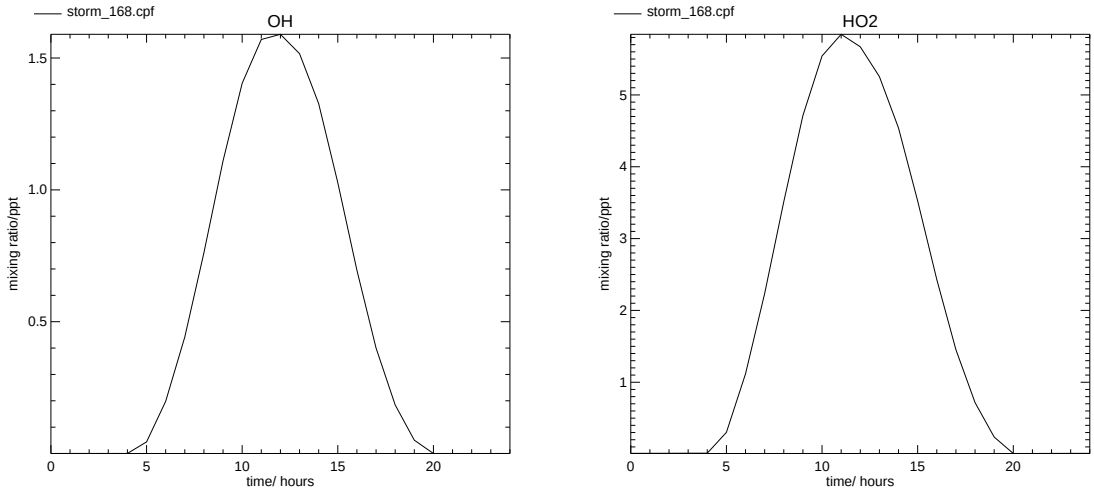

(a) OH (b) HO_2

Figure 1.4: *As for £gure 1.3, but for* OH *and* HO_2.

but do form short-lived compounds, such as HOCl, HOBr, H_2O_2 and HNO_4. The formation and subsequent destruction of these species does not represent a net source or sink of HO_x, but does affect the partitioning. For example, cycle 5 converts HO_2 to OH.

Cycle 5:

$$HO_2 + ClO \rightarrow HOCl + O_2 \tag{1.29}$$

$$HOCl + h\nu \rightarrow OH + Cl \tag{1.30}$$

$$net : \mathbf{HO_2 + ClO \rightarrow OH + Cl + O_2}$$

Chlorine Chemistry

Although many chlorine compounds are emitted into the troposphere from, for example, volcanic eruptions or sea spray, most are water soluble and are removed from the atmosphere by wet deposition. Most chlorine that reaches the stratosphere is in the form of halogenated organic compounds, such as the chloro¤uorocarbons (CFCs), as shown in £gure 1.5. These molecules are insoluble and are not oxidised by OH. Molina and Rowland (1974) suggested that these molecules, which are

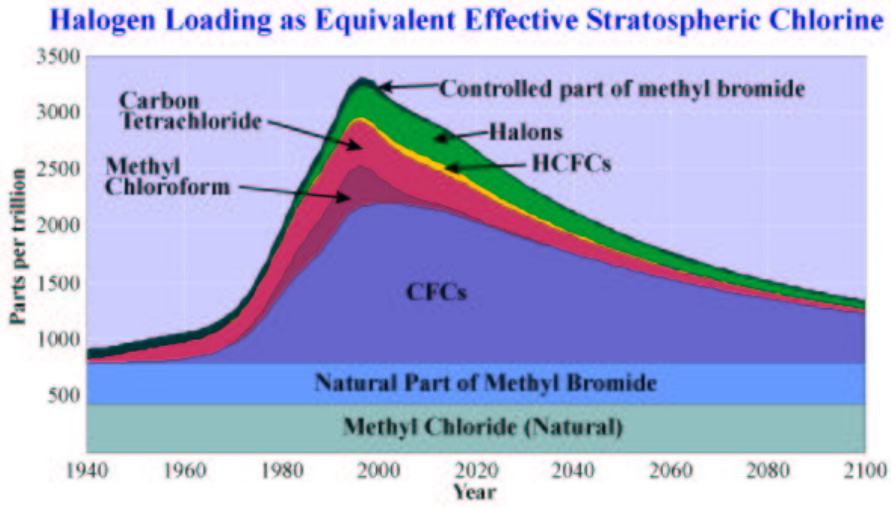

Figure 1.5: *Historical trend and future prediction of atmospheric equivalent chlorine loading. The equivalent chlorine loading of a species is its atmospheric abundance multiplied by the number of chlorine atoms it contains. For species that contain bromine atoms an additional factor is included to account for that atom's greater effectiveness in destroying ozone (see section 1.2.3). Figure available from http://afeas.org*

extremely stable in the troposphere, could be transported into the stratosphere and broken down by intense ultra-violet radiation. The inorganic chlorine that is produced is called Cl_y.

The chlorine atoms which are released can destroy ozone in the upper stratosphere in catalytic cycles requiring atomic oxygen such as

Cycle 6:

$$Cl + O_3 \rightarrow ClO + O_2 \tag{1.31}$$

$$ClO + O \rightarrow Cl + O_2 \tag{1.32}$$

$$net : \mathbf{O_3 + O \rightarrow 2O_2}.$$

As these reactions show, the main active chlorine species are Cl and ClO, which, together, are known as Cl_x.

The main chlorine reservoirs are chlorine nitrate ($ClONO_2$), and hydrochloric acid (HCl). $ClONO_2$ is formed by reaction 1.33, coupling chlorine chemistry to that of nitrogen,

$$ClO + NO_2 \xrightarrow{M} ClONO_2. \tag{1.33}$$

Chlorine nitrate is destroyed mainly by photolysis, but also by oxidation in the upper stratosphere. HCl is longer lived, and is formed by reaction 1.34 and a number of less important processes. HCl is converted back to Cl_x by oxidation by OH.

$$CH_4 + Cl \rightarrow HCl + \dot{CH_3} \tag{1.34}$$

Bromine Chemistry

The chemistry of bromine in the stratosphere is roughly analogous to that of the other important halogen, chlorine. The main source gases of inorganic bromine, or Br_y, are halogenated organic compounds. The active species are Br and BrO, together known as Br_x. The main reservoirs are bromine nitrate ($BrONO_2$) and hydrobromic acid (HBr).

The chemistry of bromine differs from that of chlorine, however, due to its larger atomic radius. This leads to longer, and therefore weaker, intramolecular bonds[†]. $BrONO_2$ is photolysed at longer wavelengths and, therefore, more rapidly than is $ClONO_2$; the formation of HBr by the reaction of Br with methane is endothermic, whereas the analogous chlorine reaction (1.34) is exothermic (Wayne, 2000); HBr is rapidly destroyed by OH, and also by O in the upper stratosphere. The effect of this is to decrease the lifetime of the bromine reservoirs.

Bromine is signi£cantly more effective in destroying ozone than is chlorine. The catalytic chains are much longer than those of chlorine as a greater fraction of the halogen is in the active form. For example, Lary (1997) showed that, in the upper stratosphere, the chain length of the Cl/ClO cycle is $\sim 10^3$ and that of Br/BrO is $\sim 10^4$. The chain length is the number of times the catalytic cyclic is executed before the reactive radical involved is destroyed. Daniel *et al.* (1999) calculated, using a two dimensional model, that bromine destroys ozone 45 times more effectively than does chlorine.

[†]Mean bond dissociation enthalpies at 298 K($\Delta H^{\ominus}$) are: HCl 431 kJmol^{-1}, HBr 366 kJmol^{-1} (Atkins, 1994)

The presence of bromine in the stratosphere also allows synergistic catalytic cycles involving both chlorine and bromine (McElroy *et al.*, 1986; Danilin *et al.*, 1996), such as

Cycle 7:

$$\mathrm{BrO} + \mathrm{ClO} \rightarrow \mathrm{BrCl} + \mathrm{O_2} \tag{1.35}$$

$$\mathrm{BrCl} + h\nu \rightarrow \mathrm{Br} + \mathrm{Cl} \tag{1.36}$$

$$\mathrm{Br} + \mathrm{O_3} \rightarrow \mathrm{BrO} + \mathrm{O_2} \tag{1.37}$$

$$\mathrm{Cl} + \mathrm{O_3} \rightarrow \mathrm{ClO} + \mathrm{O_2} \tag{1.38}$$

$$net : \mathbf{O_3} + \mathbf{O_3} \rightarrow \mathbf{3O_2}.$$

Thus, bromine enhances the catalytic ef£ciency of chlorine and *vice versa*. Note that this cycle does not require atomic oxygen, making it ef£cient in the lower stratosphere.

The gas phase chemistry of bromine is reviewed in Lary (1996).

1.2.4 Heterogeneous Chemistry

The previous sections have discussed the gas phase chemistry of the stratosphere. It is now recognised, however, that an important role is also played by heterogeneous reactions. That is, those occurring on, or in, condensed phases. There are a number of natural particles in the stratosphere that may act as a surface for these reactions, including sulphate aerosol and polar stratospheric clouds (PSCs). There may also be anthropogenic particles, such as alumina (aluminium oxide) from rocket launches. Alumina particles can have a large local effect, but have a limited global importance and will not be discussed further here. The sources and chemical effects of some sulphate aerosols and PSCs will be considered in the following sections.

Sulphate Aerosol

These liquid particles are mainly composed of sulphuric acid and water. The composition varies from roughly 50-80%wt sulphuric acid, depending on temperature and humidity. The primary source of sulphate in the stratosphere is carbonyl sulphide (OCS) which is emitted in the troposphere, although its origin is unclear (Finlayson-Pitts and Pitts Jr., 2000). Carbonyl sulphide is a stable molecule that is oxidised in the stratosphere by atomic oxygen radicals or by short wave ultra-violet radiation. Another important source of sulphur is sulphur dioxide, injected into the stratosphere by large volcanic eruptions such as El Chichón in 1982 and Mt. Pinatubo in 1991.

The sulphur dioxide is converted into sulphuric acid by oxidation by the hydroxyl radical in the presence of oxygen and water (Wayne, 2000).

Once the aerosol is formed, slow gravitational settling in the stratosphere and lack of removal by precipitation mean that it is long-lived. In addition it is formed into layers by rapid horizontal transport.

The rate of a heterogeneous reaction is given by

$$k^H = \frac{\overline{c} A \gamma(T)}{4} \tag{1.39}$$

where $\overline{c}$ is the thermal velocity of the reactant molecule, γ is the reactive uptake coef£cient (the fraction of collisions that result in the molecule being lost to the surface) and A is the surface area density (SAD) of the aerosol. A typical background SAD for sulphate aerosol is $1\mu\text{m}^2\text{cm}^{-3}$, but it may be as high as $30\mu\text{m}^2\text{cm}^{-3}$ following a large volcanic eruption. As k^H is proportional to the SAD, volcanic eruptions can have a signi£cant effect on stratospheric chemistry.

The most important heterogeneous reaction in the stratosphere is the hydrolysis of N_2O_5 to form the longer lived reservoir HNO_3.

$$N_2O_5 + H_2O \xrightarrow{aerosol} HNO_3 \tag{1.40}$$

As the loss reactions for HNO_3 (photolysis and oxidation by OH) remain unchanged, the ratio of $\frac{NO_x}{NO_y}$ decreases as sulphate SAD increases. This reversible process is sometimes called *denoxi£cation.*

Denoxi£cation has additional effects on the partitioning of other families, such as inorganic chlorine. $ClONO_2$ is an important reservoir for Cl_x. If we assume that $ClONO_2$ is in photochemical steady state and Cl_x is mostly in the form of ClO, we can obtain an expression for the ratio of $\frac{Cl_x}{ClONO_2}$:

$$\frac{d[ClONO_2]}{dt} = k_{ClO+NO_2+M}[ClO][NO_2] - J_{ClONO_2}[ClONO_2] = 0 \tag{1.41}$$

$$\frac{[Cl_x]}{[ClONO_2]} = \frac{J_{ClONO_2}}{k^*_{ClO+NO_2+M}[NO_2]} \tag{1.42}$$

$\frac{Cl_x}{ClONO_2}$ is inversely proportional to NO_x so denoxi£cation will increase Cl_x at the expense of $ClONO_2$ (Stimp¤e *et al.*, 1994).

A second important reaction is the hydrolysis of $BrONO_2$:

$$BrONO_2 + H_2O \xrightarrow{aerosol} HOBr + HNO_3 \tag{1.43}$$

The reaction also converts NO_y to a longer lived reservoir, adding to denoxi£cation.

Some reactions are only important at temperatures below about 200 K (see, for example, Dessler, 2000) as the uptake coef£cient increases with decreasing temperature. These reactions include:

$$ClONO_2 + H_2O \xrightarrow{aerosol} HOCl + HNO_3 \tag{1.44}$$

$$ClONO_2 + HCl \xrightarrow{aerosol} Cl_2 + HNO_3 \tag{1.45}$$

$$HOCl + HCl \xrightarrow{aerosol} Cl_2 + H_2O \tag{1.46}$$

$$HOBr + HCl \xrightarrow{aerosol} BrCl + H_2O \tag{1.47}$$

These reactions form chlorine compounds which are photo-labile, so quickly release active chlorine in sunlight. Reactions 1.44 and 1.45 also contribute to denoxi£cation.

It should be noted that the effect of increasing aerosol SAD at current halogen loadings is very different to that at 'natural' levels. Following the Mt. Pinatubo eruption active chlorine levels increased through direct activation reactions and as a consequence of denoxi£cation. This led to a global decrease in ozone lasting several years. Eruptions prior to the 1970s would have resulted in global increases in ozone as the slower rate of destruction by NO_x cycles would have been the dominant effect (Dessler, 2000).

Polar Stratospheric Clouds

Polar stratospheric clouds (PSCs) are now known to play a crucial role in polar ozone depletion (see section 1.3.1). They are clouds which form in the very cold temperatures of the polar vortices and provide a surface for several rapid chemical reactions which otherwise occur only slowly in the gas phase.

PSCs are categorised by composition and phase. Type I PSCs contain nitric acid and form below about 196 K (T_{NAT}) at an altitude of around 20 km (see, for example, Dessler, 2000). The most stable mixture of water and nitric acid under stratospheric conditions is nitric acid trihydrate

($HNO_3.3H_2O$), or NAT. Other possible compounds are nitric acid dihydrate (NAD) or more water rich hydrates. Solid particles of NAT or NAD are called type Ia. These particles usually have a radius of roughly 0.5-1μm, but recent observations by Fahey *et al.* (2001) found some particles with radii as large as 10μm. As the supply of nitric acid and water is limited in the stratosphere this is possible only if a small fraction of NAT particles grow to this size (Panegrossi *et al.*, 1996). Fueglistaler *et al.* (2002) have proposed a microphysical mechanism for the formation of these so-called *NAT rocks*. In their model, a *mother cloud* with a high density of NAT particles ($n \geq 0.01\text{cm}^{-3}$) acts as a source of NAT rocks via sedimentation. These particles fall into a region which is super-saturated with respect to NAT, grow in size and therefore sediment more rapidly. If these particles are assumed to denitrify the region below the mother cloud then the growth, and hence the acceleration, of additional particles will be inhibited. This provides the necessary reduction in particle number density.

Liquid particles of a super-cooled ternary solution (STS) of nitric acid, sulphuric acid and water are also found (e.g. Dessler, 2000). These form with no nucleation barrier so are likely to have more uniform radii. These liquid particles are called type Ib.

Type II PSCs are composed primarily of water ice, and form only below the frost point ($T_{frost} \approx$ 189 K at 20 km). These solid particles are typically larger than type I PSCs, with radii of around 5-10μm. Frozen ice particles are thought to nucleate on type I PSCs or on sulphate aerosol.

As noted above, low temperatures are needed for PSCs to form. Several groups (e.g. Dornbrack *et al.*, 2001; Carslaw *et al.*, 1999) have noted that the amount of chemical processing measured in the Arctic exceeds that predicted by the synoptic scale temperature. One possibility is that mountain waves cause mesoscale cooling that increases the occurrence of PSCs and enhances the chemical processing. Dornbrack *et al.* (2001) investigated the effect of mountain waves on PSC formation over Scandinavia. As the synoptic temperature was frequently below T_{NAT} the effect on type I PSCs was small. Type II PSCs, however, were controlled by mesoscale temperature ¤uctuations as the synoptic temperature was almost always greater that T_{frost}.

Reactions on PSCs are similar to those on aerosols. The most important ones are those

involved in *chlorine activation*:

$$\mathrm{ClONO_2 + HCl \xrightarrow{PSC} Cl_2 + HNO_3} \tag{1.48}$$

$$\mathrm{ClONO_2 + H_2O \xrightarrow{PSC} HOCl + HNO_3} \tag{1.49}$$

$$\mathrm{HOCl + HCl \xrightarrow{PSC} H_2O + Cl_2} \tag{1.50}$$

$$\mathrm{HOBr + HCl \xrightarrow{PSC} BrCl + H_2O} \tag{1.51}$$

All these reactions convert chlorine from reservoir forms to photo-labile compounds that release Cl_x in sunlight. These reactions are rapid on all PSC types (γ = 0.1-0.3; DeMore *et al.* (1997); Sander *et al.* (2000)) so even brief exposure to PSCs may destroy all the reservoir species. This processing also denoxi£es the polar air.

In addition to denoxi£cation, NO_y may also be irreversibly removed by sedimentation of PSC particles. This permanent *denitri£cation* is only signi£cant for larger ice particles and the *NAT rocks* described by Fahey *et al.* (2001). The sedimentation velocity of smaller particles means that they remove only a very small quantity of NO_y. This effect is thought to add signi£cantly to polar ozone depletion by prolonging the enhancement of Cl_x (Waibel *et al.*, 1999).

1.2.5 Temperature and General Circulation

The stratospheric circulation and the distribution of ozone are strongly coupled. Ozone absorbs strongly in the ultra-violet, visible and infra-red regions, causing a strong diabatic heating with a maximum of order 10 K/day near the stratopause (Brasseur *et al.*, 1999). This causes the distinctive vertical temperature pro£le of the stratosphere (see £gure 1.6) and affects the winds. In turn, the circulation affects ozone by advecting odd oxygen, and the temperature affects the rates of important chemical reactions. This strong coupling is possible because the timescales of the chemistry and dynamics are so similar. In fact, the dominant process depends on both altitude and latitude (see, for example, Dessler, 2000, £gure 5.14).

At pressures below about 30 mb there is a negative horizontal temperature gradient from equator to winter pole. The resulting strong zonal ¤ow means that the stratosphere tends to be well-mixed in the zonal direction (see, for example, Brasseur *et al.*, 1999).

Meridional ¤ow in the stratosphere is mainly wave driven. Rossby waves transport mass poleward in the winter hemisphere, which forces a sinking motion at the pole and a rising motion

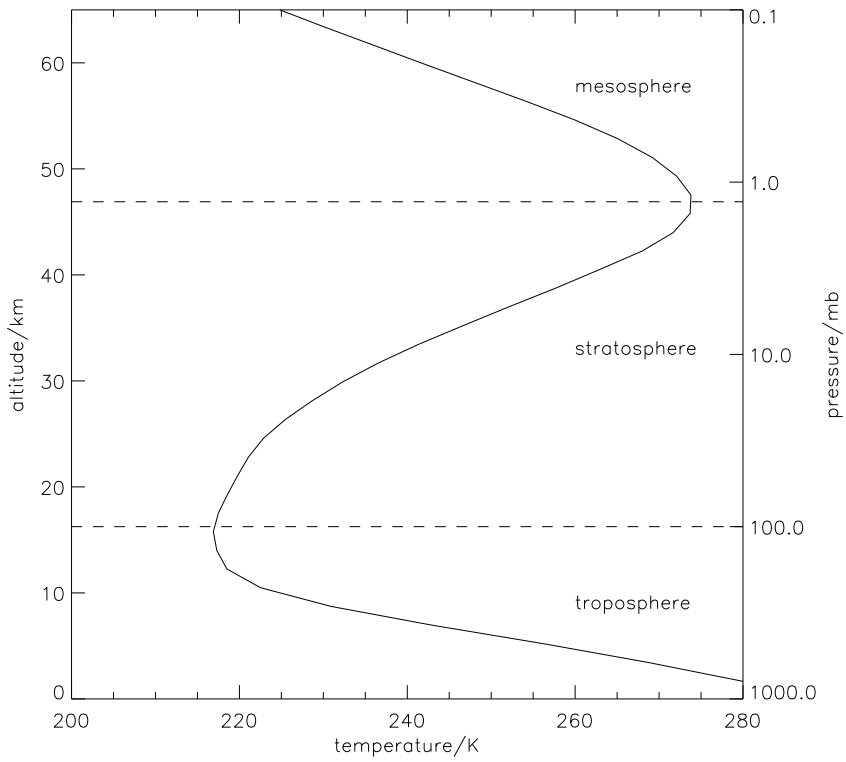

Figure 1.6: *Vertical temperature pro£le at 45° North in June. Data from Rees* et al. *(1990)*

in the summer hemisphere and in the tropics. This overturning is known as the Brewer-Dobson circulation. For more information see, for example, James (1995).

One useful measure of the ozone distribution is the total column, often measured in Dobson Units (DU) [‡]. The Brewer-Dobson circulation carries ozone from the region of maximum production in the tropical upper stratosphere towards the poles. It is here, in a region of net ozone loss, that the maximum ozone column is located. In addition, there are hemispheric differences in the circulation, and therefore in the ozone distribution, caused by differences in wave propagation (e.g. Ushimaru and Tanaka, 1994). The stronger vortex in the southern hemisphere forms a more effective barrier to mixing than does its northern counterpart. This prevents the Brewer-Dobson circulation transporting ozone quickly to the pole, so the southern hemisphere has a sub-polar maximum in the ozone column. The maximum column in the northern hemisphere is located much nearer the pole. A one year ozone climatology, showing these features and polar ozone depletion (see section 1.3.1) is shown in £gure 1.7. It is clear that the inclusion of stratospheric dynamics as well as photochemistry is needed in order to understand the global distribution of ozone.

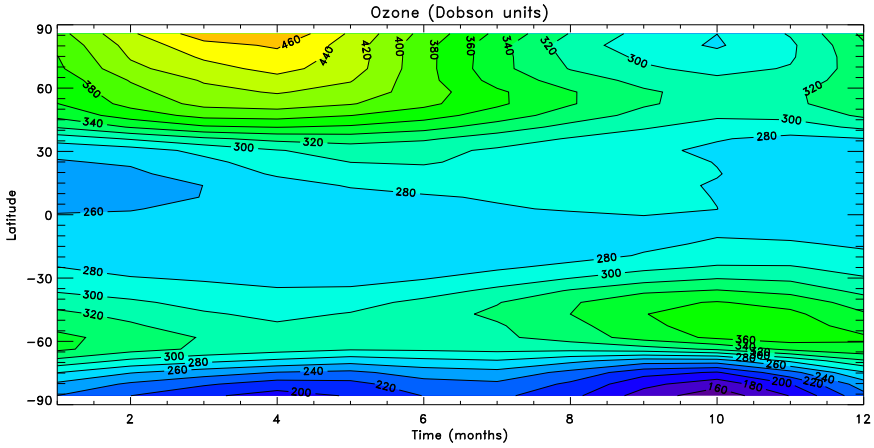

Figure 1.7: *Zonally averaged monthly ozone column climatology in DU. Data from Li and Shine (1995) derived from satellite measurements from 1985-1989. Figure courtesy of M. Joshi.*

[‡]1 DU $\approx 2.687 \times 10^{16}$ molecules cm^{-2}

1.3 Ozone Depletion

1.3.1 Polar Ozone Depletion

The dramatic ozone losses in the Antarctic spring, reported by Farman *et al.* (1985), were totally unpredicted by chemical models. The reason for this was the neglect of heterogeneous chemistry, particularly on PSCs (see section 1.2.4) that are now known to form in the particularly cold conditions of the polar night. The complex chain of events that leads to the large ozone losses found each polar spring have now been deduced and full discussions can be found in Wayne (2000), Dessler (2000), Finlayson-Pitts and Pitts Jr. (2000), Solomon (1999) and other texts. The important details, including the physical and chemical processes and hemispheric differences, will be discussed brie¤y here.

In the darkness of the polar night, the stratosphere cools as the emission of infra-red radiation is no longer balanced by absorption of solar radiation (see £gure 1.8(b)). The large meridional temperature gradient from midlatitudes to pole and the action of the Coriolis force leads to a strong zonal wind. This polar night jet forms at a latitude of about 60°in the winter hemisphere and extends from 100 mb to the upper stratosphere. In the southern hemisphere it reaches a maximum zonal velocity of around 100 ms^{-1} at an altitude of 20-35km. This jet, and the associated gradient in potential vorticity, form an effective barrier to mixing between polar and midlatitude air.

In the isolated, cold polar vortex PSCs form and the heterogeneous reactions on their surface activate chlorine and cause denoxi£cation. Type II and larger type Ia particles are heavy enough to sediment under gravity, leading to irreversible denitri£cation, and also dehydration if ice particles are formed.

Chemical processing continues throughout the winter, but ozone depletion does not begin until sunlight returns. The enhancement of $\frac{Cl_x}{Cl_y}$ means that reaction 1.52, whose rate depends on $[ClO]^2$, is ef£cient and cycle 8 can destroy ozone effectively.

Cycle 8:

$$ClO + ClO \xrightarrow{M} Cl_2O_2 \tag{1.52}$$

$$Cl_2O_2 + h\nu \rightarrow ClOO + Cl \tag{1.53}$$

$$ClOO + M \rightarrow Cl + O_2 + M \tag{1.54}$$

$$2(Cl + O_3 \rightarrow ClO + O_2) \tag{1.55}$$

$$net : \mathbf{2O_3 \rightarrow 3O_2}$$

This cycle is unimportant at midlatitudes due to the low concentration of ClO and the warmer temperatures that allow reaction 1.57 to create a null cycle:

Cycle 9:

$$\mathrm{ClO} + \mathrm{ClO} \xrightarrow{M} (\mathrm{ClO})_2 \tag{1.56}$$

$$(\mathrm{ClO})_2 \xrightarrow[>200K]{M} 2\mathrm{ClO} \tag{1.57}$$

$$net : \mathbf{null}$$

The BrO/ClO and ClO/Cl cycles also destroy signi£cant quantities of ozone. All these cycles require sunlight to proceed and can continue as long as the vortex is isolated and $\frac{\mathrm{Cl_x}}{\mathrm{Cl_y}}$ is enhanced. If denitri£cation has occured then mixing with $\mathrm{NO_x}$ rich midlatitude air must take place before $\mathrm{Cl_x}$ can be sequestered into $\mathrm{ClONO_2}$. This has the potential to prolong ozone depletion further into the spring when more light is available to drive cycles 7 and 8. Ozone is destroyed between about 15 and 21km (see £gure 1.8(a)). In the Antarctic all of the ozone in this layer may be removed (see £gure 1.9).

After sunlight returns to the polar region it begins to warm. This reduces the meridional temperature gradient, weakening the polar jet. This is followed by the £nal breakup of the vortex and complete mixing with midlatitude air.

As halogen loading has increased since the 1970s, the ozone column observed at the south pole during spring has decreased. See £gure 1.10. Although the spring ozone depletion has been recorded in both hemispheres it is both less severe and more variable in the Arctic than in the Antarctic. This is due to the different meteorology caused by greater tropospheric wave propagation over the continents of the northern hemisphere. This leads to more rapid descent in the polar vortex and, consequently, a greater adiabatic heating. In fact, the temperatures are often just above the PSC formation threshold, making the system very sensitive to variability or changes in the adiabatic heating. As the temperature is often too warm for PSCs to form, there is less chemical processing than in the southern hemisphere. This means that $\frac{\mathrm{Cl_x}}{\mathrm{Cl_y}}$ is lower than in the Antarctic and the ClO dimer cycle is much less ef£cient due to its dependence on $[\mathrm{ClO}]^2$. The ClO/BrO cycles are, therefore, relatively more important as they depend linearly on ClO. The low occurrence of PSCs also means that denoxi£cation and denitri£cation are limited, making the spring recovery faster. Denitri£cation is thought to have its largest effect when temperatures do not remain low enough for continuous heterogeneous processing by PSCs (Solomon *et al.*, 1996a). Cold Arctic winters, such as 1999/2000, that experience severe denitri£cation (Popp *et al.*, 2001) could have more serious ozone loss (Gao *et al.*, 2001).

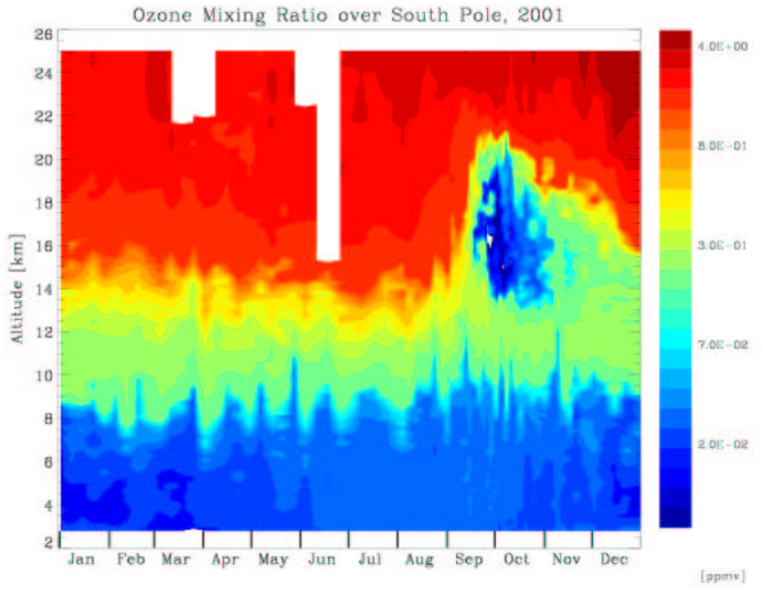

(a) Ozone mixing ratio

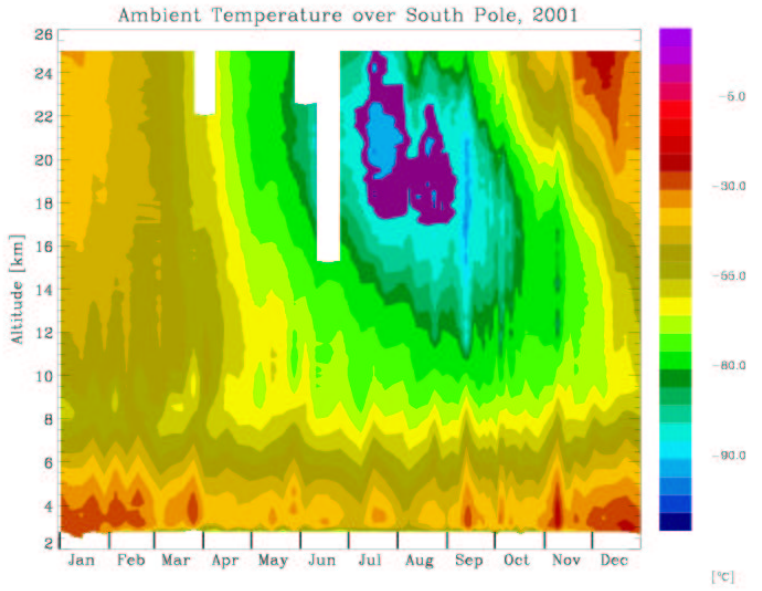

(b) Temperature

Figure 1.8: *South pole ozone and temperature plots for 2001. Large ozone depletion is seen between 15 and 21 km in September and October. Minimum temperatures are seen in July and August, increasing after sunlight returns in September. Available from http://www.cmdl.noaa.gov*

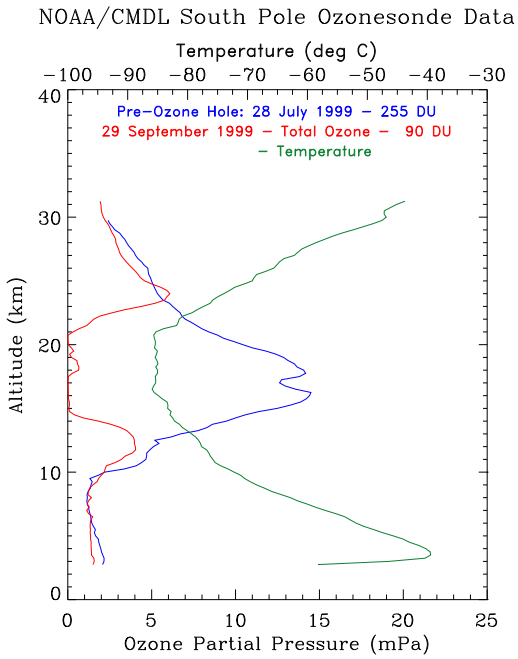

Figure 1.9: *Vertical ozone partial pressure and temperature pro£les from the NOAA Antarctic station on 29/9/99. An ozone pro£le from the preceding July is also shown, along with total ozone column data. An ozone column of less than 100 DU is measured. Sonde launched by P. Roberts and E. Sandberg of NOAA/CMDL. Available from http://www.cmdl.noaa.gov/ozwv/ozsondes/spo/ozppp2001.html*

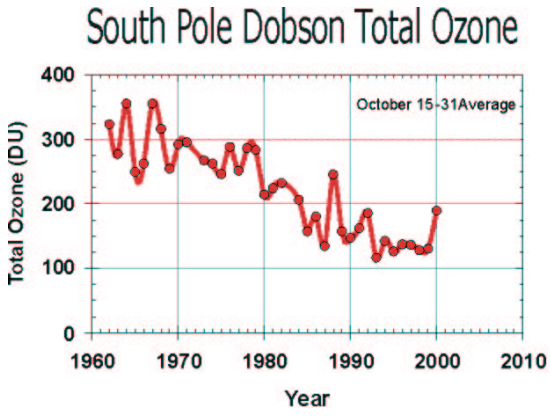

Figure 1.10: *South Pole ozone column 15-31 October average, in DU, from 1960 to 2000. A general decline is seen from the late 1970s Available from http://www.cmdl.noaa.gov/ozwv/ozsondes/spo/ozppp2001.html*

1.3.2 Midlatitude Ozone

Although the dramatic ozone losses seen in the polar spring are not seen at midlatitudes there is a clear, statistically signi£cant, downward trend at all latitudes outside of the tropics. This trend is apparent throughout the stratosphere in the data from 1979-1997 but there are distinct maxima in that trend at 15km (-7.3 $\pm$ 4.6%/decade) and 40km (-7.4 $\pm$ 2.0%/decade), and a minimum at 30km (-2.0 $\pm$ 1.8%/decade) (WMO, 1999). The trend is also apparent in the total column data shown in £gure 1.11.

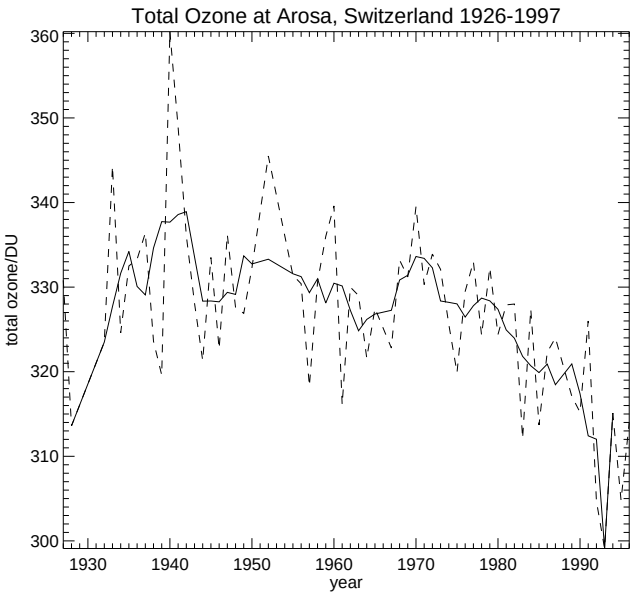

Figure 1.11: *Dashed line shows the total column ozone from Arosa, Switzerland, measured by sonde; solid line shows a £ve year moving average. There is a clear downward trend from about 1980. Data available from ftp://bach.ethz.ch/pub_read/anne/www/Arosayear.dat*

The upper stratospheric trend can mainly be explained by the increase in chlorine and bromine catalytic cycles, of the form of cycle 1, resulting from the anthropogenic emission of halogen compounds. Those involving atomic oxygen are ef£cient around 40km, and this is where the signal of man's effect on ozone was predicted to be seen.

The cause of the lower stratospheric trend is less obvious as the chemistry here is dominated by the HO_x cycles, and Cl_x cycles are inef£cient. In fact, when the effect of chlorine activation and denoxi£cation by heterogeneous reactions on aerosols are taken into account (Solomon *et al.*, 1996b, 1998) the HO_x/Cl_x and Cl_x/Br_x cycles do have a signi£cant effect at this altitude. The hydrolysis of bromine nitrate also increases HO_x concentrations, indirectly causing more ozone depletion. It has been suggested that *in situ* chlorine activation on cirrus clouds in the tropopause

region could be important for ozone depletion (Borrmann *et al.*, 1996; Solomon *et al.*, 1997). This has been both supported (e.g. Lelieveld *et al.*, 1999; Roumeau *et al.*, 2000) and contradicted (e.g Smith *et al.*, 2001) by observational evidence.

Additional causes for this trend, involving mixing with ozone-poor polar air, have also been proposed. One suggestion is that the vortex acts as a ¤*owing processor* where ozone-poor air ¤ows through the polar vortex during the spring (see, for example, Tuck *et al.*, 1993). This theory has, however, been criticised by Pyle (1995), McIntyre (1995) and Mo *et al.* (1998) who found little evidence to support it. Mixing may also occur as £laments of polar air are torn off from the vortex edge (see, for example, Orsolini, 1995; Pyle, 1995; Kirchhoff *et al.*, 1996; Flentje *et al.*, 2000) or as a single mixing event during the £nal vortex break-down (Sze *et al.*, 1989; Prather *et al.*, 1990; Manney *et al.*, 1994). Mixing with polar air can only explain part of the midlatitude trend (Randel and Wu, 1995; WMO, 1999). Knudsen and Grooß (2000) calculated that dilution accounted for approximately 40% of the depletion seen in northern hemisphere spring.

There is also a strong argument for a large dynamical contribution to the downward trend in midlatitude ozone. This may be due to, for example, a strengthening of the Arctic vortex, a change in tropopause height or a weakening of the Brewer-Dobson circulation (see, for example, Hadjinicolaou *et al.*, 2002). Hadjinicolaou *et al.* (2002) used SLIMCAT, a chemical transport model forced by European Centre for Medium Range Weather Forecasts analysis, to examine the dynamical contribution to the trend in ozone. The model used a simple relaxation chemical scheme (Cariolle and Déqué, 1986). The modelled interannual variability was in good agreement with observations, and the downward trend for 1979-1998 was at least half of that observed. The model did not include trends in halogen loading or sulphate aerosol, so the variability and trend were attributed to purely dynamical effects.

1.4 Chemistry-Climate Interactions

1.4.1 Chemistry-Climate Models

As the transport and chemical timescales of stratospheric ozone are so similar, its simulation requires a model that captures the interactions between chemistry, radiation and dynamics. As the system itself is three-dimensional, a three-dimensional model should also be used. In addition, the large interannual variability of some regions, such as the Arctic, means that long, multiannual, or even multidecadal, simulations are necessary to achieve statistically signi£cant results. Models of

this type are extremely computationally expensive, and integrating the chemical rate equations can consume around 90% of the CPU time in a coupled chemistry-general circulation model (CGCM) (Wang *et al.*, 1999).

To date, the computer power needed for long simulations using complex CGCMs has been limited. Non-interactive studies have been carried out using general circulation models (GCMs) with imposed changes in ozone or other radiatively active gases, or with chemical transport models (CTMs) using observed or off-line model dynamical £elds. Two- and three-dimensional chemical-dynamical models have also been developed. Two-dimensional, latitude-height, models have been widely used for investigating future climate scenarios, but are limited by parameterised dynamics. The existing three-dimensional models can be categorised as having either simple chemistry parameterisations or complex 'full' chemistry schemes. The various model types and their advantages and disadvantages are discussed in more detail below.

1.4.2 General Circulation Models

Many climate GCMs have been created, and these can be forced by past or future scenarios of ozone or radiatively active gases (see, for example, Rosier and Shine, 2000; Graf *et al.*, 1998). This allows the dynamical responses, such as changes in meridional circulation, wave propagation or polar vortex strength, to be investigated. Possible chemical feedbacks can be postulated, but cannot be calculated by the model.

1.4.3 Chemical-Transport Models

CTMs use observations or GCM output to force model circulation and temperature. They are computationally cheap, so can include full chemical schemes. (see, for example, WMO, 1999, chapter 12). These models have been widely used to simulate recent conditions (e.g. Chipper£eld *et al.*, 1996), perform sensitivity studies (e.g. Chipper£eld and Pyle, 1998; Massie *et al.*, 2000), and test current understanding of the physical and chemical processes involved in ozone depletion. This allows the effect of changing greenhouse gases on chemistry to be investigated. It does not, however, allow the study of interactions between chemistry, radiation and dynamics.

1.4.4 Two-Dimensional Chemical-Dynamical Models

As the zonal transport timescale is much shorter than the meridional timescale the stratosphere is generally zonally well-mixed. Two-dimensional, zonally averaged, models are, therefore, often used to investigate the long-term development of stratospheric ozone and climate. They typically have a horizontal resolution of 5-10°in latitude and 1-2 km in altitude (WMO, 1999). Transport is parameterised in terms of the meridional circulations and eddy diffusion. As two-dimensional models are computationally cheap, fairly complex chemical schemes can be incorporated, including photochemical and heterogeneous reactions. Long model integrations may easily be performed, making them suitable tools for future climate investigations (WMO, 1999, chapter 12) and sensitivity studies (see, for example, Solomon *et al.*, 1998; Tourpali *et al.*, 1997). The parameterised dynamics are, however, limiting. Important features, such as polar vortex isolation, are hard to simulate, and zonal asymmetries, such as a distorted polar vortex or synoptic scale features, are lost.

Randeniya *et al.* (2002) used the CSIRO 2-D chemical transport model to study ozone trends from 1980 to 2100. The model used updated rate coef£cients from Portmann *et al.* (1999), boundary conditions for CH_4 and N_2O from Ehhalt and Prather (2001) and low temperature aerosol chemistry from Vohralik (2002). Three 120 year integrations were performed using different scenarios for the atmospheric loading of halogens, N_2O, CH_4 and CO_2.

Rosen£eld *et al.* (2002) performed a number of future climate investigations using the GSFC coupled 2-D model. The effect of future emissions of CO_2 on stratospheric circulation and chemistry from 1980-2050 was explored.

1.4.5 Three-Dimensional Chemistry-General Circulation Models

A model with an accurate description of chemistry, radiation and dynamics, and their interactions, is needed in order to properly represent the highly coupled stratospheric system. The computational expense of including a chemical scheme in a three-dimensional climate model has limited the development and use of such complete models. A number of coupled chemistry-GCMs have, however, been developed over recent years. The chemical schemes used in these models may be broadly categorised as simple chemistry parameterisations or more complex ‘full’ chemistry schemes.

Simple Chemistry Parameterisations

These generally have idealised ozone destruction and a relaxation to climatological ozone mixing ratios. These schemes are computationally cheap, so many model integrations may be carried out, giving results that are statistically robust. This is important in regions where there is signi£cant interannual variability, such as the Arctic winter stratosphere. The parameterisations used for long simulations of stratospheric ozone have not, so far, been physically based. Generally, they must be tuned to match observations, and relax to an ozone climatology. This constrains the model response and means that changes in circulation are not accounted for.

Cariolle and Déqué (1986) used a highly parameterised chemistry scheme in a GCM adapted from a tropospheric model. In this scheme the change in ozone mixing ratio only depends linearly on temperature, the overhead ozone column, and the local ozone mixing ratio. The partial derivatives vary with latitude and pressure and are calculated at $1\frac{1}{2}$ month intervals by a two-dimensional model with a full chemical scheme. The maximum error using this parameterisation, compared to the full scheme, was found to be about 12% in the lower stratosphere. The major drawback of this scheme is that the partial derivatives must be recalculated for any changes in the atmospheric burden of other gases. This makes it unsuitable for investigating many possible future scenarios. This scheme has also been extended to account for chlorine activation on polar stratospheric clouds (Hadjinicolaou *et al.*, 1997). A 'cold tracer' is activated when the temperature drops below a PSC formation threshold at latitudes greater than 40°, and decays with a £xed e-folding time. An additional ozone loss of 5% per 24 hours occurs when the cold tracer is in sunlight.

In the study of Mahlman *et al.* (1994), using the GFDL 'SKYHI' model, an ozone climatology and a calculated anomaly are used to represent polar ozone depletion. The anomaly is generated when three conditions are met: suf£cient solar ¤ux, desiccation, and high absolute vorticity. Under these conditions the anomaly is generated (ozone is destroyed) on an arbitrary timescale of 30 days. The rate that the anomaly is destroyed (ozone recovers) is based on the rate of formation of odd oxygen, scaled by the size of the perturbation. The relaxation to an ozone climatology constrains the model response, making the method unsuitable for studies of changing climate. Ozone values calculated in using this scheme were used in the radiative calculations to examine the effect of ozone depletion in a $4\frac{1}{2}$ year simulation.

The GISS GCM has been used with parameterised chemistry by Shindell *et al.* (1998b) to investigate the effect of increasing greenhouse-gas concentrations on the rate of ozone recovery. The

photochemical scheme is a simple parameterisation based on calculations using a one-dimensional model (Shindell and de Zafra, 1996, 1997). The gas phase chemistry depends on temperature and the local radiation £eld (Shindell *et al.*, 1998a). Polar ozone loss is parameterised with chlorine activation taking place below a PSC formation threshold of 195 K, and ozone loss occurring wherever there is active chlorine and sunlight (Shindell *et al.*, 1997). The effect of bromine chemistry on ozone is only included by adding extra chlorine. This fails to account for the hemispheric differences in the importance of bromine noted in section 1.3.1. Ozone recovery rates are parameterised based on the local photochemical lifetime of ozone at a given altitude and latitude, as calculated by the one-dimensional model. Calculated ozone is used in radiative calculations and therefore affects global circulation and wave propagation. Ozone transport, however, is £xed at climatological values, using only zonal mean motions so vortex assymetries are not accounted for. Changes in ozone transport due to increasing greenhouse gases are calculated non-interactively using model winds from a GCM calculation without interactive chemistry.

Complex Models

These state-of-the-art models attempt to represent all the physical and chemical processes in the atmosphere that are important in determining ozone mixing ratios. The use of a full scheme means that the diurnal cycles of important species are calculated. This can be validated to some extent by observations, which lends con£dence to the method. Such a scheme, however, must solve a stiff set of ordinary differential equations, which forces the model to use a very short timestep, usually of the order of minutes. In addition, as the concentrations of many species are calculated these species must also be advected by the model. The computational expense of this means that only a few relatively short model integrations are possible.

A critical assessment of current chemistry-climate GCMs (CGCMs) has been made by Austin *et al.* (2002). A summary of the dynamical models is given in table 1.1 and the chemical schemes are summarised in table 1.2. Austin *et al.* (2002) found that, despite the range of model resolutions, in both the horizontal and vertical dimensions, all the models gave a reasonable representation of current ozone amounts and patterns. The models calculated the northern hemisphere March maximum in total column to between +1.4% and +16.9%, and the southern hemisphere October maximum column to between -4.8% and +19.9%.

A problem typical of many GCMs is a *cold pole*, as explained by Austin *et al.* (2002). The southern hemisphere high latitudes are 5-10 K too cold as the Brewer-Dobson circulation is too

Model	Horizontal Resolution	Vertical Levels/ Upper Boundary	Gravity Wave Drag	References
UMETRAC	$2.5^\circ \times 3.75^\circ$	64/0.01 mb	non-orographic	Austin (2002)
CMAM	T32	65/0.0006 mb	non-orographic	de Grandpré *et al.* (2000)
MAECHAM	T30	39/0.01 mb	non-orographic	Austin *et al.* (2002)
E39/C	T30	39/10 mb	orographic	Schnadt *et al.* (2002), Hein *et al.* (2001)
UIUC	$4^\circ \times 5^\circ$	25/1 mb	orographic	Rosanov *et al.* (2001)
CCSR/NIES	T21	34/0.01 mb	orographic	Takigawa *et al.* (1999), Nagashima *et al.* (2002)
GISS	$8^\circ \times 10^\circ$	23/0.002 mb	non-orographic	Shindell *et al.* (1998b)
ULAQ	$10^\circ \times 20^\circ$	26/0.04 mb	Rayleigh friction	Pitari *et al.* (2002)

Table 1.1: *Summary of dynamical models of current CGCMs. Resolution is in degrees latitude $\times$ degrees longitude or in terms of wavenumber truncation for spectral models. A horizontal spectral resolution of T21 corresponds to approximately 5.5° and T42 to about 2.5°.*

weak. This is a problem for CGCMs as the models produce PSCs over too large an area and, therefore, destroy too much ozone. One solution (Austin *et al.*, 2000) is to adjust the temperatures used in the heterogeneous scheme to correct the problem. This tuning makes the model more realistic but does not account for the fact that gas phase reactions will also be affected by the temperatures. Catalytic ozone loss may, therefore, be too slow. Austin *et al.* (2002) note that increasing the horizontal resolution and incoporating a non-orographic gravity wave drag scheme reduces the cold pole problem and makes these temperature adjustments unnecessary.

Another issue raised by Austin *et al.* (2002) is the representation of sedimentation. A few models have simple parameterisations of this process, but only the ULAQ model has a detailed microphysical scheme. Currently, no model accounts for the large NAT particles observed by Fahey *et al.* (2001). It was noted in section 1.2.4 that the denitri£cation caused by sedimentation can prolong ozone depletion.

Experimental design was also discussed by Austin *et al.* (2002). The model integrations performed can be divided into *timeslice* or *transient* runs. Timeslice runs repeat several realisations of the same conditions typical of a particular year. The advantage of this method is that the variability of the model can be more easily assessed. A ten year, or preferably longer, integration is needed for this purpose. Transient runs give a continuous integration over the period of interest with changing concentrations of halogens and well-mixed greenhouse gases. A model run covering a historical period can be easily compared with observations, but provides only one

Model	Chemical Scheme	PSC Scheme	Particle Sedimentation	References
UMETRAC	family	LTS/ice or NAT/ice	yes	Austin (1991)
CMAM	family	LTS/ice	no	de Grandpré *et al.* (1997)
MAECHAM	family	NAT/ice	yes	Steil *et al.* (1998)
E39/C	family	NAT/ice	yes	Steil *et al.* (1998), Hein *et al.* (2001)
UIUC	full	NAT/ice	yes	Rosanov *et al.* (1999)
CCSR/NIES	family	NAT/ice	no	Takigawa *et al.* (1999)
GISS	parameterised	parameterised	no	Shindell *et al.* (1998b,a)
ULAQ	family, diurnally averaged	NAT/ice	yes	Pitari *et al.* (1992, 2002)

Table 1.2: *Summary of chemical models of current CGCMs. All PSC schemes are equilibrium models except that of the ULAQ model which is a full microphysical scheme. Particle sedimentation refers to the process of denitri£cation and/or dehydration following the formation of large solid particles in the polar night.*

realisation within the envelope of natural variability. It also allows, in theory, the future evolution of the atmosphere under a particular climate change scenario to be predicted, within the bounds of model error and variability. That variability can be assessed by examining, for example, a ten year period within the run. Ensembles of model runs may be used to assess the signi£cance of future prediction and of historical simulations, although Austin *et al.* (2002) note that, as each model will have a particular systematic bias, comparing a number of models may have additional value.

In order to reduce model cost, many of the chemical schemes in the CGCMs use a family approximation (see, for example, Austin, 1991) to extend the model timestep, fast solvers or just simple parameterisations (see table 1.2). For example, UMETRAC, as described in Austin *et al.* (1997) and Butchart and Austin (1996), uses a family method for short-lived species, and compact tracer relationships (Plumb and Ko, 1992) for longer lived species such as H_2O and total nitrogen. Vohralik *et al.* (1998) have shown this introduces only small errors, but that the errors are greatest when the mixing ratios of source gases, such as the halocarbons, are changing over time. The Canadian Middle Atmosphere Model (CMAM) also uses the family approximation in conjunction with the fast reduced Jacobian solver described in Sandilands and McConnell (1997).

1.4.6 Chemistry-Climate Predictions

The near-global decreases in stratospheric ozone seen over the last two decades are attributable to the anthropogenic increase in halogen loading. The Montreal Protocol and its subsequent amend-

ments (see, for example, WMO, 1999) limit the production of ozone depleting substances and the stratospheric halogen burden is expected to decrease over the 21st century (see section 1.2.3). All other factors being constant, stratospheric ozone should return to levels seen prior to the 1980s over this time. Several important factors, however, are not expected to remain constant. For example, stratospheric temperatures have decreased over recent decades due to the increase in greenhouse gases and ozone depletion (see, for example, WMO, 1999; Ramaswamy *et al.*, 2001). Emissions of methane and nitrous oxide have a chemical, as well as radiative, in¤uence on ozone and there is also a positive trend in stratospheric humidity, although both the magnitude and cause remain a subject of debate (see, for example, Zhou *et al.*, 2001). These changes could hasten or delay the rate of ozone recovery. The ozone distribution when halogen loading drops to natural, "background", levels will also be affected. If catalytic loss is enhanced then ozone may never recover to 1980 values, whereas if ozone loss cycles are inhibited a super-recovery may take place. Although the detrimental effects of ozone depletion are well studied (see, for example Xiong and Day, 2001), the consequences of an increase in global ozone are not known.

Stratospheric Cooling

Austin *et al.* (1992) were the £rst to suggest that a stratospheric cooling, resulting from increased long-wave emission by carbon dioxide, could lead to an Arctic ozone hole similar to that seen in the Antarctic if chlorine levels remained high. They proposed that ozone depletion would be increased if additional heterogeneous processing took place following enhanced PSC formation at lower temperatures. More recent studies using three-dimensional chemical-general circulation models (CGCMs) have predicted that ozone recovery could be delayed by stratospheric cooling. As ozone loss itself has a cooling effect, the possibility of a positive feedback exists.

Shindell *et al.* (1998b) used a GCM with a simple chemical parameterisation to predict future ozone concentrations. They performed two model simulations from 1959-2070. One included greenhouse gas forcings and one did not. Ozone recovery in the northern hemisphere in the greenhouse gas experiment was delayed by about a decade due to additional ozone loss in a cooler stratospheric vortex. The greenhouse gas-induced cooling caused changes in planetary wave propagation, leading to a more stable vortex with fewer sudden warmings. Austin and Butchart (1994) have suggested that this would be a necessary condition for an Arctic ozone hole.

Austin *et al.* (2000, 2001), using a more complex model, performed a number of "snapshot" or timeslice integrations. These were each of one year, using conditions appropriate for each £ve

year period from 1979-2055. This model predicted a faster initial recovery of the Antarctic ozone hole than did Shindell *et al.* (1998b), followed by a second minimum in the 2035-2045 time period, before £nal recovery. The second minimum was caused by increased formation of ice PSCs due to greenhouse gas-induced cooling. The large interannual variability of the northern hemisphere vortex made it dif£cult to draw conclusions from this small number of short model runs.

Nagashima *et al.* (2002) also used a complex chemistry-GCM to perform future climate simulations. They presented integrations from 1986-2050, with and without greenhouse gas forcing. They found that increasing greenhouse gases altered the stratospheric circulation, reducing the poleward heat ¤ux. This led to a colder northern polar vortex with enhanced ozone depletion compared to the unforced case. This result was statistically signi£cant but small compared to that seen by Shindell *et al.* (1998b). No signi£cant difference was seen between the forced and unforced cases in the southern hemisphere for ozone or temperature.

Schnadt *et al.* (2002) found quite different behaviour using their chemistry-GCM ECHAM4.L39(DLR)/CHEM. They present three timeslice model integrations, each of 20 years with an additional 4 year spin-up period. The conditions used in the three runs were appropriate for 1980, 1990 and 2015. They found that the additional radiative cooling due to increased greenhouse gas mixing ratios led to a slight increase in PSC formation in the southern hemisphere. Consequently, southern hemisphere ozone loss was greater in 2015 than in 1990, despite lower chlorine mixing ratios. In the northern hemisphere, however, their model had enhanced planetary wave activity in 2015. This compensated for the long-wave cooling by greenhouse gases and resulted in an overall warming of more than 4 K in the winter lower stratosphere. This, together with a reduction in chlorine, resulted in a clear increase stratospheric ozone.

In contrast to the enhanced ozone depletion predicted by many models in polar regions, stratospheric cooling is expected to moderate *in situ* midlatitude and tropical ozone loss by slowing gas phase catalytic cycles. This mechanism has been known for many years and was predicted to counteract upper stratospheric ozone loss in future scenarios with increasing halogen loading (Haigh and Pyle, 1982). Cooling also reduces the ratio O/O_3 (Rosen£eld *et al.*, 2002) which further slows catalytic loss. Rosen£eld *et al.* (2002) found, using the Goddard Space Flight Center coupled two-dimensional model, that increasing CO_2 caused globally averaged ozone to recover to the 1980 value approximately 10 years faster. The model also indicated a super-recovery by 2050 relative to 1980.

Nitrous Oxide

The effect of increasing nitrous oxide concentrations was also calculated by Randeniya *et al.* (2002). Nitrous oxide is an important source of stratospheric NO_x. As NO_x cycles control the concentration of odd oxygen in the mid stratosphere, an increase in nitrous oxide could affect *in situ* midlatitude ozone loss. Randeniya *et al.* (2002) calculated that a future scenario of increasing nitrous oxide but stable methane would lead to a decrease in the midlatitude ozone column during the period 2050 to 2100, despite increases in ozone below about 20km and above 35km. This model, however, did not include the radiative effect of increasing carbon dioxide.

Methane

Randeniya *et al.* (2002) also looked at the effect of increasing methane. Overall it led to an increase in ozone as odd oxygen is produced in the lower stratosphere as methane was oxidised. Chlorine loss cycles can also be slowed by methane as Cl_x is converted to HCl *via* reaction 1.34,

$$CH_4 + Cl \rightarrow CH_3 + HCl. \tag{1.58}$$

These processes dominated the additional ozone loss caused by HO_x generated during methane oxidation.

Water Vapour

Estimates of the trend in lower stratospheric water vapour range from 73.1 ± 16.3 ppb/year (Evans *et al.*, 1998) to 123.1 ± 18.3 ppb/year (Nedoluha *et al.*, 1998). Although there is still uncertainty in this trend several groups have calculated that it may be partly responsible for a cooling of the lower stratosphere (Forster and Shine, 1999, 2002; Dvortsov and Solomon, 2001) and additional ozone loss (Shindell, 2001). In the upper and lower stratosphere ozone loss will be increased by additional HO_x and also the repartitioning of chlorine to an active form via reaction 1.59. In the middle stratosphere $\frac{NO_x}{NO_y}$ will be reduced via reaction 1.60 and ozone loss will be slowed.

$$HCl + OH \rightarrow H_2O + Cl \tag{1.59}$$

$$NO_2 + OH \xrightarrow{M} HNO_3 \tag{1.60}$$

Dvortsov and Solomon (2001) used a two-dimensional model to calculate that continued increases in stratospheric humidity would result in a delay of about a decade in ozone recovery. Kirk-Davidoff *et al*. (1999) also note that increased stratospheric humidity increases the likelihood of PSC formation in the Arctic, leading to additional spring polar ozone loss while halogen loading is high.

Feedback Mechanisms

All chemical changes to the stratosphere are buffered by a radiative-chemical negative feedback. If ozone decreases the temperature decreases which slows catalytic loss. Shindell and Grewe (2002) estimate that this reduces all ozone perturbations by $\sim$20%. Another negative feedback is important when the whole column in considered, as in Haigh and Pyle (1982). If ozone in the upper atmosphere is reduced then the ¤ux of ultra-violet increases at lower levels, leading to increased ozone production. This feedback has been dubbed *self-healing*. An increase in upper level ozone leads to *reverse self healing*.

1.5 Thesis Aims

The aim of this thesis is the development of a fast chemical scheme for general circulation models. There currently exist a number of coupled chemistry general circulation models, but none of the physically based chemical schemes are computationally ef£cient enough to allow many long model integrations. This new model will allow the investigation of a greater number of future scenarios and the uncertainties associated with climate change.

Chapter 2 describes a photochemical box (zero-dimensional) model and a comparison with a similar established model. In chapter 3 a method of generating a fast chemical parameterisation is described. The photochemical box model is used to initialise this parameterisation and the model is validated. Chapter 4 describes a series of idealised experiments to investigate chemistry-climate interactions and motivate further experiments with complex models. Chapter 5 details the coupling of the chemical parameterisation with a three-dimensional general circulation model and some coupled chemistry integrations. Conclusions are presented in chapter 6.

CHAPTER TWO

STORM - A Stratospheric Chemical Box Model

Chemical box (or zero-dimensional) models are useful tools to study the chemistry of the atmosphere. As the effects of transport are ignored, these models are unsuitable for studies longer than typical mixing timescales. This may be days, hours or minutes depending on the region of the atmosphere. These models can, however, be useful in several ways. For example, they may be used to study the sensitivity of the chemical system to changes in species mixing ratios (see chapter 4), or the uncertainty of photochemical rate constants (see, for example, Fish and Burton, 1997). Coupled to Eulerian or Lagrangian dynamical models they enable the study of the effect of dynamics on chemistry (see, for example, Millard *et al.*, 2002).

In this chapter the new photochemical box model STORM (Stratospheric Ozone Reduced Model) is described. Section 2.1 discusses methods used to solve the system of ordinary differential equations that describe the behaviour of a photochemical model. Details of STORM are presented in section 2.2 and the model is compared to an established and independent photochemical box model in section 2.3. In chapter 3 of this work the STORM chemical box model is used to initialise a parameterised chemical scheme for CGCMs, and in chapter 4 it is used to perform a series of idealised climate change experiments.

2.1 Ordinary Differential Equation (ODE) Solvers

A chemical system can be represented as a set of kinetic ordinary differential equations (ODEs), such as

$$\begin{aligned} \frac{\partial n_i}{\partial t} &= P_i - L_i = S_i \\ i &= 1, 2, ..., N \end{aligned} \tag{2.1}$$

where S_i is the photochemical source term for species i, n_i is its concentration and P_i and L_i are its production and loss terms respectively. P_i and L_i represent the reactions in which i is a product or reactant, respectively. They are written as

$$P_i = \sum_{j,l \neq i} k_{jl} n_j n_l + \sum_{l \neq i} J_l n_l \tag{2.2}$$

$$L_i = n_i \left(\sum_l k'_{il} n_l + J_i \right). \tag{2.3}$$

where J_i and J_l are the photodissociation coef£cients, and k_{jl} and k'_{il} are the rate constants. If we de£ne the vectors **c** and **S** to be

$$\mathbf{c} = (n_1, n_2, ..., n_N) \tag{2.4}$$

and

$$\mathbf{S} = (S_1, S_2, ..., S_N) \tag{2.5}$$

then the chemical system can be written as

$$\frac{\partial \mathbf{c}}{\partial t} = \mathbf{S}(t, \mathbf{c}(t)). \tag{2.6}$$

The time dependence of **S** is mainly due to rapid changes in the rate of photochemical reactions, particularly at sunrise and sunset.

Although the set of ODEs described in equation (2.6) can be solved numerically, the computational cost of this is high. A solver for chemical rate equations should ideally be accurate, stable, positive-de£nite and mass-conserving (see, for example, Jacobson, 1999). The chemical

rate equations typically have timescales ranging over several orders of magnitude, which means that the set of ODEs is extremely stiff, forcing the timestep of the model to be short to preserve numerical stability. For example, explicit solvers, where the time derivatives of concentrations are evaluated at the previous timestep, must use a timestep no longer than the e-folding time of the shortest lived species. A simple example of an explicit solver is the forward Euler solution given in equation 2.7.

$$n_i(t_m) - n_i(t_{m-1}) = \Delta t(P(t_{m-1}) - L_i(t_{m-1})) \tag{2.7}$$

Due to the need for a short timestep, this method is not generally used in atmospheric chemical modelling.

2.1.1 Fast ODE Solvers

In order to circumvent this timestep problem, a number of fast solvers have been developed to solve the ODEs ef£ciently. Many of these are based on Gear's backward differentiation method (Gear, 1967). This method is accurate, but unsuitable for large systems or three-dimensional modelling due the computational expense. Less expensive schemes have been developed. For example Jacobson and Turco (1994) and others have taken advantage of the sparseness of the Jacobian matrix, $\frac{\partial \mathbf{S}}{\partial \mathbf{c}}$, in combining Gear's method with sparse matrix and computer optimisation techniques to increase the ef£ciency of the method. Sandilands and McConnell (1997) used a solver that broke the Jacobian into small units that could be solved more ef£ciently. The smaller units corresponded to chemical 'families' (see below). Sun *et al.* (1994) used an implicit-explicit hybrid method, separating the species into a fast group and a slow group. The fast group were solved as a stiff set of ODEs and slow group as a non-stiff set. Ramaroson *et al.* (1992) described a semi-implicit symmetric technique that avoided the many iterations required for Gear's method. This method is used in STORM, and is described in more detail below.

2.1.2 Mechanism Reduction

Several alternative methods have been proposed for dealing with the problem of solving stiff chemical systems. A mechanism may be reduced in size, allowing more rapid solution, or reduced in stiffness to allow a longer timestep.

Redundant species are those which do not signi£cantly affect necessary species (that is, those whose concentrations must be known) either directly or indirectly. If these species can be

identi£ed they may be removed from the mechanism, allowing a simple mechanism reduction. Redundant species may be identi£ed by an inspection method (see, for example, Tomlin *et al.*, 1997), or by a more sophisticated analysis of the Jacobian of the kinetic system, given in equation 2.8 (see, for example, Okino and Mavrovouniotis, 1999).

$$\mathbf{J} = \frac{\partial \mathbf{S}}{\partial \mathbf{c}} = \begin{vmatrix} \frac{\partial S_1}{\partial n_1} & \cdots & \frac{\partial S_1}{\partial n_N} \\ \vdots & & \vdots \\ \frac{\partial S_N}{\partial n_1} & \cdots & \frac{\partial S_N}{\partial n_N} \end{vmatrix} \tag{2.8}$$

Each element of the Jacobian, $(\partial S_i)/(\partial n_j)$, represents the change in rate of production of species i with a change in concentration of species j, thus giving information about the relative importance of each species. The important species can then be identi£ed, in an iterative process, as those which make the largest contribution to the chemical tendency, S, of necessary species. The remaining species may then be removed from the mechanism. This objective method can be ef£ciently automated, making it suitable for larger, complex, mechanisms. This has mainly been used by groups modelling the kinetics of combustion or of enzymes (see for example, Delgado and Liao, 1995). Its use in atmospheric chemistry is complicated by the time dependence of **S** caused by the diurnal cycle of photolysis.

Another common strategy is known as the *family method* or *lumping* (see, for example, Austin, 1991). Here, species in rapid equilibrium are grouped together in the ODEs. The partitioning between these species can then be calculated using photochemical steady-state assumptions (see, for example, Jacobson, 1999). This method reduces the stiffness of the system as each family will have a longer lifetime than its individual members.

2.2 Stratospheric Ozone Reduced Model (STORM)

STORM is based on the model described in Fish and Burton (1997) and Fish *et al.* (2000), but has been extensively revised and updated. The original version of the model was written in FORTRAN77. STORM has been rewritten in FORTRAN90, taking advantage of the additional features of this language such as pointers, dynamic memory allocation and array arithmetic. This makes the model more computationally ef£cient in terms of both CPU* time and memory.

*Central Processor Unit

Two versions of STORM are used in this work. STORM-H (for "halogenated") includes 39 species and 153 reactions. STORM-NH (for "non-halogenated") includes 19 species and 68 reactions. The species calculated by each model are listed in table 2.1. The reactions included in STORM-H are shown in the Annex to this chapter.

Both models account for heterogeneous reactions on sulphate aerosol, NAT and ice (see section 2.2.3). STORM-NH assumes that for each $CH_3^{\cdot}$ radical formed, two HO_2 molecules are generated. This assumption, used in early versions of the TOMCAT and UGAMP chemical models (Chipper£eld, 1993), parameterises the production of O_x during methane oxidation. Clearly, it is less accurate than an explicit calculation. STORM-H has a more detailed methane oxidation scheme using the species shown in table 2.1. Temperatures may be speci£ed or follow the climatology of Rees *et al.* (1990). Sulphate surface area may also be speci£ed.

Model	**Species**
STORM-NH	O_3, O, $O(^1D)$, NO, NO_2, NO_3, N_2O_5, N_2O, H, H_2, OH, HO_2, H_2O_2, H_2O, HNO_3, HNO_4, HONO, CH_4, CO
STORM-H	O_3, O, $O(^1D)$, NO, NO_2, NO_3, N_2O_5, N_2O, Cl, Cl_2, ClO, ClOO, OClO, Cl_2O_2, $ClONO_2$, HOCl, HCl, Br, Br_2, BrO, BrCl, $BrONO_2$, HOBr, HBr, H, H_2, OH, HO_2, H_2O_2, H_2O, HNO_3, HNO_4, HONO, CH_4, CH_3O_2, CH_3O, HCHO, CO

Table 2.1: *Species calculated by versions of the STORM chemical box model*

2.2.1 Integration Scheme

STORM uses a semi-implicit symmetric (SIS) integration scheme (Ramaroson *et al.*, 1992) to calculate the chemical tendency in equation 2.1. The change in concentration over one timestep is

given by

$$\begin{aligned} n_i(t_{m+1}) - n_i(t_m) = \quad & \frac{\Delta t}{2} \sum_{j,l \neq i} (k_{jl}(t_m) n_j(t_{m+1}) n_l(t_m) + k_{jl}(t_m) n_j(t_m) n_l(t_{m+1})) \\ & + \frac{\Delta t}{2} \sum_{l \neq i} (J_l(t_m) n_l(t_{m+1}) + J_l(t_{m+1}) n_l(t_m)) \\ & - \frac{\Delta t}{2} \sum_{l} (k'_{il}(t_m) n_i(t_{m+1}) n_l(t_m) - k'_{il}(t_m) n_i(t_m) n_l(t_{m+1})) \\ & - \frac{\Delta t}{2} (J_i(t_m) n_i(t_{m+1}) - J_i(t_{m+1}) n_i(t_m)) \end{aligned} \tag{2.9}$$

$i = 1, 2, \ldots, N.$

The £rst two terms represent P_i (equation 2.2) and the second two terms represent L_i (equation 2.3). This scheme strictly conserves the number of atoms, but does not ensure non-negative values. This problem can be overcome by making the second and fourth terms on the right-hand side of equation 2.9 fully implicit. The second term becomes

$$\Delta t \sum_{l \neq i} J_l(t_m) n_l(t_{m+1})$$

and the fourth term becomes

$$\Delta t J_i(t_m) n_i(t_{m+1}).$$

This fully implicit version of the equation will decrease the accuracy of the method but will not affect the stability. STORM may be run using either the semi- or fully-implicit scheme, unlike earlier versions of the box model which only included the semi-implicit scheme.

2.2.2 Photolysis Scheme

The rate of photolysis reaction depends on

$$J = \int_{\lambda} \sigma(\lambda) \phi(\lambda) q(\lambda) d\lambda, \tag{2.10}$$

where σ is the absorption cross section of the molecule, ϕ is the quantum yield[†] for dissociation, and q is the solar ¤ux.

[†]The quantum yield of a process is the fraction of molecules that undergo that process for each photon absorbed.

In STORM the recommendations of DeMore *et al.* (1997) and Sander *et al.* (2000) are used for σ and ϕ_{diss}. The solar ¤ux is calculated using the method of Meier *et al.* (1982), which is widely used in atmospheric photochemical models. This scheme calculates the source function, which is the value by which the ¤ux at the top of the atmosphere must be multiplied by to £nd the ¤ux at a given level. It includes terms for the direct beam, the multiply scattered ¤ux, the ground re¤ection of the direct beam and the ground re¤ection of the multiply scattered ¤ux. The inclusion of multiple scattering and albedo means that the ¤ux of radiation of wavelength greater than about 310nm is greater in the lower stratosphere than at higher altitudes (see Meier *et al.*, 1982, £gure 4). It assumes isotropic scattering in a plane parallel atmosphere. Spherical geometry is included for large solar zenith angles and rates are calculated for zenith angles up to 100°.

Photolysis rates for each species are calculated off-line and are stored as interpolated look-up tables. Linear interpolation (Press *et al.*, 1992) is used to £nd the rate at each timestep. This part of the model has also undergone revision. One small change is that photolysis rates for the timestep t to $t+1$ are calculated as a mean of the rates at times t and $t+1$. This improves the stability when the rates are changing rapidly, such as at sunrise and sunset. This allows the model to use a timestep that is typically about twice as long. This averaging doubles the number of calls to the interpolation routine, but this calculation is quite ef£cient. The photolysis scheme in Fish and Burton (1997) used look-up tables depending on solar zenith angle and altitude; a constant ozone pro£le was assumed. This approximation made the model unsuitable for global calculations with changing ozone pro£les. The tables would have to be recalculated to investigate the effect of changing ozone. The scheme has now been improved to allow for changing ozone columns by calculating rates depending on solar zenith angle, pressure and overhead ozone column. The drawbacks of this approach are the additional computer time required to generate the look-up tables, which then require more memory to store, and the additional expense of trilinear, rather than bilinear, interpolation.

2.2.3 Heterogeneous Scheme

The rate of a heterogeneous reaction, as noted in section 1.2.4, depends on the reactive uptake coef£cient,γ. The recommendations of Sander *et al.* (2000) for γ are used in STORM. Many reactions also depend on the composition of the sulphate aerosol and the parameterisation of Hanson *et al.* (1994), equation 2.11, is used to calculate this. The percentage of sulphuric acid by weight

is calculated using the expression,

$$W(wt.\%\mathrm{H_2SO_4}) = \frac{(-14.458 + 0.62456)T + 3565}{44.777 + 1.3204Z - 0.19988T}. \tag{2.11}$$

where $Z = lnP(H_2O)$ (P in mb and T in K). This scheme assumes equilibrium between gas and condensed phases. Nitric acid trihydrate (NAT) and water ice polar stratospheric clouds are calculated using the scheme of Hanson *et al.* (1994). The equilibrium vapour pressure of HNO_3 over NAT is given by

$$\log P(\mathrm{HNO_3})_{eqm} = m(T) \times \log P(\mathrm{H_2O}) + b(T) \tag{2.12}$$

where

$$m(T) = -2.7836 - 0.00088T \tag{2.13}$$

and

$$b(T) = 38.9855 - 11397/T + 0.009179T, \tag{2.14}$$

where $P(\mathrm{H_2O})$ is the partial pressure of H_2O (P in torr). The equilibrium vapour pressure of water over ice is given by

$$P(\mathrm{H_2O})_{eqm} = 6.1078 \times e^{(21.875 \times (T-273.16)/(T-7.66))}, \tag{2.15}$$

where pressure is in mb and T in C. At low temperatures, if these equilibrium vapour pressures are lower than the partial pressures of HNO_3 or H_2O then NAT or ice is formed:

$$[\mathrm{HNO_3}]_{solid} = [\mathrm{HNO_3}]_{gas} - [\mathrm{HNO_3}]_{eqm} \tag{2.16}$$

$$[\mathrm{H_2O}]_{solid} = [\mathrm{H_2O}]_{gas} - [\mathrm{H_2O}]_{eqm}. \tag{2.17}$$

NAT is assumed to have a radius of $0.01\mu m$ and ice a radius of $5\mu m$. NAT is assumed to nucleate on sulphate aerosol, and ice to nucleate on NAT. No nucleation barrier is assumed as small scale temperature ¤uctuations are likely to provide the necessary super-cooling.

2.2.4 Kinetic Data

The kinetic rate data used by the model have also been updated. The latest recommendations of DeMore *et al.* (1997) and Sander *et al.* (2000) are now used. These are NASA data sets that are widely used in atmospheric models.

Bimolecular reactions are given in the Arrhenius form,

$$k(T) = A \times e^{\left(\frac{-E}{RT}\right)}, \tag{2.18}$$

where R is the gas constant, A is the Arrhenius factor and E is the activation energy (T in K). A, E and a measure of uncertainty are given in the recommendations.

Termolecular reactions involve deactivation by collision with a third body and are of the form,

$$A + B \rightleftharpoons [AB]^* \stackrel{M}{\rightarrow} AB. \tag{2.19}$$

These reactions are strongly pressure dependent and are given in the form,

$$k_0 = k_0^{300}(T/300)^{-n} cm^6 molecule^{-2} s^{-1}. \tag{2.20}$$

The rate is limited at high pressure and that rate takes the form,

$$k_\infty = k_\infty^{300}(T/300)^{-m} cm^6 molecule^{-2} s^{-1}. \tag{2.21}$$

An effective second order rate constant is found using the £tted formula,

$$k(Z) = \left(\frac{k_0(T)[M]}{1 + (k_0(T)[M]/k_\infty(T))}\right) 0.6^{(1+[\log_{10}(k_0(T)[M]/k_\infty(T))]^2)^{-1}}. \tag{2.22}$$

Values of k_0, k_∞, m and n are given in the tables, together with uncertainties.

Reactions which proceed by thermal decomposition are given equilibrium constants, K, and the rates of unimolecular reactions may be calculated from these:

$$A + B \underset{k_b}{\overset{k_f}{\rightleftharpoons}} AB$$

$$k_f = K \times k_b$$

The equilibrium constant is temperature dependent and is given in the form

$$K(T)/cm^3 molecule^{-1} = A \times e^{\frac{B}{T}}, \tag{2.23}$$

and A and B are given.

For photolysis reactions recommendations are given for the absorption cross section and quantum yield for dissociation. Following the recommendation of Wennberg (2001), the rate of HNO_4 photolysis is increased by $1 \times 10^{-5} s^{-1}$ to account for additional photodissociation in the near-IR (Roehl *et al.*, 2002). This increases the rate signi£cantly at high solar zenith angles and improves the representation of HO_x.

2.3 Model Validation

In chapter 3 the STORM stratospheric chemical box model is used to initialise the FASTOC parameterisation for coupled chemistry-general circulation models. The results of this parameterisation can only, at best, be as good as those of the initialisation model. The behaviour of STORM must, therefore, be tested and evaluated to ensure it is a suitable tool.

Although comparison with measurements may seem the best way to examine the model's performance, a comparison with a second box model is preferred for several reasons:

- Equivalent initial and boundary conditions may be speci£ed in the models, ensuring that this is not a source of discrepancy.
- Environmental parameters may be carefully chosen to test the model under various conditions, representative of different regions of the atmosphere.
- Model output may be compared at all times, and is not limited by temporally or spatially sparse measurements. This allows both the diurnal and long-term behaviour of the system to be investigated.
- Uncertainty in kinetic rate data and, indeed, the neglect of chemical or physical processes, would make a comparison with observations more a test of the state of scienti£c knowledge than one of small model de£ciencies.

Here, STORM is compared to the ASAD (A Self-contained Atmospheric chemistry coDe) model (Carver *et al.*, 1997a,b). ASAD has been used extensively for both stratospheric (Knudsen

and Grooß, 2000; Sinnhuber *et al.*, 1999) and tropospheric (Toyota *et al.*, 2001; Wild and Prather, 2000; Stockwell *et al.*, 1999; Fish *et al.*, 1999) problems and model validation (Gil *et al.*, 2000). It can be considered to reproduce the mixing ratios of stratospheric species accurately. All such models are limited, however, by uncertainty in chemical kinetic parameters. For example, Fish and Burton (1997) estimated that ozone depletion in the Arctic could only be calculated with an uncertainty of $\sim$25% and midlatitude ozone depletion with an uncertainty of $\sim$50%. Minor processes and reactions may also be neglected because of limited computer power.

The formulation of ASAD is discussed in section 2.3.1; the comparison experiments are outlined in section 2.3.3; in section 2.3.4 results are presented, systematic differences between the models are discussed and, where possible, the likely reasons are identi£ed.

2.3.1 The ASAD Model

ASAD is a package that solves the system of kinetic rate equations. It is designed to be coupled to other models that calculate advection, emission or deposition. It may also be run as a box model. The model is described in Carver *et al.* (1997a), but a brief description will be given here.

There are a number of numerical integrators supplied with ASAD. IMPACT (IMPlicit Algorithm for Chemical Time-stepping) detailed in Carver and Stott (2000) is a fast implicit scheme based on that described by Stott and Harwood (1993). It allows this use of chemical families and a timestep of about ten minutes. Alternatively the user may choose a quasi-steady state approximation, a standard NAG (Numerical Algorithms Group) routine for stiff systems (D02EAF), or the SVODE (Variable coef£cient stiff ODE) integrator (Brown *et al.*, 1989). Here, the IMPACT integrator was used.

ASAD calculated 35 species using 147 reactions. The kinetic data were taken from both JPL (NASA Jet Propulsion Laboratory) (DeMore *et al.*, 1992) and IUPAC (International Union of Pure and Applied Chemistry, http://www.iupac-kinetic.ch.cam.ac.uk) sources. The photolysis rates are calculated using the scheme described by Lary and Pyle (1992a,b), which is based on Meier *et al.* (1982), Nicolet *et al.* (1982) and Anderson (1983). This scheme uses the rate recommendations of DeMore *et al.* (1992).

2.3.2 Model Differences

Some differences between the models should be anticipated for several reasons. The use of different rate data can alter the partitioning and abundance of all families (Portmann *et al.*, 1999).

ASAD (see section 2.3.1) uses older JPL recommendations than does STORM (see section 2.2.4). Also, the two models differ in which minor species and reactions they include, and ASAD uses the family approximation while STORM calculates all species, other than O_x, explicitly. Differences may also be attributed to the photolysis schemes and assumptions about the overhead ozone column. Chipper£eld (1993) noted that different photolysis schemes prevent chemical models from producing identical results even when the same photochemical data is used.

Finally, it should be noted that the comparison of two chemical models in the same point in space is a particularly stringent test. The rates of some important photolysis reactions change rapidly with height, as indicated in £gure 2.1. These sensitive reactions include the production of odd oxygen,

$$O_2 + h\nu \rightarrow 2O, \tag{2.24}$$

and of $O(^1D)$,

$$O_3 + h\nu \rightarrow O_2 + O(^1D). \tag{2.25}$$

The latter species also in¤uences the production of HO_x through, for example, reaction 2.26,

$$O(^1D) + H_2O \rightarrow 2OH, \tag{2.26}$$

and the oxidation of methane. Consequently, the mixing ratios of many species vary by several orders of magnitude in the space of a few kilometres in the vertical direction (see, for example, Brasseur *et al.*, 1999, Appendix C).

2.3.3 Experimental Details

Following the model inter-comparison of Chipper£eld (1993), a series of 100 day model integrations were performed. Each integration began on Julian day 331 (November 26th). The conditions were chosen to compare the two models in the lower, middle and upper stratosphere in mid-latitudes, and in the polar lower stratosphere. The temperature was held constant during each run, except in the polar case which experienced two polar stratospheric cloud (PSC) events of lower temperatures to simulate a typical Arctic winter. The conditions of each experiment are summarised in table 2.2.

Concentrations of long-lived species, and those of the NO_x, Cl_x, Br_x and O_x families, were matched at the start of each experiment. Species mixing ratios were stored every hour in order to resolve the diurnal cycles.

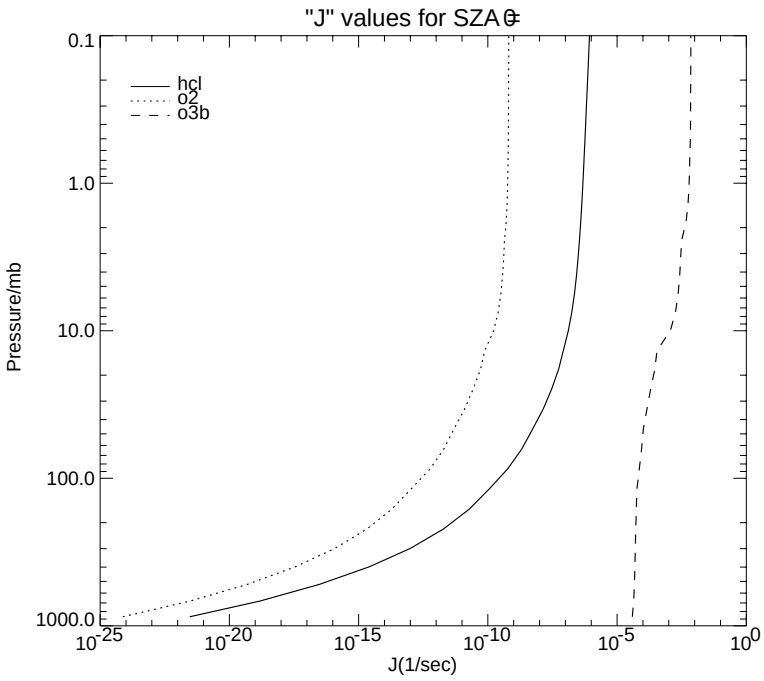

Figure 2.1: *Photolysis rates for* $HCl \rightarrow H + Cl$, $O_2 \rightarrow O + O$, *and* $O_3 \rightarrow O_2 + O(^1D)$ *for a solar zenith angle of 0°, calculated using STORM.*

2.3.4 Results and Discussion

Odd Oxygen

There is good agreement between the two models in each test case. C01 and C03 are regions of net ozone loss and the two models' similar behaviour (£gures 2.2(a) and 2.2(c)) indicates that the rate of gas phase catalytic destruction is roughly the same. C04 is a region of net ozone production. The rate of production is slightly greater in ASAD at the start of the run, but is equal after about 1000 hours (£gure 2.2(d)), indicating similar rates of oxygen photolysis in each model.

Nitrogen Species

The partitioning between NO_x species is similar in all cases (£gure 2.3). Storm generally has less HNO_4 than does ASAD, particularly in the lower stratosphere (£gure 2.3(d)). This is due to the improved representation of long-wavelength photolysis of HNO_4 in STORM.

There is some difference in the $\frac{NO_x}{NO_y}$ ratio in C01, C02 and C04, as indicated by the amount of HNO_3 in £gure 2.4. This is likely due to differences in the rate of photolysis of HNO_3 as there is little difference between the models in C03 which is dominated by gas phase and heterogeneous chemistry, with little photolysis. The JPL recommendations were updated signi£cantly in DeMore

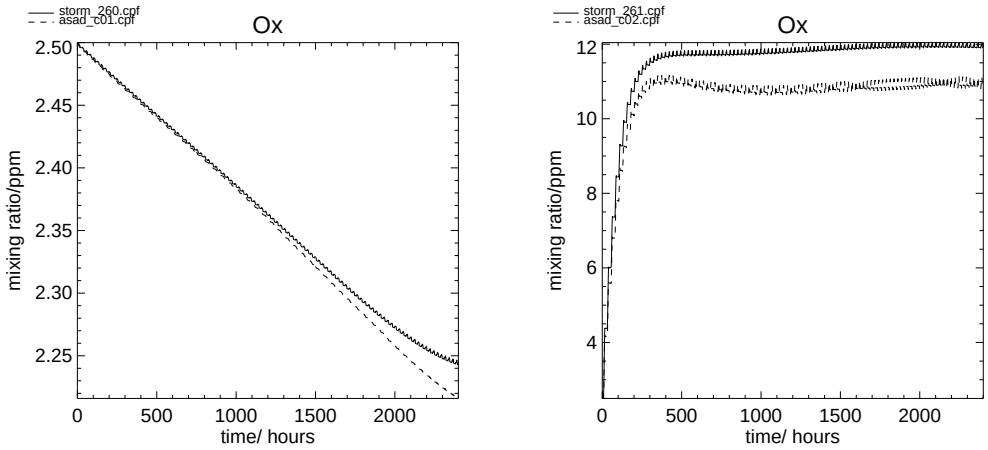

(a) C01 (b) C02

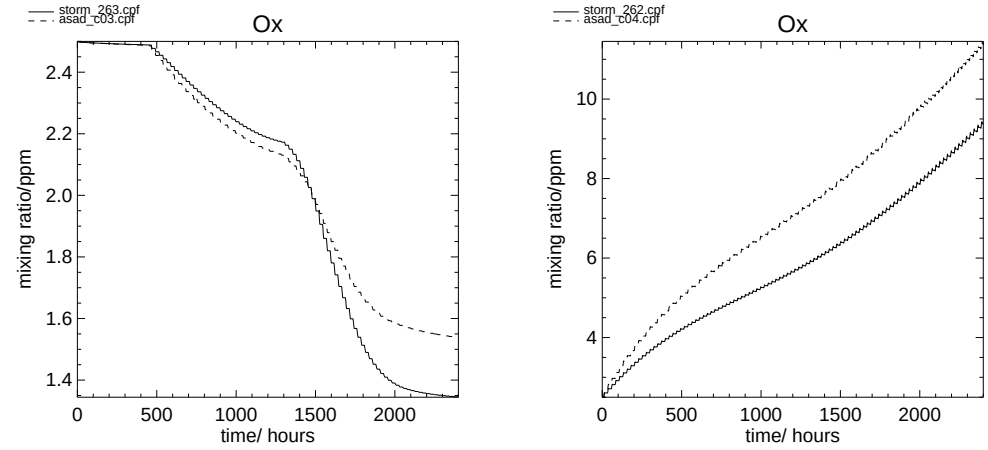

(c) C03 (d) C04

Figure 2.2: *Odd oxygen for ASAD (dashed) and STORM (solid) in a) C01, b) CO2, c) CO3 and d) C04.*

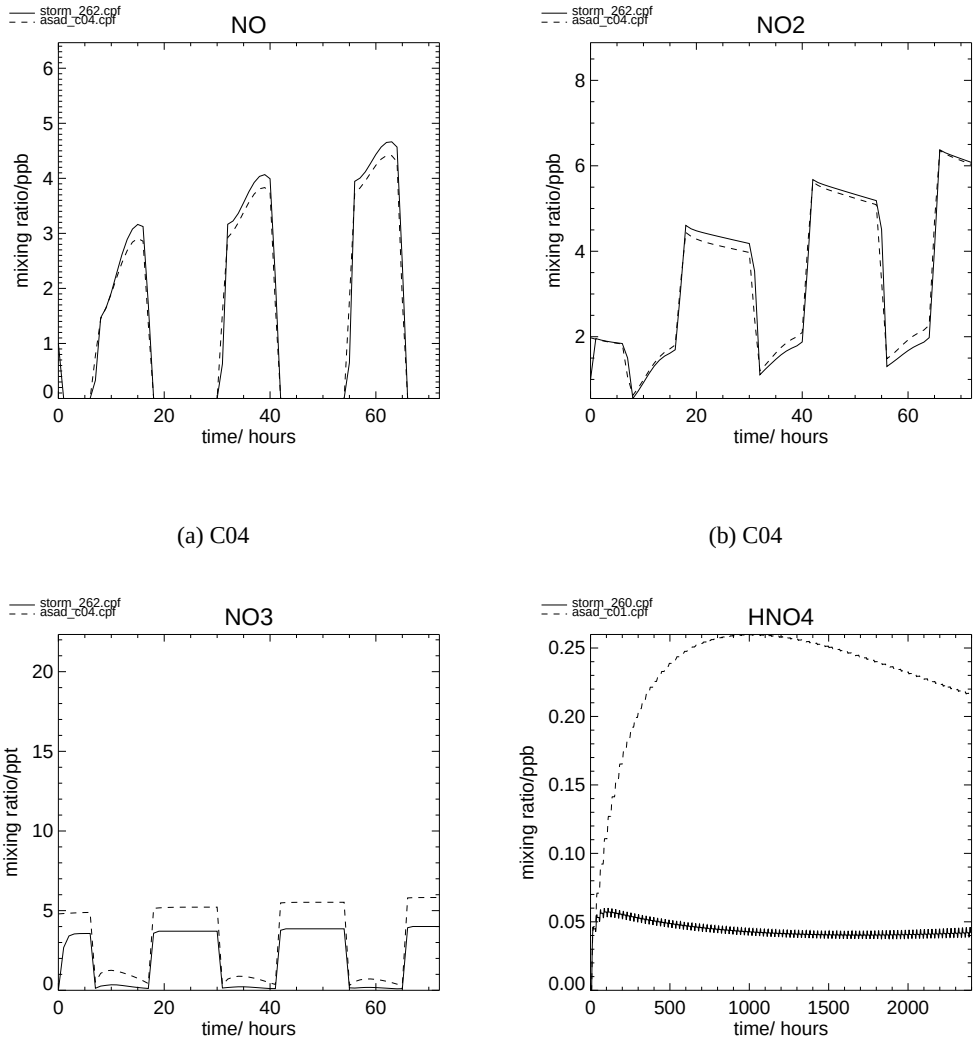

(a) C04

(b) C04

(c) C04

(d) C01

Figure 2.3: NO_x *species in C04 (£rst three days shown to highlight diurnal cycle) and pernitric acid in C01 (full run shown) for ASAD (dashed) and STORM (solid).*

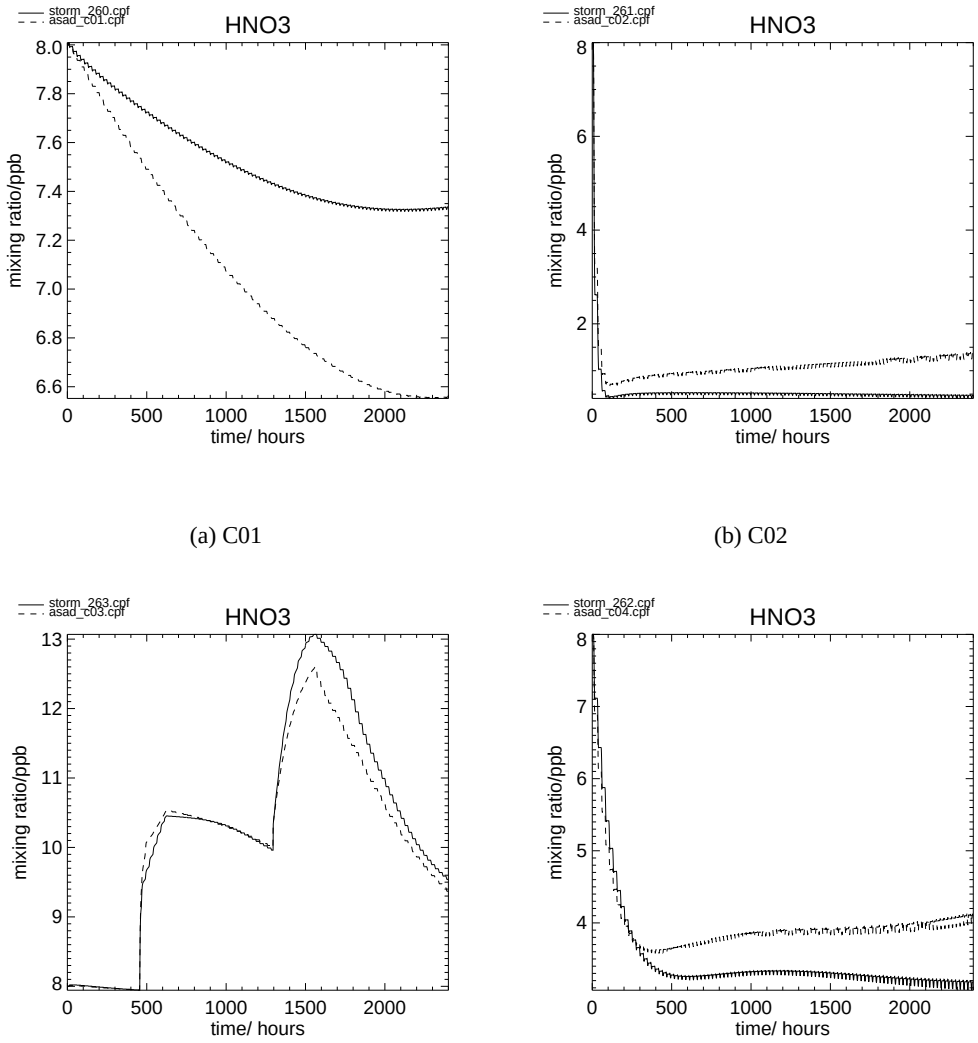

(a) C01

(b) C02

(c) C03

(d) C04

Figure 2.4: *Nitric acid for ASAD (dashed) and STORM (solid) in all test cases.*

experiment	latitude/degrees N	pressure/mb	temperature/K
C01	40	50	210
C02	40	3	240
C03	65	50	*210
C04	40	10	220

Table 2.2: *Conditions used in the comparison experiments. $*$ Experiment C03 included two "PSC events" between days 19-25 and 54-64 when the temperature was reduced to 192K*

et al. (1994) and slightly in DeMore *et al.* (1997), so the STORM code will differ from the Lary and Pyle (1992a,b) code.

Halogens

The behaviour of Cl_x and Br_x is very similar in the two models. As with nitrogen species it is the partitioning between reservoirs and active species that indicates larger discrepancies. Again as with nitrogen, this is due to different rates of photolysis. In the lower stratosphere where the rate of

$$\mathrm{HCl} + h\nu \rightarrow \mathrm{H} + \mathrm{Cl} \tag{2.27}$$

is slow and the rate of oxidation,

$$\mathrm{HCl} + \mathrm{O}(^1\mathrm{D}) \rightarrow \mathrm{OH} + \mathrm{Cl}, \tag{2.28}$$

is limited by the low mixing ratio of $\mathrm{O}(^1\mathrm{D})$, ASAD has just 7% more HCl than does STORM after 100 days (2.5(a)). In the upper stratosphere STORM has nearly 30% more HCl than does ASAD (£gure 2.5(b)). This can be attributed to different photolysis rates of reaction 2.27 as the mixing ratios of $\mathrm{O}(^1\mathrm{D})$ are within a few percent.

The agreement between STORM and ASAD is even better for bromine species than for chlorine (£gure 2.6). As photolysis reactions of bromine species are fast under most conditions the partitioning is controlled mainly by gas phase reactions.

Hydrogen Species

There is good agreement between the models in the HO_x budget (£gure 2.7). The greatest difference is seen in C04, where ASAD produces 30% more HO_x than does STORM. This may be

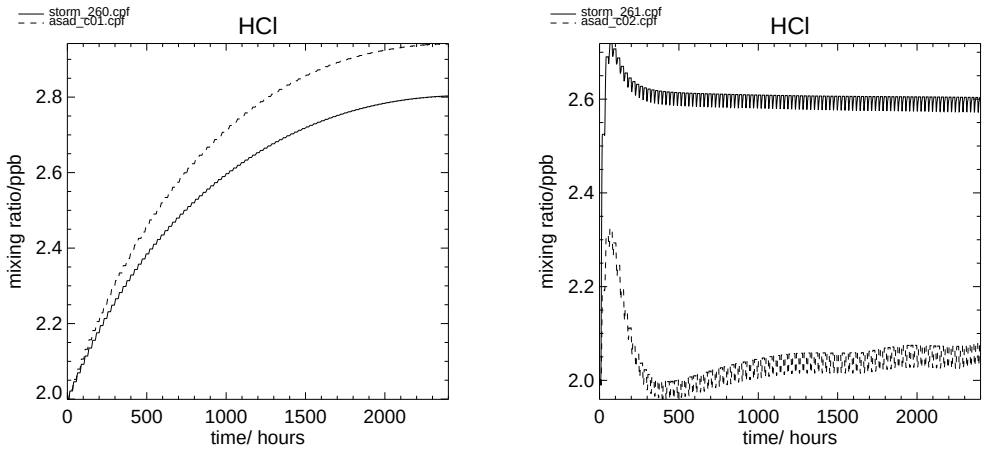

(a) C01 (b) C02

Figure 2.5: HCl *in a) C02 and b) C04 (£rst three days shown to highlight diurnal cycle) for ASAD (dashed) and STORM (solid).*

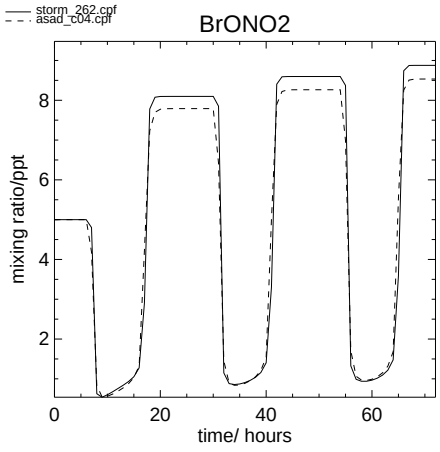

Figure 2.6: $BrONO_2$ *in C04 (£rst three days shown to highlight diurnal cycle) for ASAD (dashed) and STORM (solid).*

caused by the larger $O(^1D)$ mixing ratios in ASAD at this level. Sensitivity tests indicated that a change in altitude of 1-2 kilometres was suf£cient to give agreement in the HO_x budget in the two models in this case.

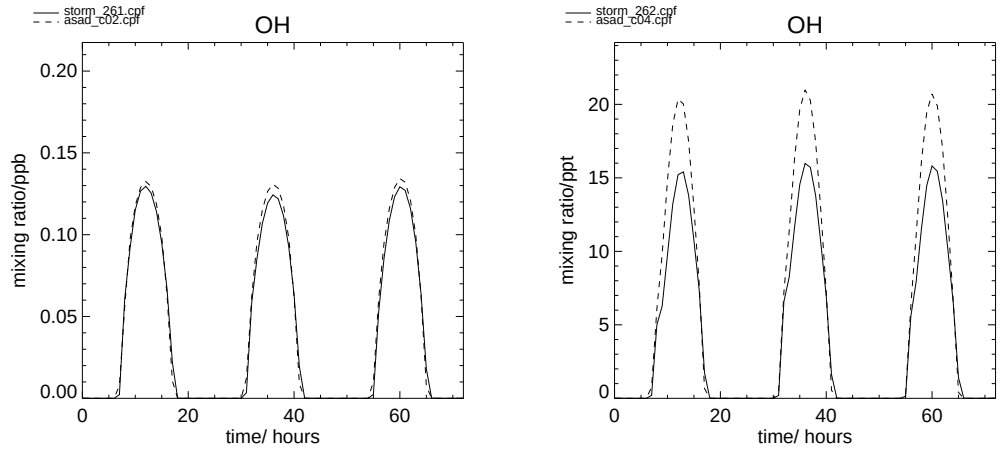

(a) C02 (b) C04

Figure 2.7: HO_x *in a) C02 and b) C04 for ASAD (dashed) and STORM (solid).*

Heterogeneous Reactions

As ASAD does not account for heterogeneous reactions on sulphate aerosol, C03 is the only experiment that allows surface reactions to be compared. Both models use similar *equilibrium* parameterisations for PSCs but include different reactions. STORM uses updated parameterisations for reactions 2.29 and 2.30 from Sander *et al.* (2000).

$$N_2O_5 + H_2O \rightarrow 2HNO_3 \tag{2.29}$$

$$BrONO_2 + H_2O \rightarrow HOBr + HNO_3. \tag{2.30}$$

Although these differences lead to some disagreement for minor species such as HOBr (£gure 2.8), ozone is generally insensitive to this. The most signi£cant reactions, such as

$$N_2O_5 + H_2O \rightarrow 2HNO_3 \tag{2.31}$$

$$ClONO_2 + H_2O \rightarrow HOCl + HNO_3 \tag{2.32}$$

$$BrONO_2 + H_2O \rightarrow HOBr + HNO_3 \tag{2.33}$$

$$ClONO_2 + HCl \rightarrow Cl_2 + HNO_3 \tag{2.34}$$

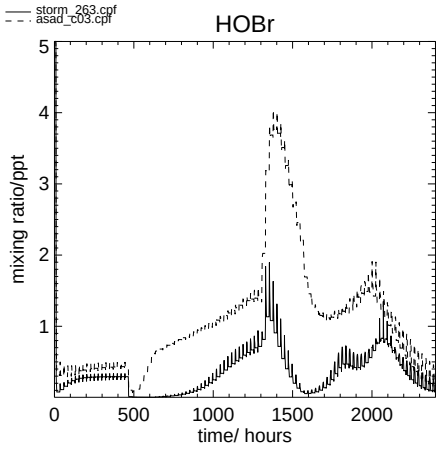

Figure 2.8: HOBr *in C03 for ASAD (dashed) and STORM (solid).*

are fast enough that almost all HCl and $ClONO_2$ are removed as soon as the temperature falls below the PSC formation threshold. Some small differences can be seen, however (£gure 2.9). For example, STORM destroys slightly more $ClONO_2$ and slightly less HCl than does ASAD. Overall though, the models destroy these key species at a similar rate.

2.4 Comparison with Observational Data

In order to con£rm that the model simulates realistic chemistry, STORM was also compared to observational data. Data from the BLISS (Balloon-Borne Laser In-Situ Sensor) instrument (Webster *et al.*, 1990) were used to provide a diurnal cycle of NO_2. Following the method Webster *et al.* (1990), the model was initialised at 10mb on 13th September at 30°N using measured values of O_3 and HNO_3.

The results from the comparison are shown in £gure 2.10. The agreement with the observations is excellent, indicating that STORM is simulating a realistic chemical system.

2.5 Chapter Summary

In this chapter the ordinary differential equations that represent the photochemical system were described and methods of solving them were discussed. A photochemical box model based on that described by Fish and Burton (1997), using the latest laboratory rate data, has been developed.

This model has been compared to a well-established model, ASAD. The STORM and ASAD chemical box models are in good agreement in both regions of ozone production and ozone loss. The gas phase and heterogeneous reactions on PSCs produce very similar results. Unfortunately ASAD does not allow reactions on sulphate to be assessed. Greater differences are seen in some photolysis reactions and this is attributed to the sensitivity of these reactions to the calculated extinction of solar radiation.

A further experiment has been performed to compare the box model with observational data. The BLISS diode laser spectrometer were used to compare the diurnal cycle of NO_2. STORM produced a diurnal cycle in excellent agreement with the observations.

It is concluded that STORM compares well to ASAD and is a suitable tool to generate a fast parameterisation of stratospheric chemistry.

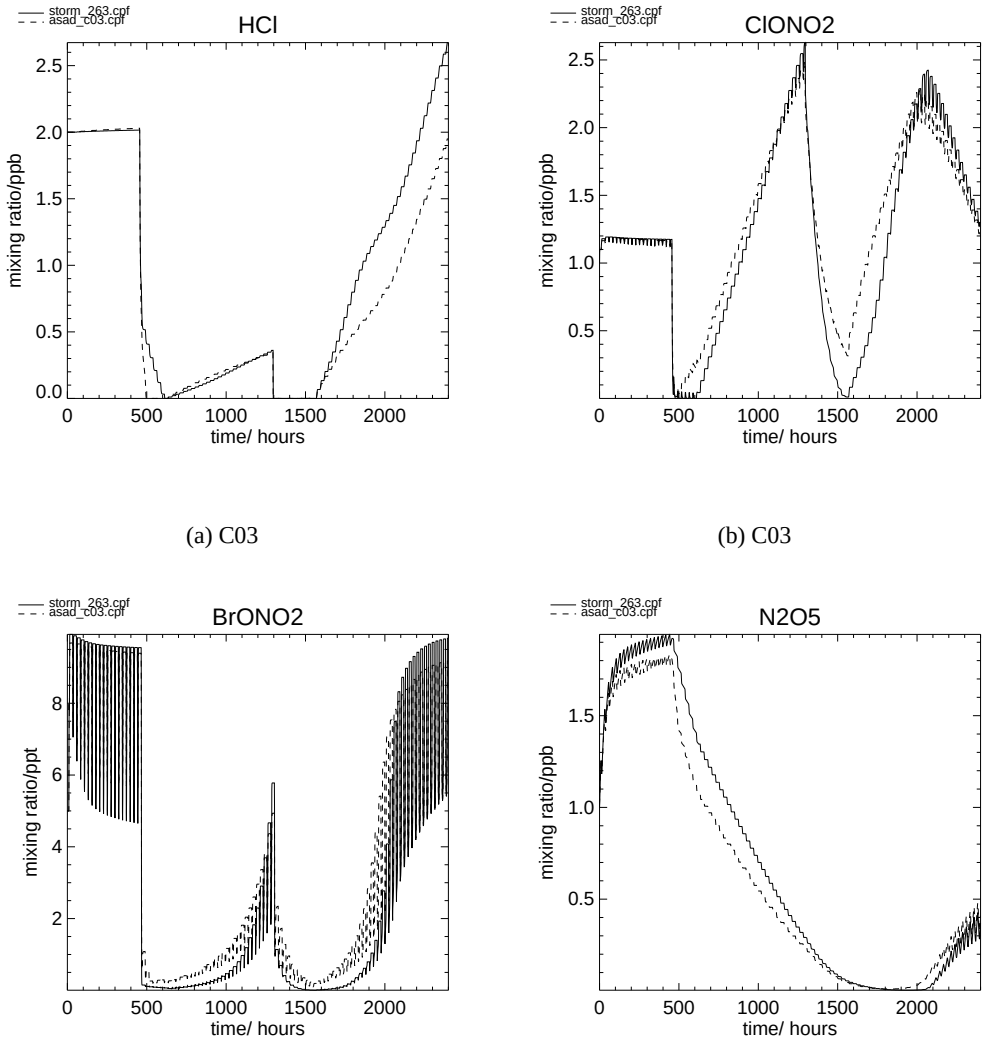

(a) C03

(b) C03

(c) C03

(d) C03

Figure 2.9: *Reservoir species in C03 for ASAD (dashed) and STORM (solid).*

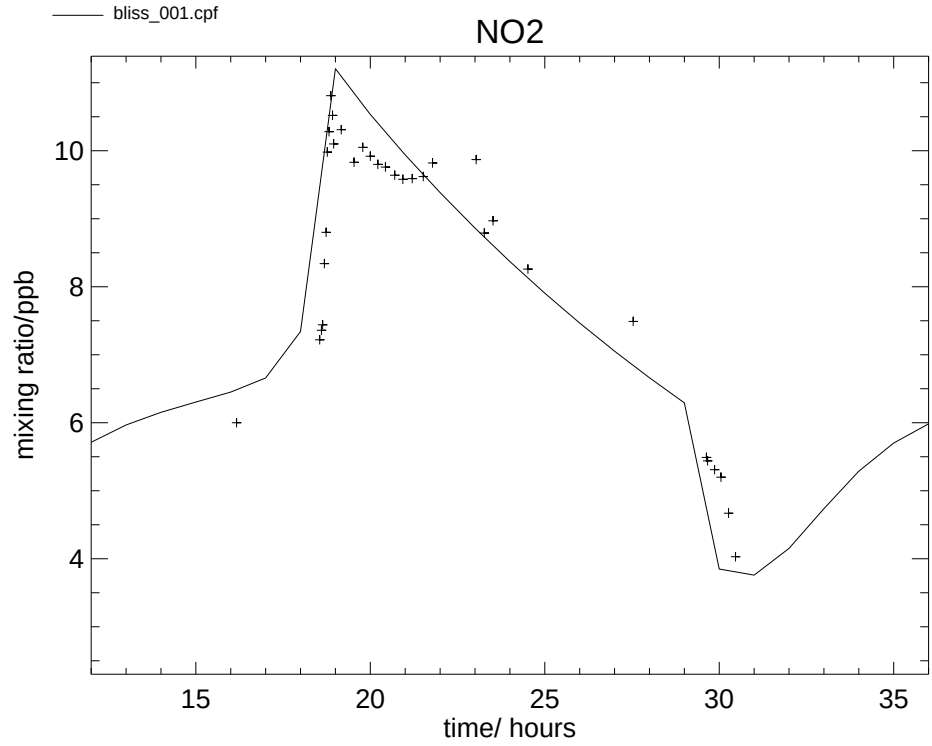

Figure 2.10: Comparison of BLISS September 1998 ¤ight measurements at 30 km of [NO_2] against time with model predictions of [NO_2]

Annex to Chapter 2

List of Reactions Included in STORM						
O	$+$	O_3	$\rightarrow$	O_2	$+$	O_2
$O(1d)$	$+$	O_2	$\rightarrow$	O	$+$	O_2
$O(1d)$	$+$	H_2	$\rightarrow$	OH	$+$	H
O	$+$	H_2	$\rightarrow$	OH	$+$	H
$O(1d)$	$+$	N_2	$\rightarrow$	O	$+$	
$O(1d)$	$+$	O_3	$\rightarrow$	O_2	$+$	O_2
$O(1d)$	$+$	O_3	$\rightarrow$	O	$+$	O
$O(1d)$	$+$	H_2O	$\rightarrow$	OH	$+$	OH
$O(1d)$	$+$	CH_4	$\rightarrow$	CH_3O	$+$	H
$O(1d)$	$+$	CH_4	$\rightarrow$	CH_3O_2	$+$	H
$O(1d)$	$+$	CH_4	$\rightarrow$	$HCHO$	$+$	H_2
$O(1d)$	$+$	HCl	$\rightarrow$	O	$+$	HCl
$O(1d)$	$+$	HCl	$\rightarrow$	H	$+$	ClO
$O(1d)$	$+$	HCl	$\rightarrow$	OH	$+$	Cl
$O(1d)$	$+$	Cl_2	$\rightarrow$	O	$+$	Cl_2
$O(1d)$	$+$	Cl_2	$\rightarrow$	ClO	$+$	Cl
$O(1d)$	$+$	N_2O	$\rightarrow$	N_2	$+$	O_2
$O(1d)$	$+$	N_2O	$\rightarrow$	NO	$+$	NO
NO	$+$	O_3	$\rightarrow$	NO_2	$+$	O_2
NO_2	$+$	O_3	$\rightarrow$	NO_3	$+$	O_2
O	$+$	NO_2	$\rightarrow$	NO	$+$	O_2
NO_3	$+$	O	$\rightarrow$	NO_2	$+$	O_2
NO	$+$	NO_3	$\rightarrow$	NO_2	$+$	NO_2
NO_3	$+$	NO_3	$\rightarrow$	NO_2	$+$	NO_2

(continued)							
ClO	+	O	→	Cl	+	O_2	
Cl	+	NO_3	→	ClO	+	NO_2	
ClO	+	NO	→	NO_2	+	Cl	
Cl	+	O_3	→	ClO	+	O_2	
Cl	+	CH_4	→	HCl	+	CH_3O_2	
Cl	+	$HCHO$	→	HCl	+	HO_2	+ CO
O	+	OH	→	H	+	O_2	
O	+	HO_2	→	OH	+	O_2	
H	+	O_3	→	OH	+	O_2	
H	+	HO_2	→	OH	+	OH	
H	+	HO_2	→	H_2	+	O_2	
OH	+	O_3	→	HO_2	+	O_2	
OH	+	H_2	→	H_2O	+	H	
OH	+	OH	→	H_2O	+	O	
OH	+	HO_2	→	H_2O	+	O_2	
OH	+	$HOCl$	→	ClO	+	H_2O	
OH	+	$OClO$	→	$HOCl$	+	O_2	
OH	+	CO	→	HO_2	+	O_2	
OH	+	CH_4	→	H_2O	+	CH_3O_2	
OH	+	$HCHO$	→	H_2O	+	HO_2	+ CO
NO_2	+	CH_3O	→	$HCHO$	+	$HONO$	
CH_3O	+	O_2	→	$HCHO$	+	HO_2	
CH_3O_2	+	NO	→	CH_3O	+	NO_2	
HO_2	+	O_3	→	OH	+	O_2	
H	+	NO_2	→	OH	+	NO	
HO_2	+	NO	→	NO_2	+	OH	
O	+	HCl	→	Cl	+	OH	
OH	+	ClO	→	Cl	+	HO_2	
OH	+	ClO	→	HCl	+	O_2	
OH	+	HCl	→	Cl	+	H_2O	
HO_2	+	Cl	→	HCl	+	O_2	

(continued)							
HO_2	+	Cl	→	OH	+	ClO	
OH	+	HNO_3	→	H_2O	+	NO_3	
O	+	H_2O_2	→	OH	+	HO_2	
OH	+	OH	→	H_2O	+	O	
OH	+	H_2O_2	→	H_2O	+	HO_2	
OH	+	$ClONO_2$	→	HNO_3	+	ClO	
HO_2	+	HO_2	→	H_2O_2	+	O_2	
HO_2	+	HO_2	→	H_2O_2	+	O_2	
OH	+	$HONO$	→	H_2O	+	NO_2	
O	+	$OClO$	→	ClO	+	O_2	
O	+	$HOCl$	→	ClO	+	OH	
O	+	$ClONO_2$	→	ClO	+	NO_3	
HO_2	+	ClO	→	$HOCl$	+	O_2	
NO	+	$OClO$	→	NO_2	+	ClO	
Cl	+	H_2	→	HCl	+	H	
Cl	+	H_2O_2	→	HCl	+	HO_2	
Cl	+	$OClO$	→	ClO	+	ClO	
Cl	+	$ClOO$	→	Cl	+	Cl	
Cl	+	$ClOO$	→	ClO	+	ClO	
ClO	+	ClO	→	Cl_2	+	O_2	
ClO	+	ClO	→	$OClO$	+	Cl	
ClO	+	ClO	→	$ClOO$	+	Cl	
Cl	+	$ClONO_2$	→	Cl_2	+	NO_3	
Cl	+	Cl_2O_2	→	Cl	+	Cl	+ Cl
HNO_4	+	O	→	NO_3	+	HO_2	
OH	+	HNO_4	→	H_2O	+	NO_2	
O	+	BrO	→	Br	+	O_2	
O	+	$HOBr$	→	OH	+	BrO	
Br	+	HO_2	→	HBr	+	O_2	
BrO	+	OH	→	Br	+	HO_2	
HO_2	+	BrO	→	$HOBr$	+	O_2	

(continued)						
BrO	+	NO	$\rightarrow$	Br	+	NO_2
BrO	+	ClO	$\rightarrow$	Br	+	$OClO$
BrO	+	ClO	$\rightarrow$	Br	+	$ClOO$
BrO	+	ClO	$\rightarrow$	$BrCl$	+	O_2
$BrCl$	+	O	$\rightarrow$	BrO	+	Cl
Br	+	Cl_2O_2	$\rightarrow$	$BrCl$	+	Cl
$O(1d)$	+	HBr	$\rightarrow$	OH	+	Br
OH	+	HBr	$\rightarrow$	H_2O	+	Br
O_3	+	Br	$\rightarrow$	BrO	+	O_2
N_2O_5			$\stackrel{M}{\rightarrow}$	NO_3	+	NO_2
Cl_2O_2			$\stackrel{M}{\rightarrow}$	ClO	+	ClO
$ClOO$			$\stackrel{M}{\rightarrow}$	Cl	+	O_2
HNO_4			$\stackrel{M}{\rightarrow}$	HO_2	+	NO_2
O	+	O_2	$\rightarrow$	O_3		
$O1D$	+	N_2	$\rightarrow$	N_2O		
H	+	O_2	$\rightarrow$	HO_2		
OH	+	OH	$\rightarrow$	H_2O_2		
O	+	NO	$\rightarrow$	NO_2		
O	+	NO_2	$\rightarrow$	NO_3		
OH	+	NO	$\rightarrow$	$HONO$		
OH	+	NO_2	$\rightarrow$	HNO_3		
NO_3	+	NO_2	$\rightarrow$	N_2O_5		
ClO	+	ClO	$\rightarrow$	Cl_2O_2		
Cl	+	O_2	$\rightarrow$	$ClOO$		
ClO	+	NO_2	$\rightarrow$	$ClONO_2$		
HO_2	+	NO_2	$\rightarrow$	HNO_4		
BrO	+	NO_2	$\rightarrow$	$BrONO_2$		
N_2O_5	+	H_2O	$\stackrel{surface}{\longrightarrow}$	HNO_3	+	HNO_3
N_2O_5	+	H_2O	$\stackrel{surface}{\longrightarrow}$	HNO_3	+	HNO_3
N_2O_5	+	H_2O	$\stackrel{surface}{\longrightarrow}$	HNO_3	+	HNO_3
N_2O_5	+	H_2O	$\stackrel{surface}{\longrightarrow}$	HNO_3	+	HNO_3

(continued)

$HOCl$	$+$	HCl	$\xrightarrow{surface}$	Cl_2	$+$	H_2O
$HOCl$	$+$	HCl	$\xrightarrow{surface}$	Cl_2	$+$	H_2O
$HOCl$	$+$	HCl	$\xrightarrow{surface}$	Cl_2	$+$	H_2O
$ClONO_2$	$+$	H_2O	$\xrightarrow{surface}$	$HOCl$	$+$	HNO_3
$ClONO_2$	$+$	H_2O	$\xrightarrow{surface}$	$HOCl$	$+$	HNO_3
$ClONO_2$	$+$	H_2O	$\xrightarrow{surface}$	$HOCl$	$+$	HNO_3
$ClONO_2$	$+$	HCl	$\xrightarrow{surface}$	Cl_2	$+$	HNO_3
$ClONO_2$	$+$	HCl	$\xrightarrow{surface}$	Cl_2	$+$	HNO_3
$ClONO_2$	$+$	HCl	$\xrightarrow{surface}$	HNO_3	$+$	Cl_2
$HOBr$	$+$	HCl	$\xrightarrow{surface}$	$BrCl$	$+$	H_2O
$HOBr$	$+$	HCl	$\xrightarrow{surface}$	$BrCl$	$+$	H_2O
$BrONO_2$	$+$	H_2O	$\xrightarrow{surface}$	$HOBr$	$+$	HNO_3
$BrONO_2$	$+$	H_2O	$\xrightarrow{surface}$	$HOBr$	$+$	HNO_3
$ClONO_2$	$+$	HBr	$\xrightarrow{surface}$	$BrCl$	$+$	HNO_3
$ClONO_2$	$+$	HBr	$\xrightarrow{surface}$	$BrCl$	$+$	HNO_3

CHAPTER THREE

FASTOC - A Fully Equivalent Operational Model

In chapter 1 it was stated that three-dimensional coupled chemistry-general circulation models were needed to make predictions about the future development of the ozone layer. A number of models were discussed and it was noted that the number and length of integrations using these models were limited by their computational expense. This chapter concerns alternatives to these complex chemical schemes and the development of a fast chemical model, FASTOC (FAst STratospheric Ozone Chemistry).

Section 3.1 explores a range of fast parameterisations for atmospheric chemistry and the Fully Equivalent Operational Model (FEOM) technique is presented in section 3.2. This technique is implemented in section 3.3 to generate the FASTOC model. This model is compared to that of Shorter *et al.* (1999) in section 3.4 and is validated in section 3.5. A summary is given in section 3.6. In chapter 5 of this thesis, FASTOC is coupled to the Reading Intermediate General Circulation Model, and used for perform some climate change experiments.

3.1 Fast Chemical Models

Although many relatively fast chemical models have been developed, they are generally still too computationally expensive to perform many long integrations in a GCM (see section 1.4.5). Other, more parameterised schemes, are also discussed in section 1.4.5. Whilst these allow longer integrations they possess other disadvantages which limit their applicability. Another possibility is to replace the ordinary differential equation (ODE) solver with an inexpensive parameterisation that accurately represents the system. The basis of these *input-output* models is that each output

variable can be described as a function of a number of known input variables:

$$g(x) = g(x_1, x_2, \ldots, x_n). \tag{3.1}$$

These functions may, therefore, be "learned" by sampling the system. For example, a number of simulations would be performed using an ODE solver to map input variables, such as temperature and pressure, to values of the output variables, such as $\chi_{\mathrm{O_x}}$. The functions must then be represented in some easy way that allows the calculation of output variables. There are a number of different methods for creating these surrogate models.

Blasco *et al.* (2000) and Chen *et al.* (2000) describe the use of arti£cial neural networks in representing large chemical mechanisms. They report that this may be a suitable method for multidimensional simulations. Spivakovsky *et al.* (1990) used a series of polynomials to parameterise the chemistry of tropospheric OH. Turanyi (1994) extended this approach using orthonormal polynomials. Bell *et al.* (2000) describe a polynomial representation of the chemistry of a turbulent ¤ame, where the functions are generated dynamically during the simulation. This reduces the computational effort if regions of the input-space are not sampled. Lowe and Tomlin (2000a,b) also use a set of polynomials to represent chemical systems. They also simplify the system by reducing its order. The chemical system is viewed as a multi-dimensional phase space, and a set of conditions as a point in that space. As the fast processes reach equilibrium all trajectories in the chemical phase space rapidly converge (Sportisse and Djouad, 2000), and the system can be represented as a lower dimension manifold.

The limitation of these input-output models is the effort required to sample the input-space. This cost, that is the number of points in the input space that need to be evaluated, C, increases exponentially with the number of input variables, n. That is written

$$C = s^n \tag{3.2}$$

where s is the number of sample points taken for each variable. This has been referred to as the "curse of dimensionality" by Rabitz and Aliş (1999). This cost makes many of these methods unsuitable for high order systems if computational ef£ciency is required. Of the methods described above only that of Lowe and Tomlin (2000a,b) attempts to reduce the order of the system. A conceptually simpler method for representing high order systems has been proposed by Rabitz

et al. (1999) (see also Rabitz and Aliş (1999) and Aliş and Rabitz (2001)). This involves generating a fully equivalent operational model (FEOM) using a high dimensional model representation (HDMR).

3.2 Fully Equivalent Operational Models

The so-called cut-HDMR presented by Rabitz *et al.* (1999) decomposes the function in equation 3.1 into a sum of correlated functions of increasing order as in equation 3.3.

$$\begin{aligned} g(x_1, x_2, \ldots, x_n) = \quad f_0 \quad & + \sum_{i=1}^{n} f_i(x_i) \\ & + \sum_{1 \le i < j \le n} f_{ij}(x_i, x_j) \\ & + \ldots \\ & + f_{1,2,\ldots,n}(x_1, x_2, \ldots, x_n) \end{aligned} \tag{3.3}$$

The f_0 term represents a zeroth order effect which is constant throughout the input-space. It is evaluated at an arbitrary reference point, or cut-centre, y. The second term, $f_i(x_i)$ represents the effect of each variable acting independently. It is evaluated along the axis of x_i through y. The $f_{ij}(x_i, x_j)$ term represents pairs of variables acting cooperatively and is evaluated on a plane through y. Further terms describe higher order correlations between variables, with the £nal term accounting for any residual effect. Each term is an arbitrary function and is generally non-linear. The construction of the HDMR is shown graphically in £gure 3.1. The functions are de£ned so as to remove their dependence on lower order functions. This ensures that each function makes a unique contribution to $f(x)$:

$$f_0 = f(y) \tag{3.4}$$

$$f_i = f^i(x_i) - f_0 \tag{3.5}$$

$$f_{ij} = f^{ij}(x_i, x_j) - f^i(x_i) - f^j(x_j) - f_0 \tag{3.6}$$

where f_i means that all variables except i are given the same value to that at y.

The construction of the HDMR means that an exact solution for $f(x)$ is obtained at any level of truncation of equation 3.3. It has been shown that for most physical systems only low-order terms are signi£cant (Shorter *et al.*, 1999, 2000; Wang *et al.*, 1999) and higher order terms

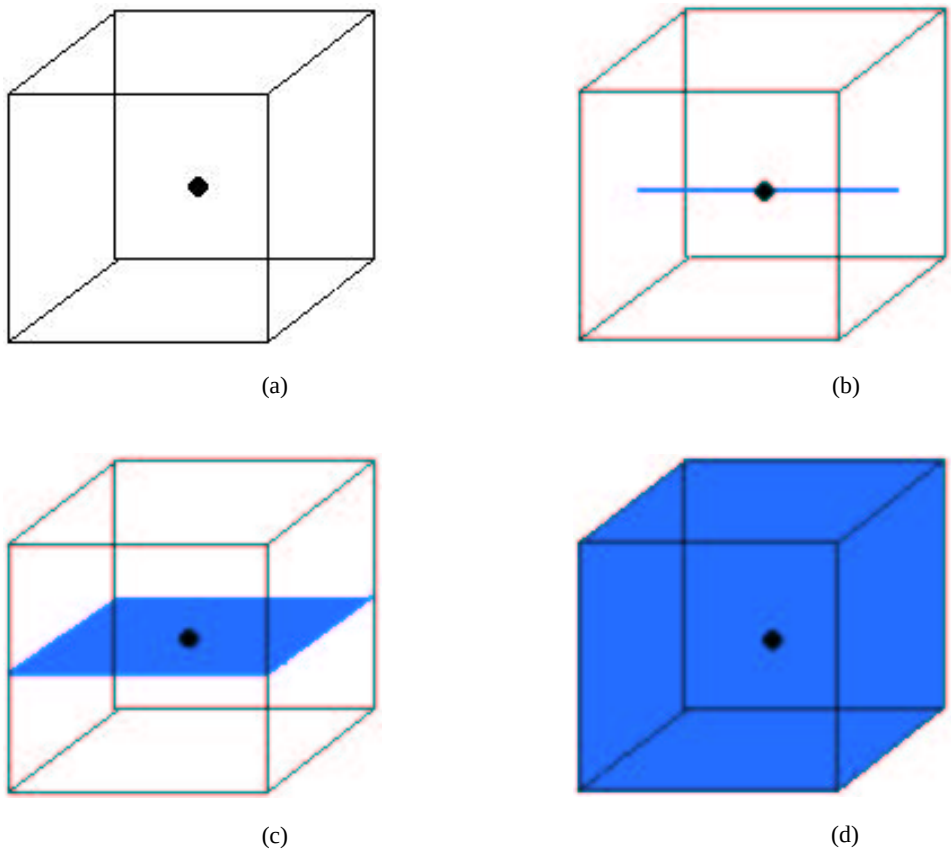

Figure 3.1: *These cubes represent an HDMR system with three input variables. (a) shows the reference point, y; (b) shows a £rst order function as a line cutting through y; (c) shows a second order function as a plane cutting through y; (d) shows a third order function which allows the whole cube to be sampled.*

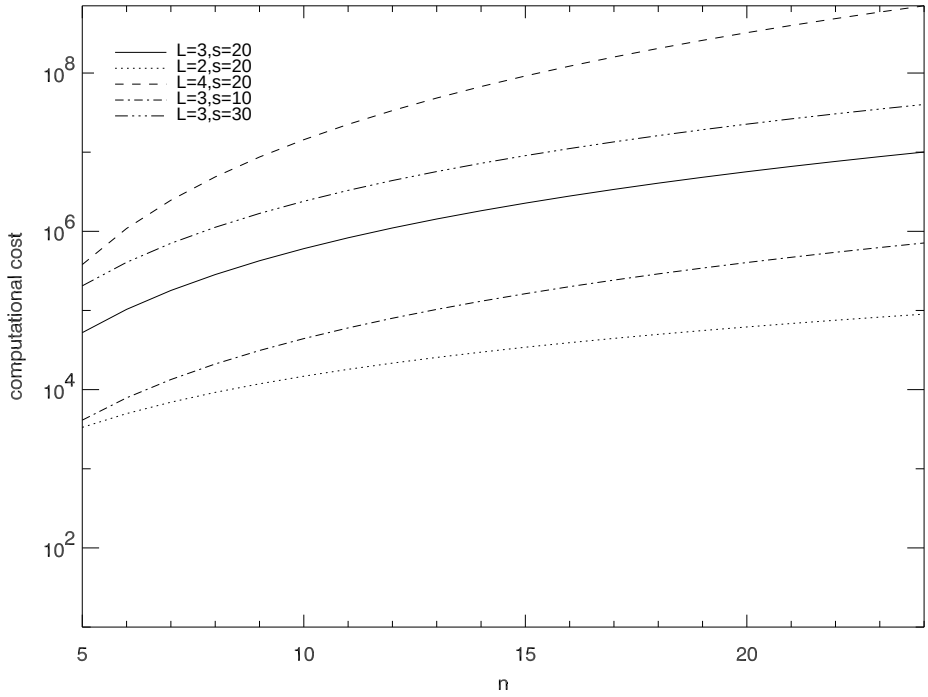

Figure 3.2: *Computational cost, calculated using equation 3.7, of generating FEOMs of various values of n, L nd s*

may be neglected with only small error. Typically, second or third order terms have been found to be adequate. The choice of y should become less important as enough terms are included to give convergence.

The computational cost of generating a FEOM is given by

$$C_{HDMR} = \sum_{i=0}^{L} \frac{n!}{(n-i)!i!}(s-1)^i. \tag{3.7}$$

where L is the highest order of signi£cant correlation (Rabitz *et al.*, 1999). Calculated values of C for various values of n, L and s are shown in £gure 3.2. If $L << n$ then equation 3.7 is dominated by the largest term. If $s >> 1$ then $C_{HMDR} \approx \frac{(sn)^L}{L!}$. The cost scales polynomically with n, rather than the exponential dependence traditionally found (equation 3.2). A comparison with traditional input-output models is shown graphically in £gure 3.3.

The HDMR may be used to construct a Fully Equivalent Operational Model (FEOM). This uses the functions as low dimensional look-up tables that can be ef£ciently interpolated.

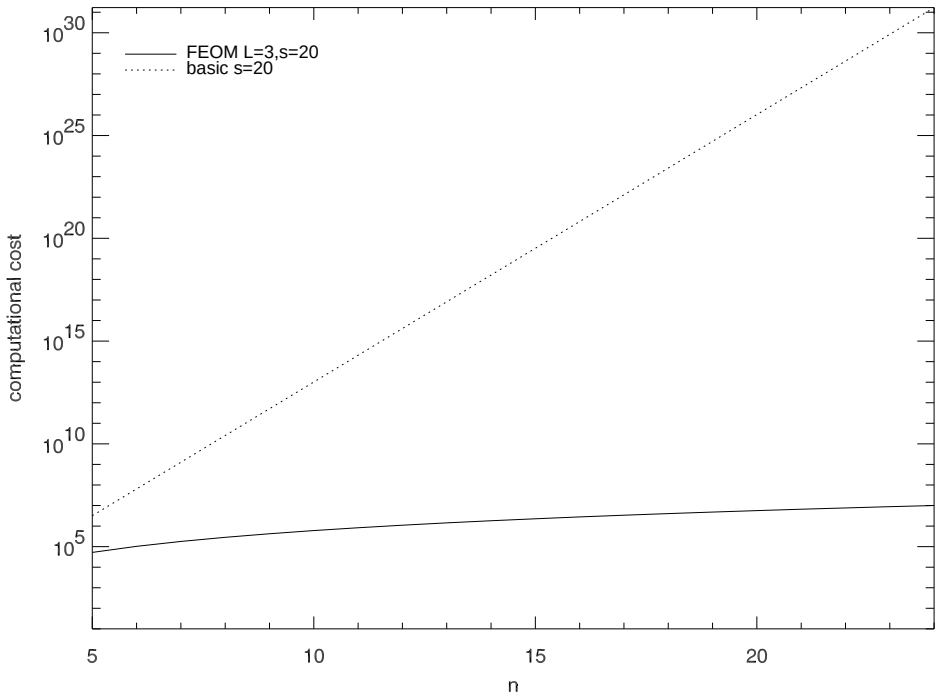

Figure 3.3: *Computational cost of generating traditional input-output models (equation 3.2) and FEOMs of the same dimension (equation 3.7)*

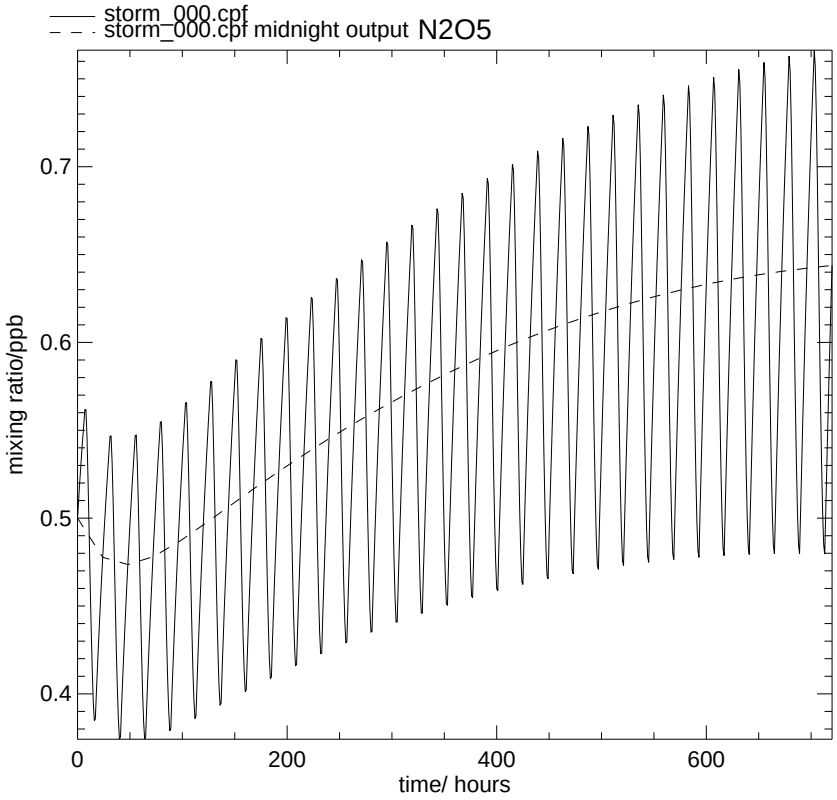

Figure 3.4: N_2O_5 *STORM-NH output hourly (solid line) and daily at midnight (dashed line) for 30 days from 1st January at 45°N at 50mb. The long term development is not affected by the diurnal variation, but is forced by environmental parameters which change over longer timescales.*

3.2.1 Choice of Variables

Rabitz and Aliş (1999) suggest that, in most cases, no special effort is required to achieve low-order convergence. They note, however, that it is desirable to choose input variables that have clear distinct roles. This criterion helps to ensure that high order correlations are weak and that the higher order terms in the expansion are small. The analysis of the system is simpli£ed if variables are physical quantities, or convenient transformations of those values.

3.3 FASTOC

A Fully Equivalent Operational Model has been generated for the STORM-NH stratospheric chemical box model (see section 2.2). The construction of the FASTOC model will be described here.

Although the stratospheric chemical system is a stiff one (see section 2.1), the long-term

development of the system is forced by longer-lived species and environmental parameters such as temperature and solar insolation. Shorter-lived species rapidly achieve equilibrium with these longer timescale variables. This is consistent with the the £ndings of Sun *et al.* (1994), Sportisse and Djouad (2000) and Lowe and Tomlin (2000a,b). This concept is illustrated in £gure 3.4. If, as in this work, the focus is on a relatively long-lived species, such as odd oxygen, a long model timestep can be used if the restriction of using an ODE solver is lifted. Following the approach of Shorter *et al.* (1999) a 24 hour timestep was chosen for this model. It must be stressed that this is not the same as a traditional ODE solver with a long timestep. The latter method would assume that rate constants were unchanged throughout the timestep, perhaps as a diurnal average. Even if numerical stability can be achieved, this clearly introduces errors, particularly for photolysis reactions (Smith, 1995). Using the FEOM method, a full diurnal cycle is included implicity in each 24 hour timestep. This is achieved by calculating each point in the FEOM functions by running the box model for a full day using appropriate initial and boundary conditions. The output mixing ratios are, therefore, midnight values rather than diurnal averages.

It was found that second order terms were insuf£cient to achieve acceptable results over a large part of the stratosphere. As the number of calculated species, and therefore also the number of input variables, was kept small, the cost of including third order terms was not prohibitive.

In order to reproduce the chemical system accurately, input variables that describe all the important processes must be included. Gas phase reactions depend on temperature and pressure, so clearly these must be used. The inclusion of heterogeneous reactions requires the use of sulphate surface area as an input. The representation of photolysis, however, is problematic. The choice of parameters that describe these reactions is now discussed further.

3.3.1 Photolysis Parameters

A 24 hour timestep in the FASTOC model means that there must be a function, or combination of functions, that describe the effect of daily integrated photolysis. The choice of this function is not immediately obvious. To begin, the traditional way of calculating photolysis rates is considered. The instantaneous rate of a photolysis reaction is given by

$$J = \int_{\lambda} \sigma(\lambda)\phi_{diss}(\lambda)q(\lambda)d\lambda, \tag{3.8}$$

where σ is the absorption cross section of the molecule, ϕ_{diss} is the quantum yield* for dissociation, and q is the solar ¤ux. The solar ¤ux depends on the attenuation by ozone, oxygen and aerosol. σ and ϕ_{diss} are constant, so it is the integral of q over all λ and daylight hours that must be calculated. Functions for pressure and overhead ozone column provide much of the information, but the diurnal cycle remains unknown. A number of different functions were tested for this purpose.

Solar Insolation

The solar insolation at the top of the atmosphere, Q, is the integral of $\cos\theta$ over daylight hours, where θ is the solar zenith angle (Liou, 1980, see, for example,). It is given by

$$Q = S(\sin\phi\sin\delta\frac{H}{2} + \cos\phi\cos\delta\frac{H}{2}), \tag{3.9}$$

where S is approximately constant and H is the day length in radians. This is a reasonable function as it gives information about the total energy entering the system to drive photolysis. It increases with increasing day length and with decreasing solar zenith angle, which is desirable. It does not, however, discriminate between these variables. Similar values of Q are found at the summer pole and in the tropics, but for different reasons. Some reactions, such as the photolysis of O_2,

$$O_2 + h\upsilon \rightarrow O + O, \tag{3.10}$$

are fast in the tropics but very slow at the large solar zenith angles found at the poles. These reactions will, therefore, be poorly represented. Clearly in a model where ozone is the most important species the production of odd oxygen must be well represented.

Day Length

In the case of solstice conditions the day length in monotonic from pole to pole and can give a good estimate of the photolysis at each latitude. The system can then be evaluated along this line determining the response as a function of day length. The results are, however, poor during equinox conditions when all latitudes have a day length of 12 hours. In this case photolysis is calculated to be equal at all latitudes whereas in fact the solar zenith angle is also important for reactions such as 3.10 . At high latitudes this results in an over-production of ozone at equinox.

*The quantum yield of a process is the fraction of molecules that undergo that process for each photon absorbed.

Latitude and Day of Year

For a given pressure level and overhead ozone column the photolysis rate depends on the solar zenith angle, θ. This is usually calculated using the expression

$$\cos(\theta) = \sin(\phi)\sin(\delta) + \cos(\phi)\cos(\delta)\cos(t_h), \tag{3.11}$$

where ϕ is the latitude, δ is the solar declination angle and t_h is the local hour angle[†]. The declination angle is found by

$$\delta(radians) = \cos\left[\frac{2\pi}{360}(d - 172)\right] \tag{3.12}$$

for day, d, of a 360 day model year[‡].

The information required to capture a unique diurnal cycle is, therefore, contained in the latitude and day of year. In theory this means that all the necessary information is available and correct at all latitudes and times of year. It was noted in section 3.2.1, however, that variables with clear and distinct roles should be chosen to ensure low order convergence of the FEOM. These variables do not ful£ll this criterion as both must be accounted for if their effect is to be known. For example, at a latitude of 80°N the chemistry will be very different in summer and winter. Therefore, although all the necessary information is available, high order functions are needed to give an accurate reproduction of the system.

Noon Zenith Angle and Day Length

An alternative solution that is used in this work is to use the noon solar zenith angle, θ_n, and the number of daylight hours, Λ. These variables also de£ne a unique diurnal cycle if $0 < \Lambda < 24$ (see £gure 3.5). These variables have the advantage that they have consistent £rst order effects, so should be less strongly coupled.

In order to use these parameters the calculation of solar zenith angle in STORM-NH, equation 3.11, is replaced by

$$\theta = a.\cos(t_h - \pi) + b \tag{3.13}$$

[†]The local hour angle is the fraction of 2π which the Earth has turned after local noon.

[‡]A 360 day year is used to simplify analysis, as it allows 12 months of equal length, and for parity with the Reading Intermediate General Circulation Model (see chapter 5).

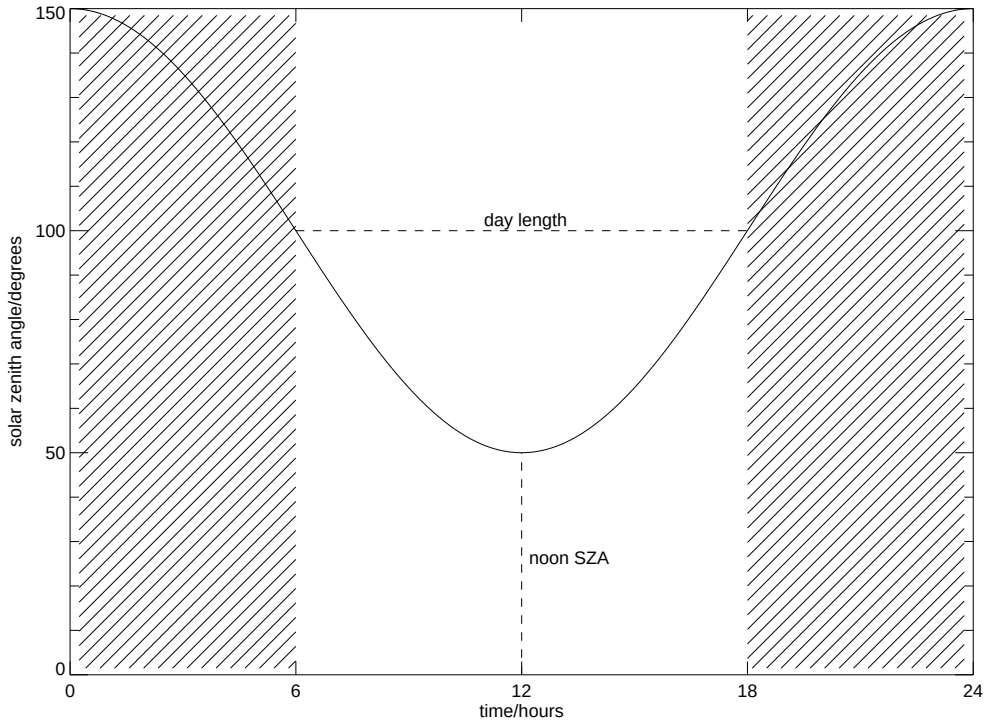

Figure 3.5: *Diurnal cycle produced by £xing day length and noon solar zenith angle. The day length is 12 hours and the noon solar zenith angle is 50°. The local sunrise angle here is set to 100°*

where

$$a = \frac{\theta_{ss} - \theta_n}{\cos(t_{ss}) + 1} \tag{3.14}$$

$$b = \frac{\theta_n \cos(t_{ss}) + \theta_{ss}}{\cos(t_{ss}) + 1}. \tag{3.15}$$

The derivation of a and b is given in the Appendix. t_{ss} is the time of sunrise (in radians) and θ_{ss} is the local sunrise angle which depends on altitude. In this thesis, θ_{ss} was assumed to be 100°throughout the stratosphere. This is not strictly true, but is reasonable as photolysis at solar zenith angles greater than about 90°is very slow anyway. FASTOC must calculate the day length and noon solar zenith angle from the latitude and day of year. Equations 3.16 and 3.17 (see appendix) are used to calculate these quantities.

$$\theta_n = \phi - \delta \tag{3.16}$$

$$\Lambda = \frac{24}{\pi} \cos^{-1} \left(\frac{\cos(\theta_{ss}) - \sin(\phi)\sin(\delta)}{\cos(\delta)\cos(\phi)} \right) \tag{3.17}$$

A latitude-time plot of these values is shown in £gure 3.6.

For periods of twenty-four hour sunlight (polar day) it is necessary to add an additional term to account for the maximum (midnight) solar zenith angle. This is achieved by adding a factor, α to the day length function. This is de£ned as

$$\alpha = \frac{\theta_{ss} - \theta_m}{10}, \tag{3.18}$$

where θ_m is the mimimum solar zenith angle. This function allows the model to distinguish between regions of different chemistry and so improves the results during polar day.

3.3.2 FASTOC Functions and Analysis

To summarise the preceeding sections, functions are included for temperature, pressure, day length, noon solar zenith angle, overhead ozone column and sulphate surface area. It is also necessary to include the chemical species, but only those which in¤uence the long term development of the system need to be considered. To reduce the number of species that must be calculated a family approach is adopted in FASTOC for some species. O_x (O_3 + $O(^3P)$ + $O(^1D)$) and NO_x (NO

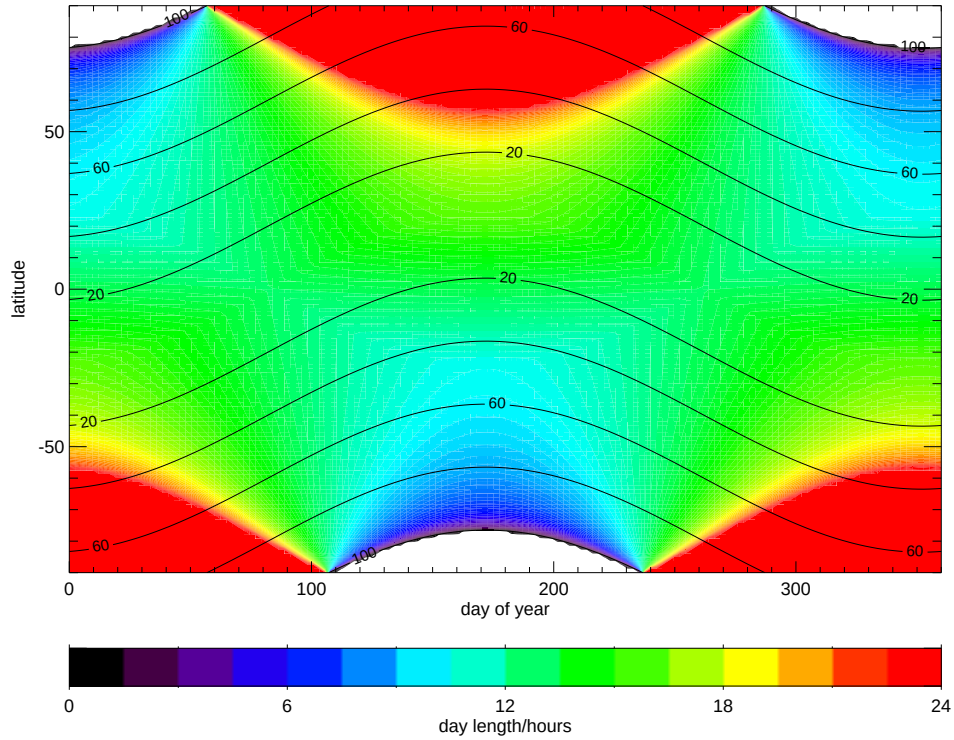

Figure 3.6: *Day length as a function of latitude and day of year. The black contours show the noon solar zenith angle. The local sunrise angle here is set to 100°*

Method	Species
family	O_x (O_3, $O(^3P)$, $O(^1D)$), NO_x (NO, NO_2, NO_3, HONO), nitric acid (HNO_3, HNO_4)
explicit	N_2O_5
implicit	H, H_2, OH, HO_2, H_2O_2
input	N_2O, H_2O, CH_4, CO

Table 3.1: *Table showing species included in FASTOC. "family" and "explicit" species are both model inputs and outputs. Those marked "input" are used as model inputs but are not calculated. Those marked "implicit" are included in STORM-NH but are neither calculated nor used as inputs by FASTOC. Chemical interactions involving these species are implicit in each model timestep.*

+ NO_2 + NO_3 + HONO) are calculated. HO_x species are not included explicitly in FASTOC, but rather the effect of HO_x chemistry is implicit by the inclusion of these species in the STORM-NH calculations used to generate the model functions. The calculation of short-lived species should be unnecessary as they will be in photochemical equilibrium over the 24 hour timestep. Another way of putting this is that if the lifetime of a species, i, $\tau_i << 24$ hours then the system will have converged onto a lower dimensional manifold. This means that the system has no memory of that species' initial mixing ratio which will, therefore, be unimportant in determining mixing ratios at the next timestep. The role of each STORM-NH species is shown in table 3.1.

Approximately 15 points were used for each function, distributed with more points in regions of function curvature and covering the range of possible stratospheric values found using the STORM chemical box model. The best results were found when the reference point was near photochemical equilibrium, found using STORM. This is expected as high order correlations will be less important near the reference point. This region of the input space is more likely to be used by the model if it is "realistic".

As well as being used as a parameterised model, the functions used in FASTOC can be used to gain physical insight into the effects of each variable or groups of variables. In addition, the magnitude of each function gives information about the dominant processes controlling the system.

To illustrate the use of FEOM functions two groups of examples are brie¤y discussed. Figures 3.7(a) and 3.7(b) shows the £rst order effects of temperature and NO_x on odd oxygen. The effect of NO_x is quite linear, but the temperature function shows the importance of accounting for non-linear £rst order effects. Figure 3.8 is the second order function showing the effect of varying NO_x and temperature simultaneously. The maximum magnitude of this function is approximately the same size as the NO_x £rst order function, demonstrating the importance of these higher order correlations. The low temperature region effectively negates the £rst order effect of NO_x because the rates of catalytic reactions are so slow that it has no effect. The high temperature region, contrastingly, magni£es the effect of the NO_x function. Due to the subtraction of lower order functions, the second order function is zero along the £rst order axes.

Figures 3.9, 3.10 and 3.11 shows the effect of changing day length on NO_y partitioning. Short days allow nitrogen to be converted to nitric acid *via*

$$N_2O_5 + H_2O \xrightarrow{aerosol} HNO_3 \tag{3.19}$$

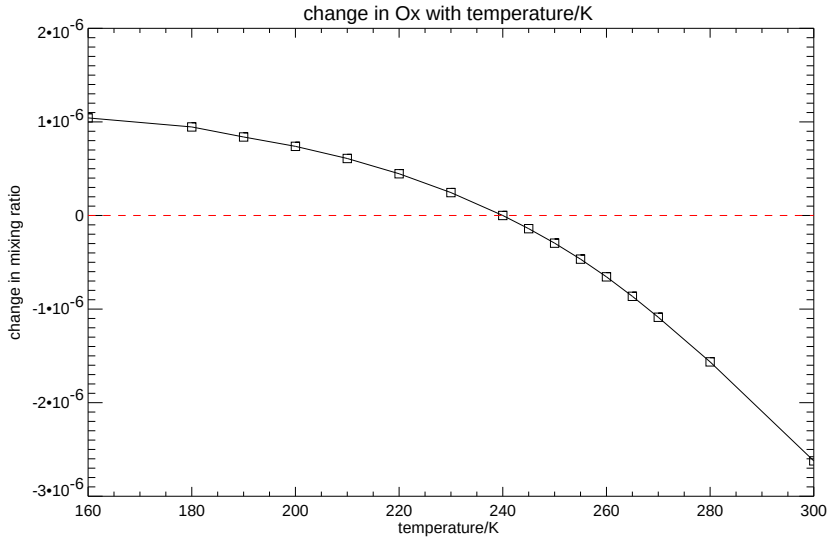

(a)

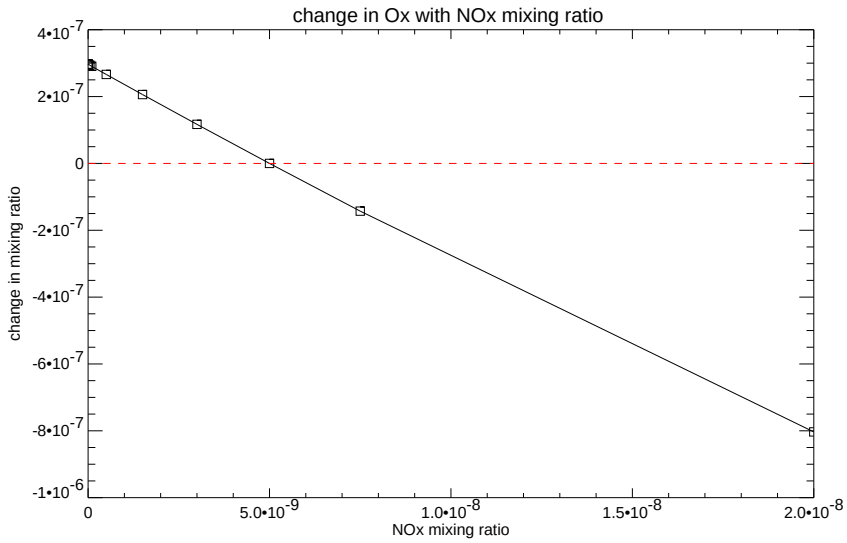

(b)

Figure 3.7: *First order functions of temperature and* NO_x *for odd oxygen in the FASTOC model.*

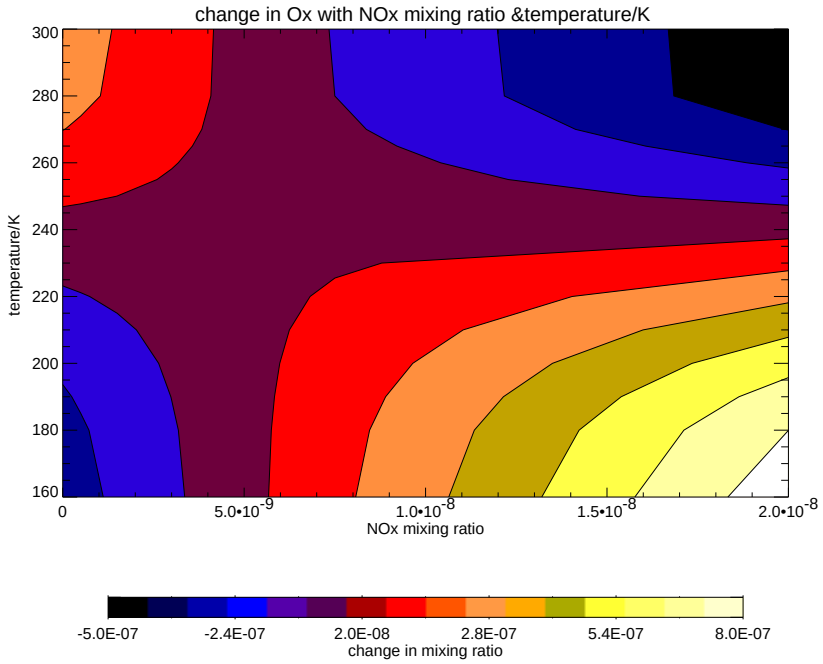

Figure 3.8: *Second order function of temperature and* NO_x *for odd oxygen in the FASTOC model.*

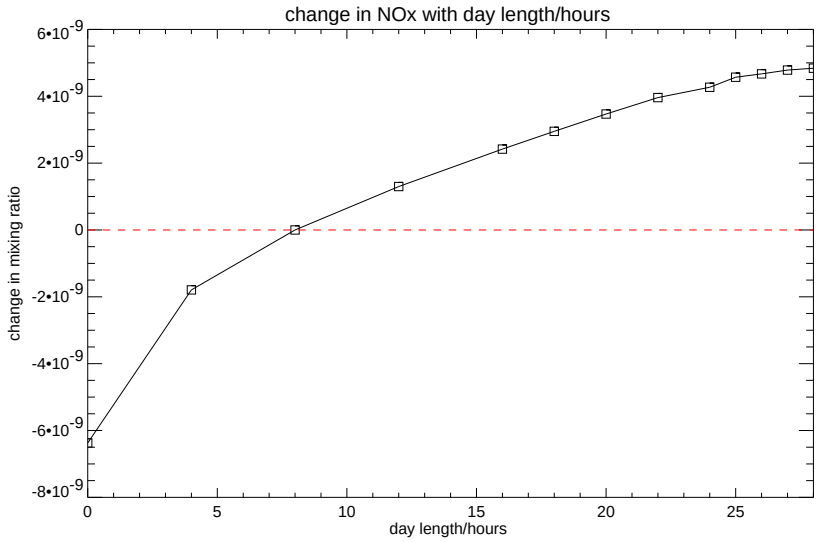

Figure 3.9: *First order day length functions for* NO_x *in the FASTOC model. Day lengths greater than 24 hours signify decreasing solar zenith angle in periods of polar day.*

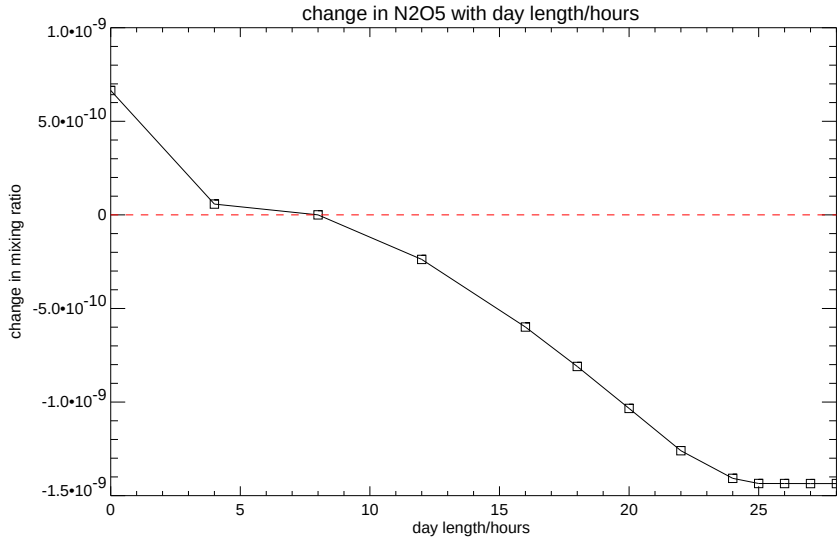

Figure 3.10: *First order day length functions for* N_2O_5 *in the FASTOC model. Day lengths greater than 24 hours signify decreasing solar zenith angle in periods of polar day.*

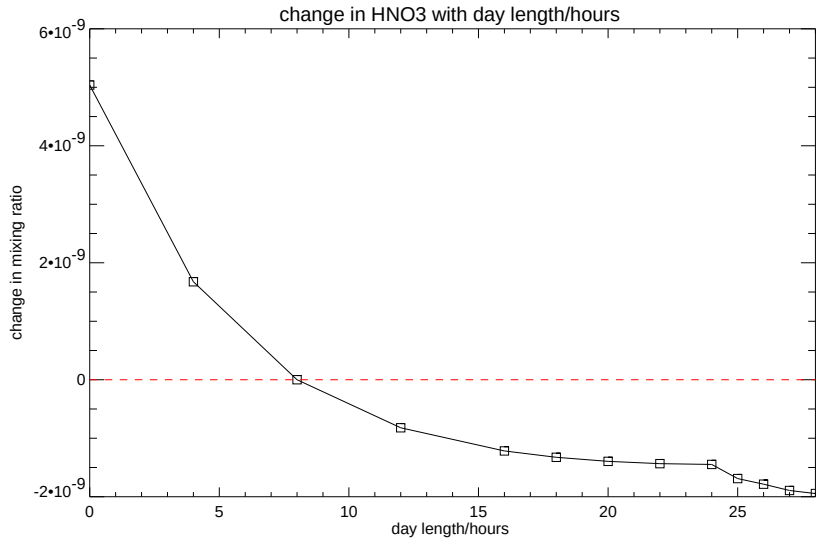

Figure 3.11: *First order day length functions for* HNO_3 *in the FASTOC model. Day lengths greater than 24 hours signify decreasing solar zenith angle in periods of polar day.*

without destruction by photolysis or oxidation by OH. N_2O_5 also increases as photolysis is reduced. Increasing day length initially leads to destruction of HNO_3 as effect of the reactions

$$HNO_3 + h\nu \rightarrow products \tag{3.20}$$

and

$$HNO_3 + OH \rightarrow NO_3 + H_2O \tag{3.21}$$

is increased. Increasing the day length beyond about 15 hours, however, has little effect as an equilibrium with

$$NO_2 + OH \rightarrow HNO_3 \tag{3.22}$$

is reached. The longer day lengths have a larger impact on N_2O_5, which is destroyed by photolysis at longer wavewlengths. The combination of these processes leads to a smooth increase in NO_x from total darkness to twenty-four hour sunlight.

As mentioned earlier, is may also be useful to know which functions are controlling the system, and which play a negligible role. A good measure of the magnitude of each function, f, is its relative importance, RI, compared to the zeroth order function, f_0. Over the course of a model integration of n timesteps it is calculated as

$$RI = \frac{\sum \left| \frac{f}{f_0} \right|}{n}. \tag{3.23}$$

If the assumption that high order terms can be neglected is valid the RI of functions should decrease with increasing order.

Examples of such a function analysis are given in £gures 3.12, 3.13, 3.14 and 3.15. Pressure and temperature are shown to be the most important environmental parameters for O_x and HNO_3. These species are sensitive to radiation at wavelengths shorter than about 350nm, through, for example, the photolysis of oxygen, and to gas phase destruction. NO_x and N_2O_5 are most affected by pressure, day length and overhead ozone column (in DU). These species are affected by longer wavelength radiation, than are O_x and HNO_3, the extinction of which is insensitive to solar zenith angle. The daily integrated photolysis will, therefore, depend more on the number of daylight hours than on the noon zenith angle. O_x, HNO_3 and N_2O_5 have their own mixing ratio as one

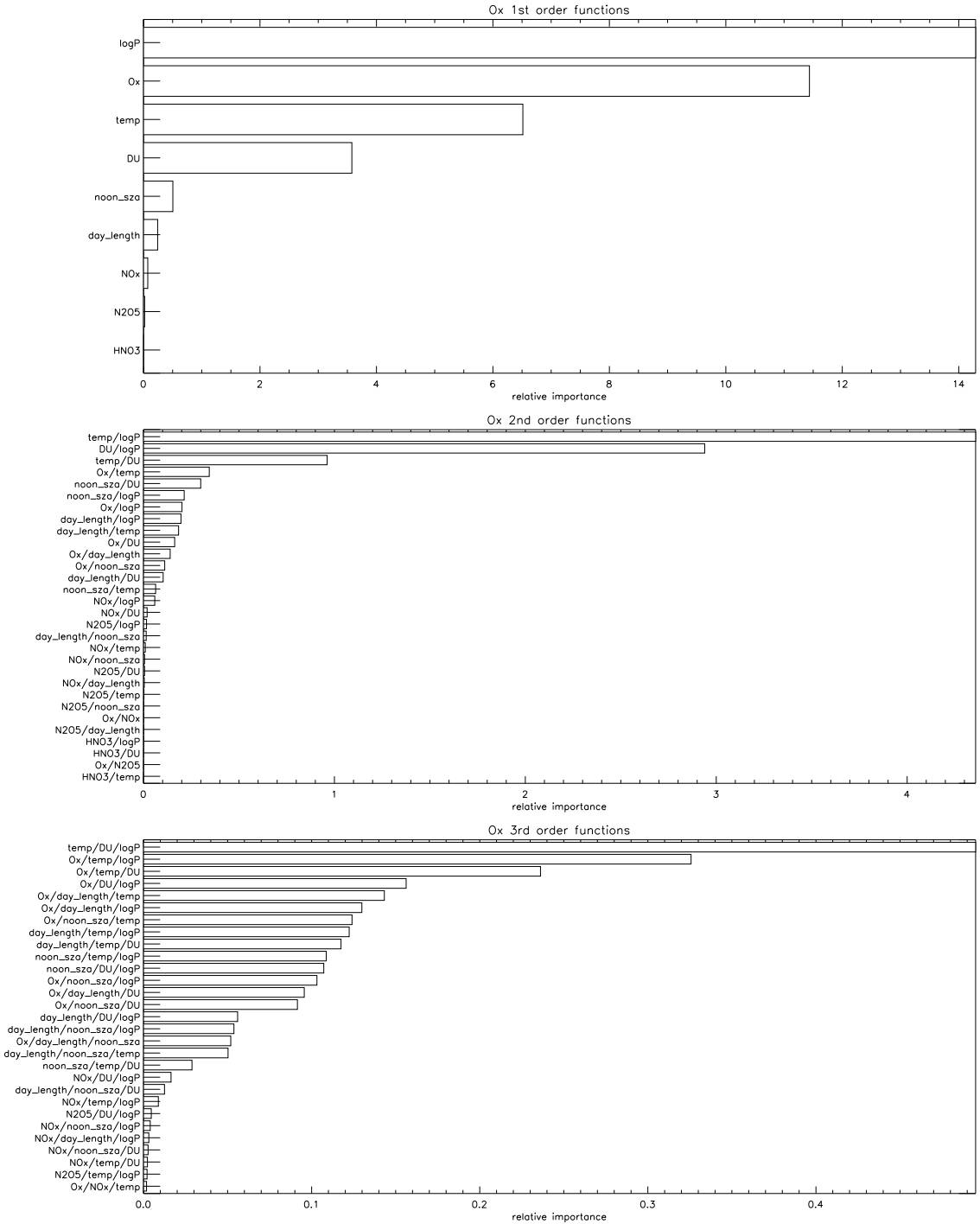

Figure 3.12: *Relative Importance of most signi£cant functions for* O_x *of a FEOM calculation at 0.3mb, 55°N lasting one year. DU is the function for overhead ozone column.*

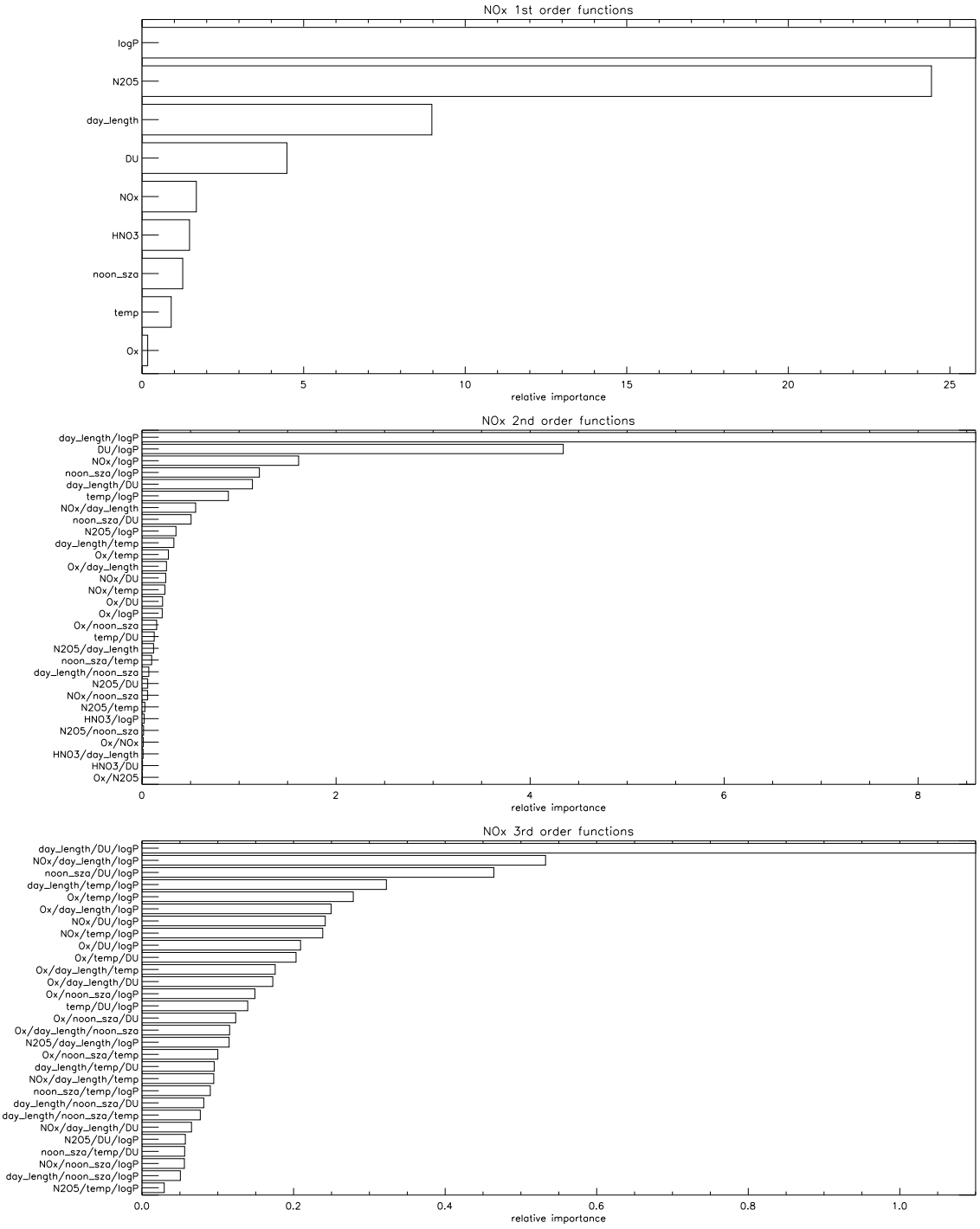

Figure 3.13: *Relative Importance of most signi£cant functions for* NO_x *of a FEOM calculation at 0.3mb, 55°N lasting one year. DU is the function for overhead ozone column.*

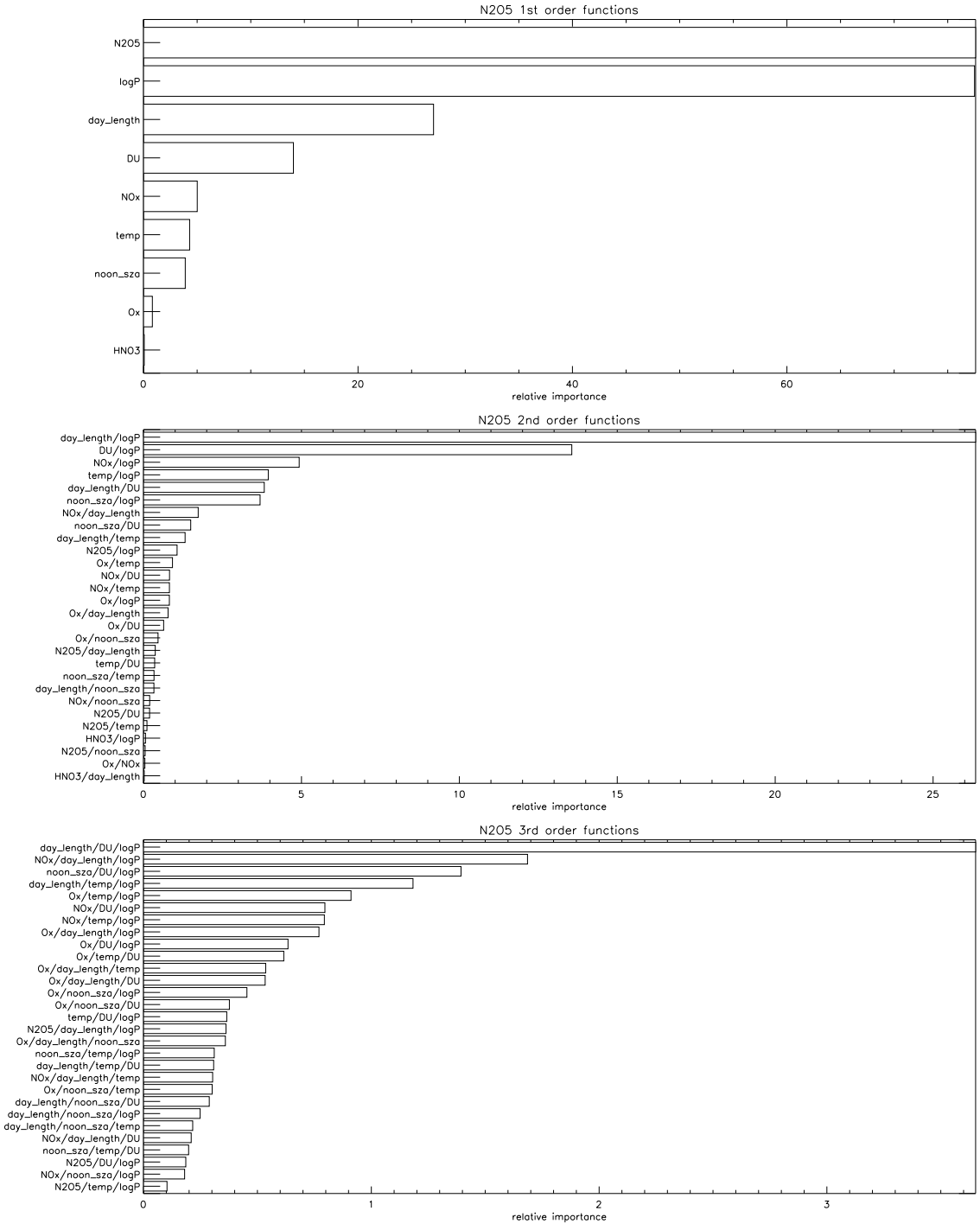

Figure 3.14: *Relative Importance of most signi£cant functions for* N_2O_5 *of a FEOM calculation at 0.3mb, 55°N lasting one year. DU is the function for overhead ozone column.*

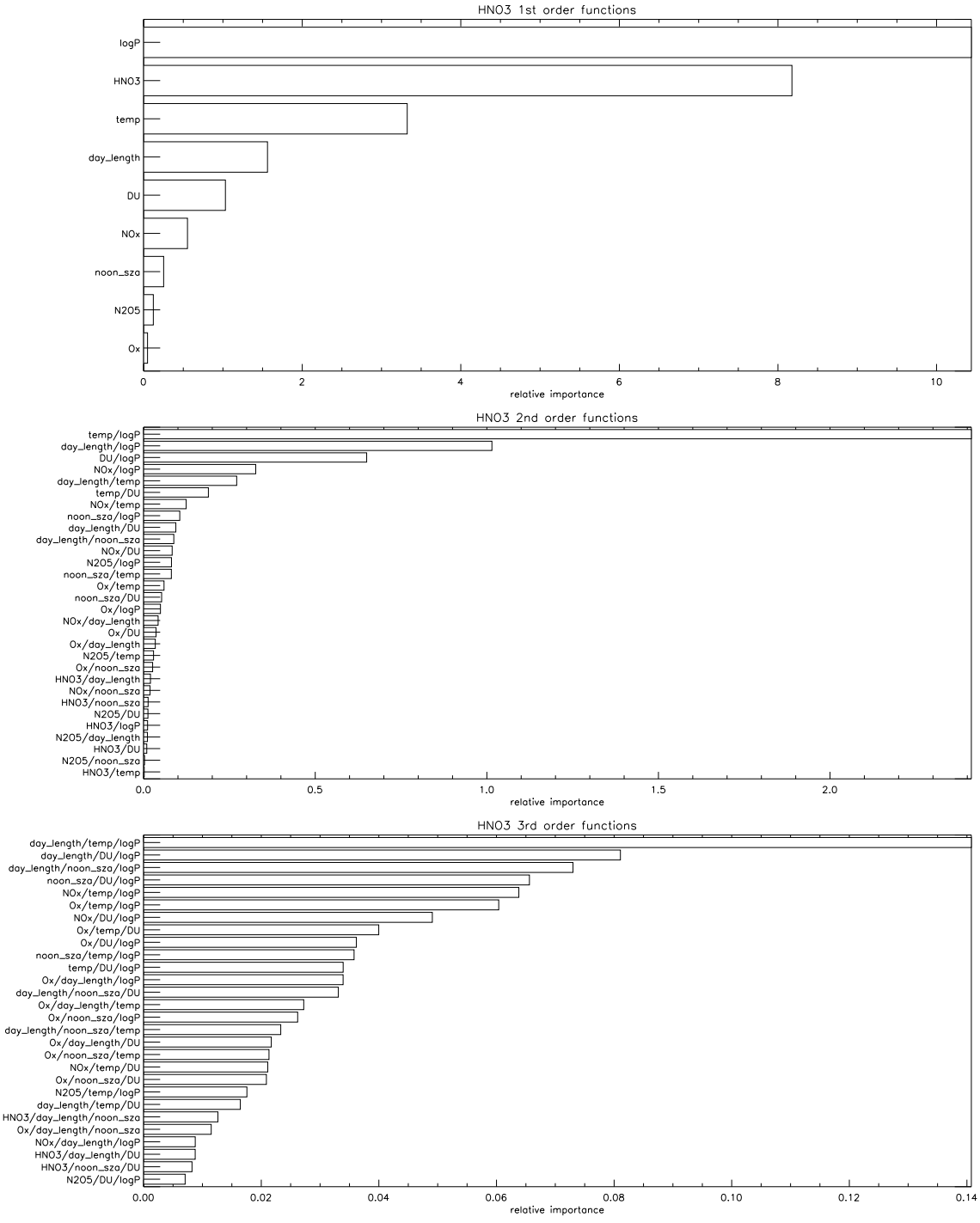

Figure 3.15: *Relative Importance of most signi£cant functions for* HNO_3 *of a FEOM calculation at 0.3mb, 55°N lasting one year. DU is the function for overhead ozone column.*

of their most important £rst order functions, suggesting a signi£cant memory in the system. NO_x depends more strongly on N_2O_5 than it does on itself, suggesting a lack of memory. NO_x, however, has some higher order in¤uences that would be lost if only £rst order terms were considered. Both NO_x and N_2O_5 have signi£cant terms of NO_x/pressure and NO_x/day length/pressure.

The RI values of the functions can also be used to reduce the computational cost of a FEOM. The functions which have a negligible impact on the solution can be identi£ed and removed from the calculation. It should be noted that if different functions are removed from the calculation of each species then the scheme will no longer exactly conserve mass. The effect of this, however, should be insigni£cant as the functions are removed speci£cally because of their minimal impact on the solution. A threshold value of $RI = 2 \times 10^{-6}$ is chosen to ensure that the effect of removing the functions is small. In the case where all the functions had an RI less than this, ignoring them will change the solution by less than 0.1%. Figure 3.16, typical of such plots, shows that around 20-40% of third order functions may be neglected. As these functions dominate the computational cost of the model, the saving is signi£cant.

3.3.3 Multiple FEOMs

As in the simple four species tropospheric chemical FEOM of Wang *et al.* (1999) it was found that a single set of FEOM functions could not capture the chemistry of the stratosphere in all locations suf£ciently well. As the chemical system varies dramatically with altitude, and time of year at high latitudes, the expansion does not converge at low order everywhere. In this case, the high order terms are signi£cant and the choice of reference point becomes important. If only low order terms are used the FEOM calculates mixing ratios that are inaccurate and possibly negative. An example of a poor representation of ozone from a FEOM is given in £gure 3.17. Here, a FEOM initialised in the middle stratosphere is used to calculate ozone at 100mb at the equator. The rate of ozone production is unrealistically high, so the region becomes a net source rather than a sink.

Wang *et al.* (1999) chose to use a different set of second order functions at every grid point in their domain in order to avoid this problem, which has an obvious computational burden. Here, the stratosphere is instead divided into regions of similar chemistry, based on the number of daylight hours and pressure. Each region has a set of third order FEOM functions. The environmental parameters chosen for each box are shown in table 3.2. A transition zone, equivalent to a few kilometres in height, is speci£ed between each vertical region where the solution is calculated by linear interpolating between the solutions using the functions above and below.

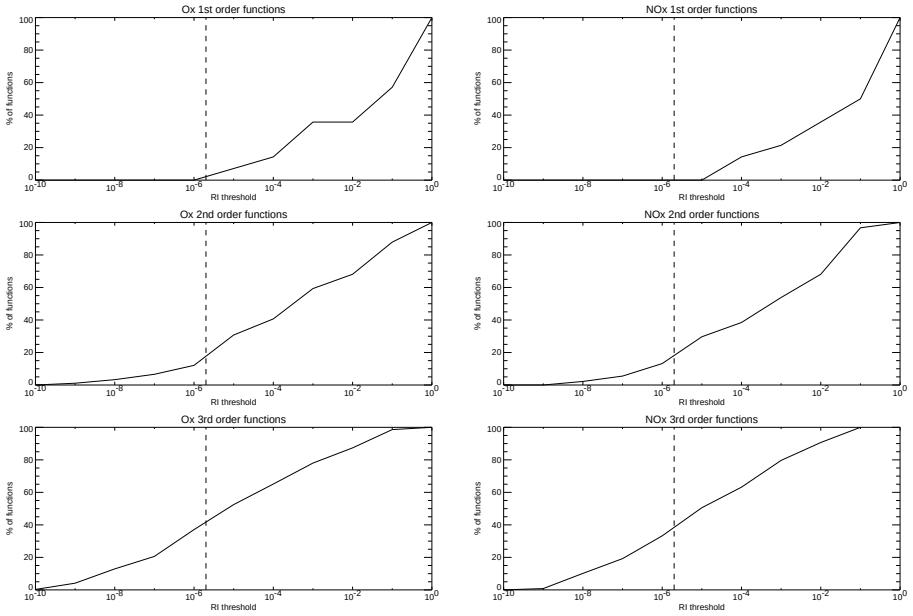

(a) O_x

(b) NO_x

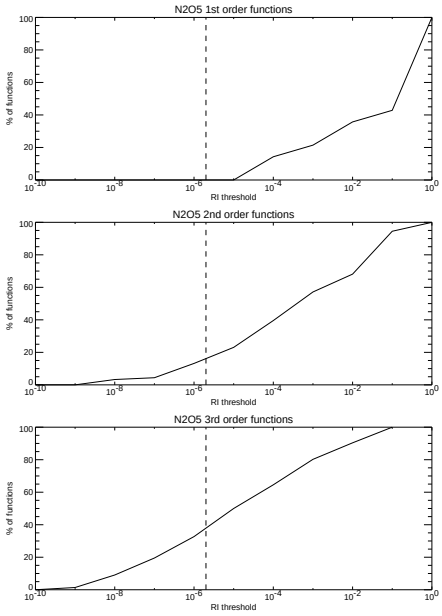

(c) N_2O_5

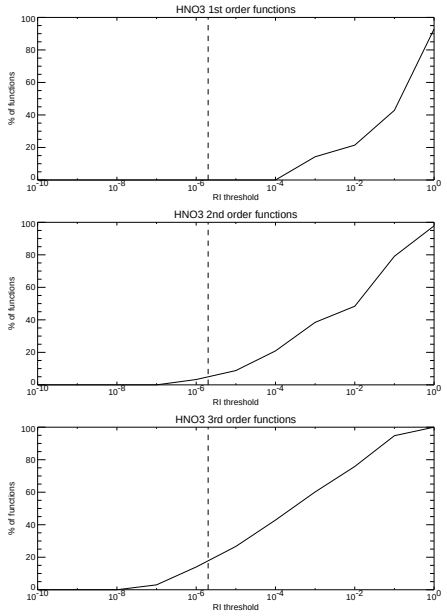

(d) HNO_3

Figure 3.16: *Figure shows the percentage of FEOM functions with a RI value greater than a threshold of 2×10^{-6}. Data from a FASTOC calculation in a two-dimensional framework (see chapter 4) from 4 to 20mb, for all latitudes not in polar day or night, lasting £ve days starting on 1st January.*

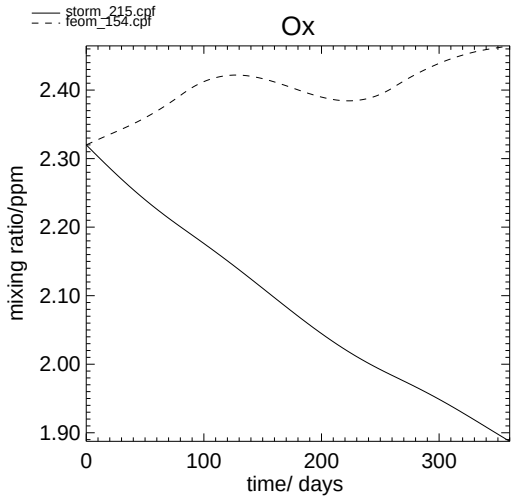

Figure 3.17: *STORM (solid) and FASTOC (dashed) calculations of one year of ozone mixing ratios at 100mb at the equator. FASTOC used a FEOM initialised at 30mb and calculates ozone production to be too high.*

Box	**log(P/mb)**	**Day length/h**	θ_n
MLSLS	2.2	15	30
MLSMS	1.7	15	30
MLSUS	1.0	15	30
MLSSP	0.0	15	30
MLWLS	2.2	9	60
MLWMS	1.7	9	60
MLWUS	1.0	9	60
MLWSP	0.0	9	60
PLDLS	2.2	26	60
PLDMS	1.7	26	60
PLDUS	1.0	26	60
PLDSP	0.0	26	60
PLNLS	2.2	0	101
PLNMS	1.7	0	101
PLNUS	1.0	0	101
PLNSP	0.0	0	101

Table 3.2: *Environmental parameters for each of the sets of third order functions used in FASTOC. MLS refers to midlatitude and tropical summer; MLW refers to midlatitude and tropical winter; PLD refers to polar day; PLN refers to polar night; LS means lower stratosphere; MS means middle stratosphere; US means upper stratosphere; SP means stratopause.*

3.4 Comparison with Shorter *et al.* (1999)

Shorter *et al.* (1999) developed a FEOM for stratospheric chemistry using the NASA GSFC 2-D atmospheric chemistry model running in 0-D. It will be referred to here as SIR99. They present a 39 species model running for several years at mid-latitude conditions. Only small errors were seen when the FEOM, using 2nd order terms, was compared to the full ODE solver model.

Although SIR99 and FASTOC both parameterise stratospheric chemistry, there are a number of important differences between them. Firstly STORM-NH uses a more sophisticated photolysis scheme than does the NASA GSFC model. In the latter model, an average photolysis rate was used during daylight hours. This approach has been shown by Smith (1995) to introduce additional errors when compared to more rigorous calculations. The approximation is reasonable for species that photolyse at wavelengths greater than about 350nm, such as NO_3 (see £gure 3.18(a)). For species that photolyse at shorter wavelengths, however, a square wave is a poor approximation to the diurnal cycle (see £gure 3.18(b)). Furthermore, each rate in SIR99 varied seasonally, based on

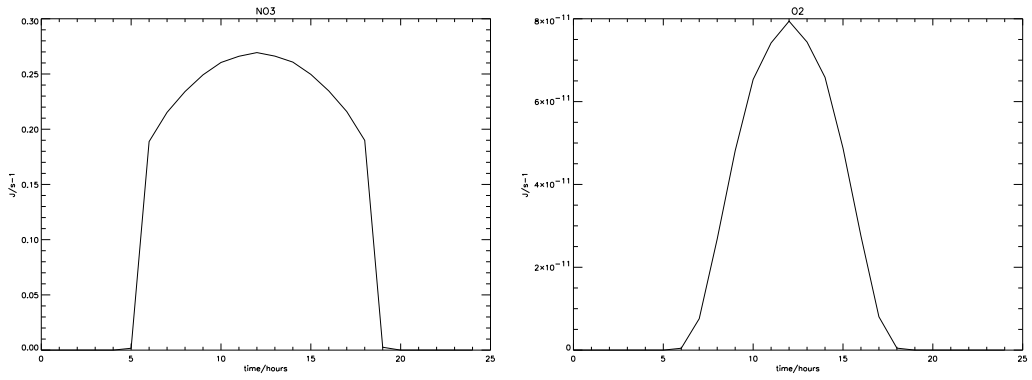

(a) NO_3 (b) O_2

Figure 3.18: *photolysis rates for a)* NO_3 *and b)* O_2 *over one day at 30km, 20° north, calculated using the STORM-NH chemical box model output hourly*

one of just £ve functional forms. These simpli£cations reduce the accuracy of the model. STORM uses a photolysis scheme based on Meier *et al.* (1982) (see section 2.2) and rates are calculated at each timestep. This method is accurate, but the large variation in photolysis rates with solar zenith and overhead ozone column is more dif£cult to parameterise. SIR99 used the functional form values as inputs to represent photolysis, but the choice of inputs is less obvious for FASTOC. A second difference is one of computational ef£ciency. SIR99 calculated the concentrations of all 39 species included in the NASA GSFC model. As noted earlier, FASTOC calculates just four

species, although it should be noted that this version does not include halogens. Even with this caveat, many species included in SIR99 are not necessary because they do not have an effect on timescales as long as 24 hours.

3.5 Model Validation

The most important test for an input-output model is that it agrees well with the model that is used to initialise it. Here FASTOC is compared to the STORM-NH chemical box model in a number of zero-dimensional tests. Each comparison lasts for one year and the temperatures are taken from Rees *et al.* (1990). The experimental conditions are shown in table 3.3. The pressures tested range from the lower stratosphere to near the stratopause in order to test that the model is suitable for global calculations. The performance of the model is assessed by calculating the percentage of days in the run that FASTOC is within a given threshold of the independent STORM-NH run.

Comparison	Pressure/mb	Latitude/degrees
LS	150	40
MS	30	0
US1	10	40
US2	1	40

Table 3.3: *Conditions used in FASTOC validation tests.*

The LS test results are good. O_x is within 1% for more than 75% of the time and within 5% at all times (£gure 3.19). NO_y partitioning is not as good, but has the correct annual cycle. FASTOC generates slightly less NO_x than does STORM-NH, but the model O_x is generally insensitive to this. It appears that the sum of NO_x plus N_2O_5 is more important due to the rapid repartioning of these species.

In the MS run (£gure 3.20) FASTOC calculates O_x to within 5% for around 70% of the time. The rate of increase is slightly overestimated, as are the maxima that occur at equinox. Overall, however, the agreement is good. The NO_y partitioning is also good, although HNO_3 is initially low in FASTOC and does not reach similar values to those of STORM-NH until after day 100.

In US1 the annual cycles of O_x are in good agreement (£gure 3.21) although FASTOC overestimates the summer maximum slightly. FASTOC calculated very similarNO_y partitioning to STORM-NH, as shown by the HNO_3 values shown in £gure 3.21. Figure 3.21 (bottom panel)

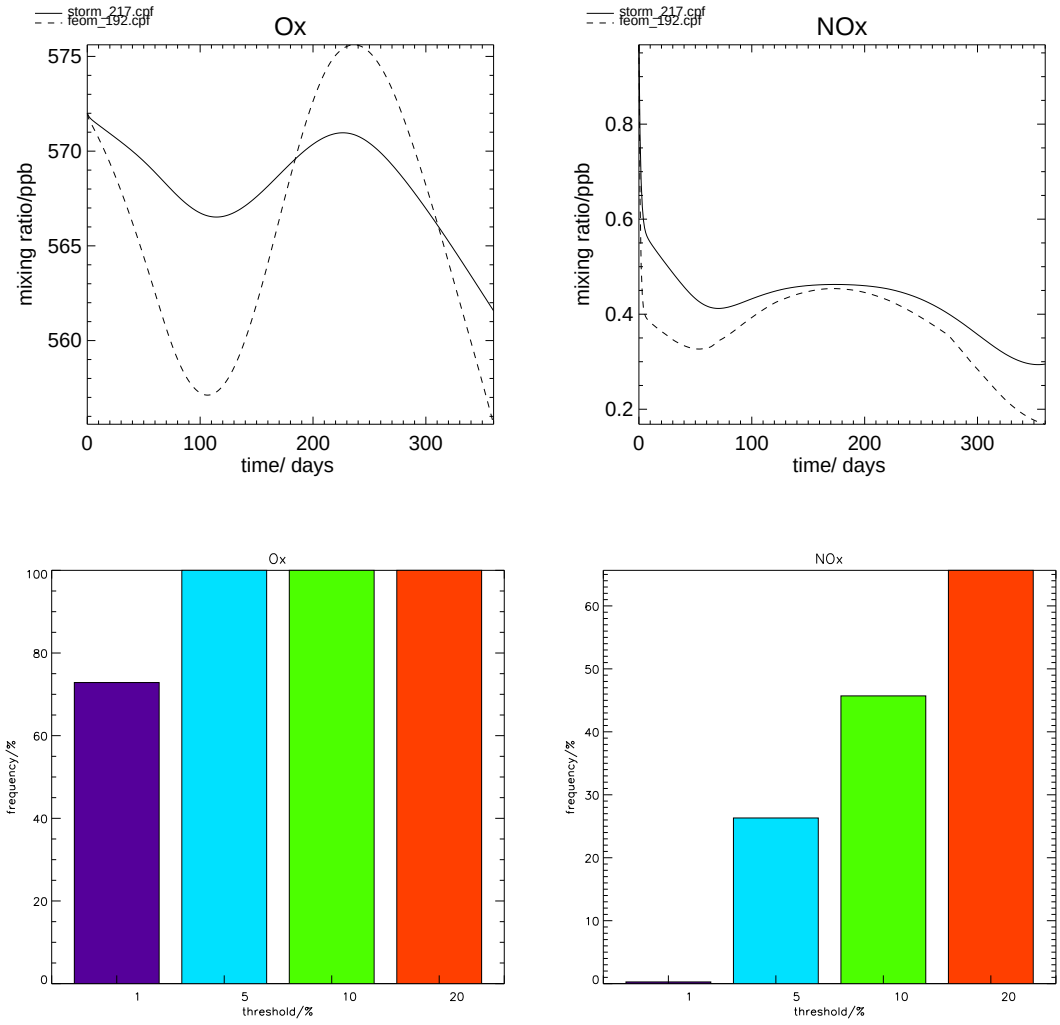

Figure 3.19: *Mixing ratio of* O_x *and* NO_x *in the LS test (top). Percentage of FASTOC days that are within a given percentage of STORM-NH values for* O_x *and* NO_x *in the LS test (bottom).*

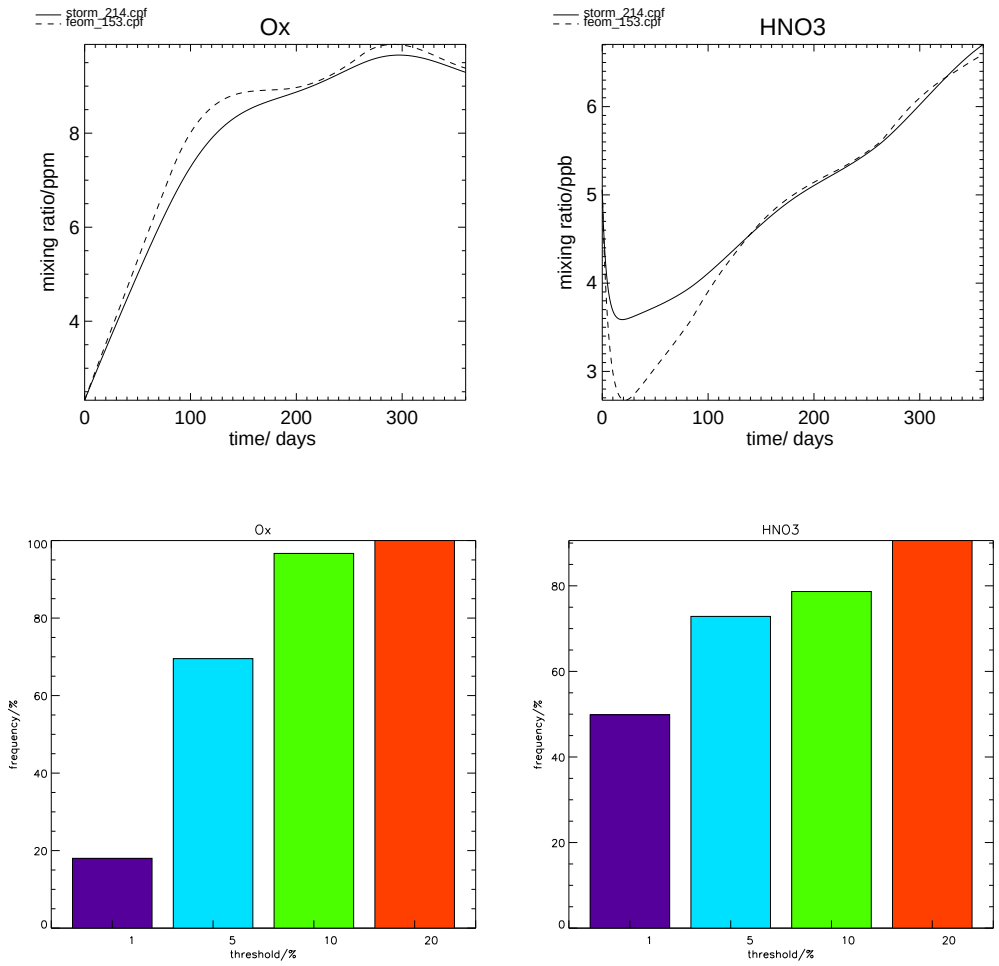

Figure 3.20: *As £gure 3.19 but for* O_x *and* HNO_3 *in the MS test.*

also shows that the O_x and HNO_3 values are typically within 5%.

The results for O_x in US2 are excellent (£gure 3.22). The O_x values here are strongly in¤uenced by temperature, as shown by the discontinuous £rst derivative of the ozone time series. This is caused by the linear interpolation that is used between monthly temperature values. The dominance of a £rst order function helps the low order convergence of the FEOM. Although the N_2O_5 value of FASTOC is frequently more than 10% away from that of STORM-NH (£gure 3.22, bottom panel) the error is never greater than 20%. In addition, the annual cycle is correct, but slightly exaggerated (£gure 3.22, top panel). The large percentage differences are due to the very low mixing ratio of N_2O_5 at this pressure, particularly in the summer.

Overall, the FASTOC model performs very well in comparison with STORM-NH. The parameterisation agrees well with the ODE solver in regions of net photochemical ozone production, net photochemical ozone loss and of rapid equilibrium. The parameterisation does not give perfect agreement as error is introduced by the truncation of equation 3.3 to third order. The results are, however, very good and FASTOC should be a suitable model for general circulation models.

3.6 Chapter Summary

In this chapter the FASTOC model has been described and tested. This fast stratospheric chemistry parameterisation is an input-output model of the FEOM type described by Shorter *et al.* (1999). This method ef£ciently samples the input space, allowing high order systems to be parameterised. The construction of FASTOC was described, and several important problems in its implementation were discussed. FASTOC was compared with the model of Shorter *et al.* (1999) and a number of differences between the models were highlighted. Finally, the FASTOC model was validated by comparing its results with those of the STORM-NH chemical box model. In chapter 5 FASTOC is coupled to a general circulation model and a number of multi-year integrations are performed.

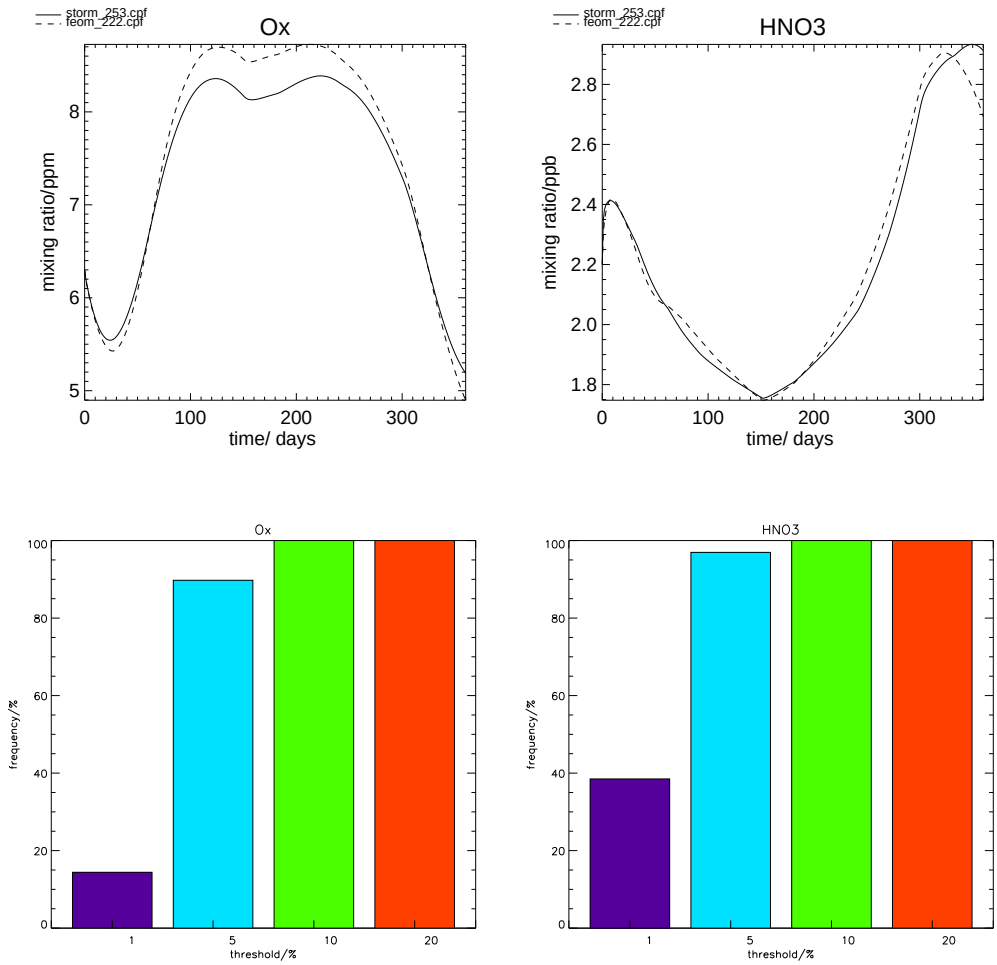

Figure 3.21: *As £gure 3.19 but for* O_x *and* HNO_3 *in the US1 test.*

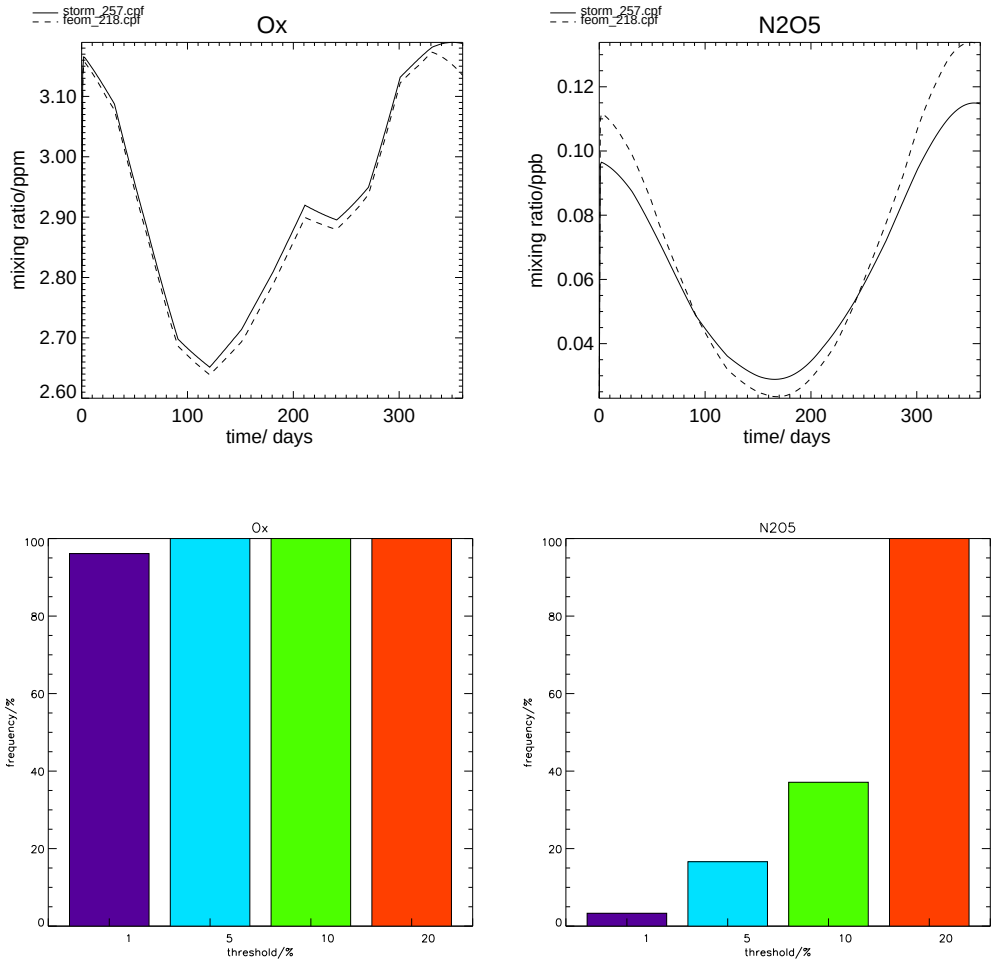

Figure 3.22: *As £gure 3.19 but for* O_x *and* N_2O_5 *in the US2 test.*

CHAPTER FOUR

Chemical Perturbation Experiments

The effect of complex chemistry-climate interactions can only be fully investigated using coupled chemical-dynamical models forced by changes in well-mixed greenhouse gases, halogens or other trace gases. It is possible, however, to examine the £rst order response of dynamics to chemical changes, or *vice versa*. Dynamical changes can be forced be imposing non-interactive trends in radiative gases, such as carbon dioxide (see, for example, Shindell *et al.*, 1998a) or ozone (see, for example, Rosier and Shine, 2000), on a GCM. Alternatively, chemical changes can be assessed by imposing changes in temperature or trace gases on a purely chemical model. These calculations, although simpli£ed, can offer an initial estimate of the magnitude of a change or attempt to separate the effects of coupled chemistry and dynamics. This information may be used to motivate further calculations with more costly, complex models.

In section 4.1 a theory for a simple estimation of the response of stratospheric chemistry to a perturbation is presented; in section 4.2 a chemical box model is used to investigate the importance of changes in temperature and source gas budgets to ozone in the upper atmosphere; section 4.3 examines the impact of the most signi£cant chemistry-climate interactions on the £nal recovery of ozone at the end of the 21st century.

4.1 Theory

The behaviour of any system that has a natural equilibrium can be studied by performing perturbation experiments. This is similar to the approach used by Haigh (1985) to examine the relationship between temperature and radiative heating. It is not necessary for the system to be at equilibrium to calculate its £nal response, as this can be calculated from the initial response if the timescale of

the relaxation is known. Consider a species n and its source function S_n.

$$S_n = P - L[n] = \frac{\partial n}{\partial t}. \tag{4.1}$$

Using a Taylor expansion of equation 4.1 to £rst order gives

$$S_n + \delta S_n \approx S_n + \left(\frac{\partial S_n}{\partial n}\right)\delta n + \ldots \tag{4.2}$$

$$\therefore \delta S_n = \left(\frac{\partial S_n}{\partial n}\right)\delta n. \tag{4.3}$$

Let

$$\alpha = -\left(\frac{\partial S_n}{\partial n}\right), \tag{4.4}$$

so

$$\delta S_n = -\alpha \delta n. \tag{4.5}$$

It can be shown that a perturbation to n from equilibrium, n_{eqm}, relaxes exponentially back to n_{eqm}:

$$\frac{\partial \delta n}{\partial t} = -\alpha \delta n \tag{4.6}$$

$$\therefore \int \frac{1}{\delta n} \partial \delta n = -\alpha \int \partial t \tag{4.7}$$

$$\therefore \delta n = \delta n_0 e^{-\alpha t}. \tag{4.8}$$

The relaxation timescale, τ, is therefore given by

$$\tau = \frac{1}{\alpha} \tag{4.9}$$

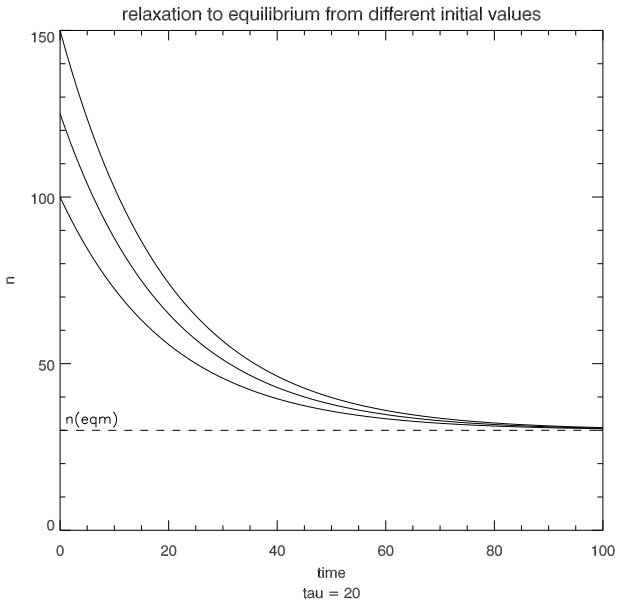

Figure 4.1: *Relaxation of n to an equilibrium value, $n_{eqm} = 30$, from initial values of 100, 125 and 150. A timescale of 20 was used in each case.*

α can be calculated empirically using a chemical code by performing perturbations to δn, as shown in £gure 4.1. δS_n is calculated for each δn, so giving α by equation 4.5. Once α is known, perturbations to S_n may be carried out and δn estimated. Here, the equilibrium value, n_{eqm}, is altered so a positive δn means a decrease in n_{eqm} as illustrated in £gure 4.2. The response is assumed to be linear in these experiments, that is τ does not change for a small perturbation. In fact changes in S_n will alter τ, so this may only be used as a £rst order estimate of the magnitude of perturbations. It is worth noting that there are several studies, such as Yang and Brasseur (2001), which have found considerable non-linear behaviour over decadal timescales in photochemical models of the stratosphere, but it is likely that such behaviour would be damped by mixing in the real atmosphere, and would not be apparent in these short experiments.

The timescale found using this method, if calculated as an instantaneous value, would be the same as that calculated using the production and loss rates as presented in section 1.2.1. In this work the long term development of the chemical system is considered so the timescale is calculated using the chemical tendency, S_n, over a full diurnal cycle.

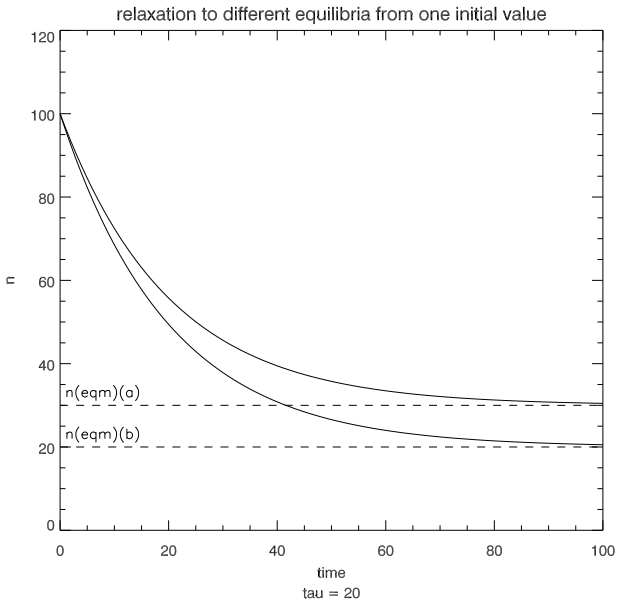

Figure 4.2: *Relaxation of n to different equilibrium values of 20 and 30 from an initial value of 100. A timescale of 20 was used in each case.*

4.2 Perturbation Experiments

In this section the simple theory of section 4.1 is applied to ozone in the upper stratosphere using a photochemical box model, STORM (see chapter 2). There are several reasons for preferring the upper stratosphere for such experiments. As the region is in rapid photochemical equilibrium, chemistry dominates dynamics and the purely chemical response will be similar to that of the real atmosphere over short timescales. Also, it is a region where ozone is sensitive to climate change as catalytic cycles of the form

Cycle 10:

$$X + O_3 \rightarrow XO + O_2 \tag{4.10}$$

$$XO + O \rightarrow X + O_2 \tag{4.11}$$

$$net : \mathbf{O_3 + O \rightarrow 2O_2},$$

where X can be Cl, Br, NO or OH, are ef£cient due to the relatively high ratio of $\frac{O}{O_3}$, which is about 10^{-3} at 3mb, Dessler (2000)).

4.2.1 Calculating α and τ

The timescale is calculated by performing several experiments perturbing ozone and calculating δS for each. The STORM chemical box model was used to £nd α, and hence τ, at 3mb at 40 °N on

1st January using mixing ratios from Brasseur *et al.* (1999), Appendix C and temperatures from Rees *et al.* (1990). Ozone perturbations of 1%, 5% and 10% were made and the change in ozone over 24 hours was recorded. The calculated values of δS are plotted in £gure 4.3

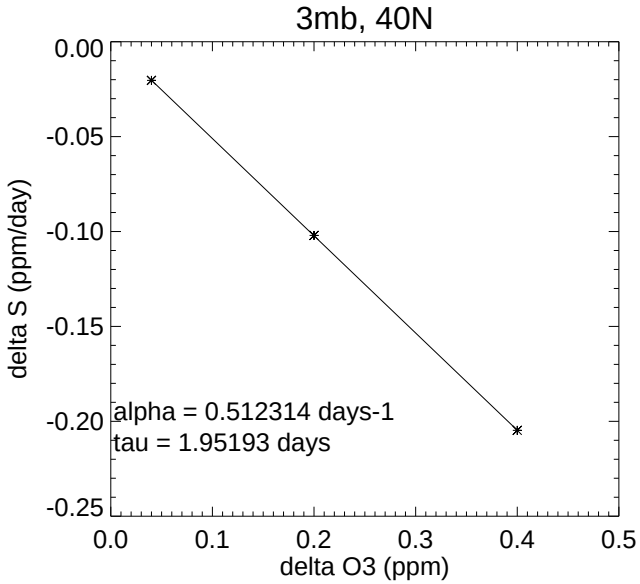

Figure 4.3: $deltaS$ *against* $delta$ O_3. *The gradient is* $-\alpha$ *for present day conditions*

A timescale of 1.95 days was calculated using the IDL LINFIT least squares £t to the data. A χ^2 goodness of £t test con£rmed that the linear £t was justi£ed. The timescale is similar to that found using timescales for annual average production and loss using the Goddard Space Flight Center two-dimensional model (Dessler, 2000).

4.2.2 Perturbation Results

Several perturbation experiments were performed, as detailed in table 4.1. The species that are perturbed are those whose abundances are likely to change over the next century because of changes in anthropogenic emissions or changes in transport across the tropopause. δO_3 is calculated using equation 4.5.

As expected, decreasing the temperature leads to an increase in ozone as the loss reactions such as

$$O + O_3 \rightarrow 2O_2, \tag{4.12}$$

Experiment	**Perturbation**	**δO_3(ppm)**	**δO_3(%)**	**%/ppm**
Δ T	-1K	$+5.8 \times 10^{-8}$	+1.0	-
Δ N	+5% (1.1ppb)	-6.8×10^{-8}	-1.1	1.00
Δ Cl	+5% (0.2ppb)	-2.0×10^{-7}	-3.3	16.5
Δ Br	+5% (1ppt)	-1.7×10^{-9}	-0.03	30.0
Δ CH_4	+5% (25ppb)	$+1.5 \times 10^{-8}$	+0.24	0.01
Δ H_2O	+5% (0.25ppm)	-6.9×10^{-9}	-0.11	0.44
Δ CO	+5% (1ppb)	$+8.1 \times 10^{-11}$	-0.001	0.001

Table 4.1: *Perturbation experiments showing the £nal adjustment of ozone in ppm and as a percentage of the original value of 6ppm at 3mb, 40°N*

are slowed. This can be understood easily in terms of the Arrhenius equation,

$$k(T) = A \times e^{\left(\frac{-E}{RT}\right)}, \tag{4.13}$$

which calculates a decrease in the bimolecular rate constant, k, for a decrease in temperature. Using values of $A = 8 \times 10^{-12}$ and $\frac{E}{R} = 2060$ (DeMore *et al.*, 1997), a decrease in temperature from 220K to 219K leads to a decrease in k of about 4%. $\frac{E}{R} = -180K$ for the reaction

$$NO_2 + O \rightarrow NO + O_2, \tag{4.14}$$

so the rate is not signi£cantly altered by small changes in temperature. The ozone increase of about 1%/K is consistent with the £ndings of Evans *et al.* (1998) and Shindell and Grewe (2002) who found, using two- and three-dimensional models respectively, an increase in ozone of 10-12% at $\sim$3mb for an approximate doubling of CO_2. Shindell *et al.* (1998a) found a cooling of $\sim$8K for a doubling of CO_2 at $\sim$3mb in their GCM and, like this study, did not include the impact of ozone changes on temperature. The current temperature trend in the upper stratosphere is $\sim$-1.5K/decade (IPCC, 2001), though this is due to ozone depletion as well as greenhouse gas increases.

Of the perturbations to active species studied here chlorine is the most signi£cant. The stratospheric halogen loading is expected to decrease by $\sim$60% by 2100 (IPCC, 2001) and this change is likely to dominate the ozone trend over this time. The perturbation to the bromine budget has a minimal effect as the concentration is so low. The results suggest that, on a molecule for molecule basis, bromine is about two times as effective at destroying ozone than is chlorine

under these conditions. This is much lower than other global estimates of about 40 (Daniel *et al.*, 1999), and is not valid under other conditions, such as in the lower stratosphere.

Nitrogen is less effective at destroying ozone at this altitude than are the halogens, but perturbations to its budget are important. Assuming that the decline of the halogen burdon will occur as predicted, the nitrogen budget is one of the greatest unknowns. The abundance of N_2O may increase by 12-90% according to IPCC (2001), leading to a similar increase in NO_x. The upper estimate would lead to an ozone depletion of comparable magnitude to the increase due to the fall in halogen loading. An increase in NO_x of 5% should lead to an increase in NO_x catalysed ozone loss by about the same amount as the rate of reaction 4.14 is proportional to [NO].

The perturbation to methane leads to a small increase in ozone, although this could be signi£cant if methane were to double as predicted by some emissions scenarios (IPCC, 2001). The increase in ozone is due partly to the formation of odd oxygen *via*

$$HO_2 + NO \rightarrow OH + NO_2 \tag{4.15}$$

$$NO_2 + h\nu \rightarrow NO + O(^1D) \tag{4.16}$$

after HO_2 is produced during methane oxidation. Methane also reduces ozone destruction by chlorine by converting it to a reservoir species through reaction 4.17,

$$CH_4 + Cl \rightarrow CH_3 + HCl. \tag{4.17}$$

This, however, does not account for the effect of an increase in water vapour which would follow an increase in methane.

An increase in water vapour is shown to lead to additional ozone loss. This is due to the catalytic loss caused by additional HO_x. As estimates of the trend in stratospheric water vapour range from 73.1 ± 16.3 ppb/year (Evans *et al.*, 1998) to 123.1 ± 18.3 ppb/year (Nedoluha *et al.*, 1998) water vapour could be a signi£cant in¤uence on ozone, as concluded by Dvortsov and Solomon (2001). This perturbation estimate is, of course, for the purely chemical effect of increasing water vapour and does not include the radiative feedback. Forster and Shine (2002) found a cooling of $\sim$0.5K in the upper stratosphere associated with an increase of 1ppm on the 1980 background water vapour. The results here suggest that such a perturbation would give a chemical ozone response of $\sim$-0.5% and a radiative-chemical response of $\sim$+0.5%.

Perturbations to the carbon monoxide budget are unlikely to have a signi£cant impact on the upper stratosphere, even if the doubling of this species predicted by some IPCC (2001) scenarios is realised.

4.3 Ozone Recovery to 2100

The question of ozone recovery toward the year 2100 is currently under debate and a number of two-dimensional model have given con¤icting results. Randeniya *et al.* (2002) found a decrease in ozone by 2100 in some scenarios due to additional catalytic destruction by NO_x. This model, however, did not include cooling due to greenhouse gas increases. Rosen£eld *et al.* (2002) found that ozone levels were higher in 2050 than in 1980 due to stratospheric cooling. The results in table 4.1 indicate that, in the absence of halogens, the effects of increasing nitrogen and radiative cooling are the most signi£cant factors controlling *in situ* ozone destruction. The two effects are similar in magnitude and opposite in sign.

These opposing processes are investigated further using a series of perturbation experiments. STORM was initialised at 3mb, 40°N with mixing ratios suitable for the year 2100 as shown in table 4.2. Methane is appropriate for the IPCC (2001) A1FI scenario; the water vapour trend is towards the lower end of the range of estimates (Evans *et al.*, 1998); the halogen loading is scaled according to the predicted equivalent effective stratospheric chlorine given in table II.2.10 of IPCC (2001).

Species	**Mixing Ratio**
CH_4	1×10^{-6}
H_2O	1.35×10^{-5}
Cl_y	4×10^{-10}
Br_y	4×10^{-12}

Table 4.2: *methane year 2000* $\times 2$*; water vapour year 2000 75ppb per year; halogens year 2000* $\times 0.4$

The perturbation timescale was recalculated, using the same method as in section 4.2.1, to be 2.35 days (see £gure 4.4), compared to 1.95 days for the year 2000 conditions. This increase is likely due to the decrease in catalytic loss rates as the halogen loading falls, and demonstrates that the assumption of a £xed timescale limits con£dence in this method when extrapolating the effect of small perturbations.

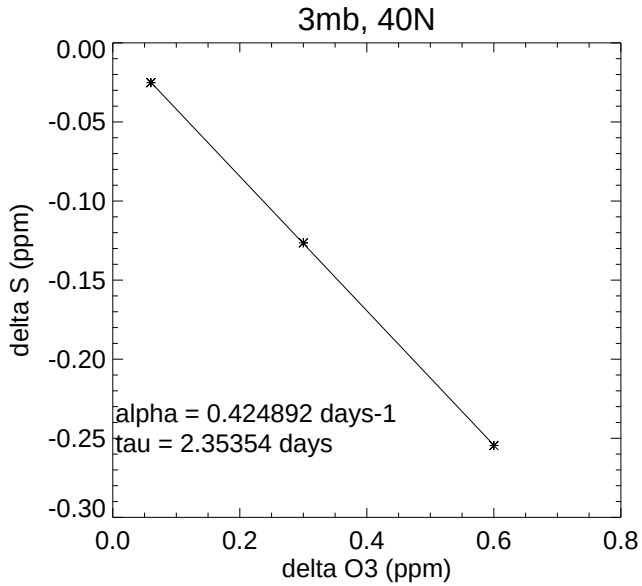

Figure 4.4: *Same as £gure 4.3 but for year 2100 conditions.*

A series of experiments were performed to calculate δO_3 for various NO_y and temperature perturbations. The results are shown in £gure 4.5.

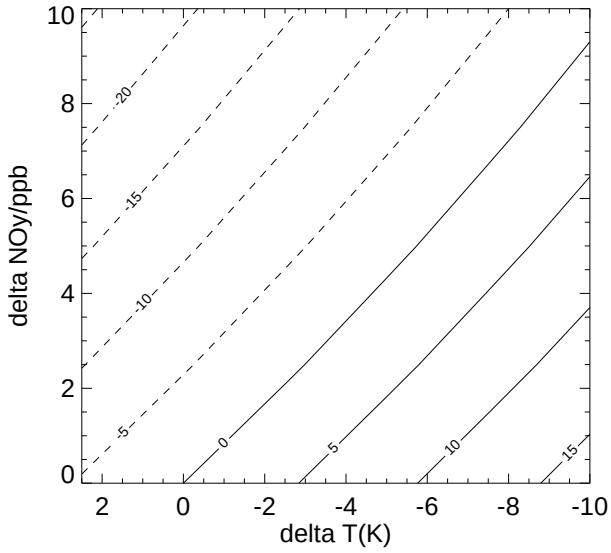

Figure 4.5: *Percentage change in ozone at 3mb, 40°N depending on* NO_y *and temperature change.*

The £gure indicates that the two effects are almost additive and that the ozone trend may be positive or negative depending on the exact scenario. The results suggest that in increase in NO_y of $\sim$5ppb at 3mb would counteract a cooling of $\sim$6K. To put these values in context, this increase

in NO_y is about 100%. About 3% of N_2O which enters the stratosphere is converted into NO_y Brasseur *et al.* (1999). If we assume that this relationship remains constant then NO_y will increase linearly with the abundance of N_2O. An N_2O increase of 100% by 2100 corresponds to the middle of estimates by the WMO (IPCC, 2001). A cooling of $\sim$6K is possible following a carbon dioxide increase of less than 100%.

The future of stratospheric ozone is, therefore, very sensitive to the future scenario that is used, and further study is required by other methods. The limitations of this approach should be noted. Ozone produced at lower levels and transported to the upper stratosphere is not taken into account. For example, additional methane may produce substantial amounts of ozone in the lower stratosphere (Randeniya *et al.*, 2002). Also, changes in ozone in the upper stratosphere have a relatively small impact on the total column as the number density is small and changes are buffered by the *self healing* effect (see section 1.4.6). The robustness of these results should be tested using a similar series of experiments using a more complex model, such as a chemistry-general circulation model. This would allow additional factors, such as dynamical or radiative changes to be included.

4.4 Chapter Summary

In this chapter a series of chemical perturbation experiments were performed. A theory for perturbation experiments was presented and applied using a chemical box model.

It was found that, after chlorine, NO_x and temperature perturbations led to the greatest change in ozone. The two perturbations were of similar magnitude and opposite in sign for perturbations of +5% NO_x and -1K. This conclusion agrees with simple considerations of reaction rates. It is concluded that the future of the ozone layer over the next century will depend strongly on the emissions path that is followed. Nitrogen species, greenhouse gases, water vapour and methane all have the potential to alter both the quantity and distribution of stratospheric ozone. These calculations suggest that further investigation is necessary to determine possible outcomes. These calculations are idealised and a chemistry-climate GCM should be used to capture further processes, such as self-healing and changes to the stratospheric circulation.

CHAPTER FIVE

IGCM-FASTOC - A Coupled Chemistry-Climate Model

This chapter will describe the formulation of a coupled chemistry general circulation model based on the FASTOC chemical parameterisation and the Reading Intermediate General Circulation Model (IGCM). The coupling of the FASTOC chemical scheme to the IGCM was carried out in conjunction with M. Bourqui and the coupled simulations were run by M. Bourqui. This chapter will also present the £rst coupled chemistry-climate experiments performed using this new model. A £fteen year timeslice experiment of 1979 conditions is performed. The model ozone is compared to observations and to other chemistry climate GCMs. As a demonstration of the model's usefulness a simulation of 2060 conditions is also carried out. This is used to explore the effects of climate change on ozone recovery. An additional experiment is performed for 2060 when changes in trace gas concentrations are not allowed to affect the radiation scheme. This "chemistry only" experiment allows some of the effects of changing dynamics and chemistry to be seperated. Changes in ozone, temperature and zonal mean zonal wind will be examined. It is emphasised that the aim of this chapter is to illustrate that FASTOC can be used as a tool for simulations of future ozone, rather than present a set of detailed calculations which were not possible in the timescale of this thesis.

5.1 The Intermediate General Circulation Model

The Reading Intermediate General Circulation Model is described brie¤y in Forster *et al.* (2000) and Rosier and Shine (2000), but some details will be given here. The model is intermediate in the sense that the physical parameterisations are simple enough to allow many long model integrations

to be performed relatively quickly, yet the physical processes have enough detail that it simulates a reasonably realistic atmosphere. For example, the wind and temperature structures are reasonable and it reproduces realistic stratospheric sudden warmings (Rosier *et al.*, 1999). The model does have problems, however. In common with many GCMs (Pawson *et al.*, 2000; Austin, 2002), it suffers from stratospheric temperatures that are too cold. Consequently, the zonal mean zonal winds in the stratosphere are also too fast. The northern polar vortex, in particular, is too strong due to cold polar temperatures. The IGCM is a spectral model based on that described by Hoskins and Simmons (1975). The radiation scheme is based on that of Morcrette (1991) which includes water vapour, carbon dioxide, ozone and some minor species, as well as clouds. Gravity wave drag is parameterised by a simple *Rayleigh Friction* type scheme. Non-orographic gravity wave drag is not included. In the work reported here it is run at T21 horizontal resolution (roughly $5^\circ \times 5^\circ$lat-long) with 26 levels vertical levels from the surface to 0.1mb and around 14 levels in the middle atmosphere. The coarse horizontal resolution does not preserve sharp gradients of tracers and may lead to other dynamical problems, but is computationally cheap. Spectral advection is used, which is not positive de£nite and may not be locally conservative. Sea surface temperatures are £xed, reducing the freedom of the model to develop its own background state.

The IGCM has previously been used to investigate the effect of ozone trends on stratospheric temperature and circulation (Rosier *et al.*, 1999; Rosier and Shine, 2000). In these experiments the three dimensional monthly mean ozone climatology of Li and Shine (1995) was used, along with trends taken from Randell and Wu (1999). In that version of the model no chemical scheme was included so it was not possible to simulate chemistry-climate interactions.

5.2 IGCM-FASTOC

The coupling between chemistry and dynamics in this CGCM is achieved by including the calculated ozone in the radiative and chemical schemes and by the advection of chemical species by the dynamical model. As in the case of the radiation scheme in the IGCM, the chemical source term is calculated once per day. The IGCM has 64 dynamical timesteps per day so $\frac{1}{64}$ of the chemical source is added at each timestep in order to aid stability. O_x, NO_x, N_2O_5 and HNO_3 are calculated by FASTOC and advected by the IGCM. H_2O, CH_4, N_2O and CO are £xed as seasonally varying three-dimensional climatologies. Data for CH_4, stratospheric water vapour, HNO_3 and N_2O are taken from the UARS data set from the HALOE, CLAES and MLS instruments. Details may be found in Randel *et al.* (1998). Data for CO, N_2O_5 and NO_x are taken from a SLIMCAT chemi-

cal transport model reference atmosphere*. The ozone climatology was appropriate for 1979 and taken from Li and Shine (1995). An aerosol climatology may also be used. This monthly averaged data was derived from the satellite instruments SAGE I, SAGE II, SAM I and SME I over the period 1979-1997 by the NASA Langley Research Center (M. Bourqui, personal communication).

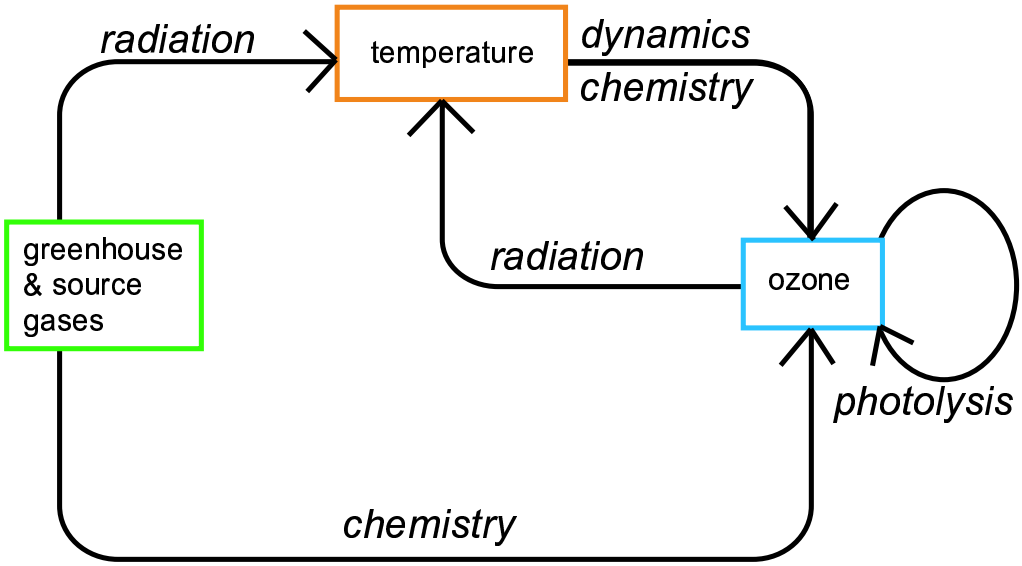

Figure 5.1: *Chemistry climate interactions included in FASTOC-IGCM. Changes in atmospheric gases have chemical and radiative effects; temperature changes have a chemical effect on ozone and affect dynamics; ozone perturbations affect temperature and have a feedback on the ozone column through the "self-healing" effect.*

This con£guration of the model allows several important interactions to be investigated, as represented in £gure 5.1. Trends in greenhouse gases and chemical source gases may be speci£ed. The resulting temperature changes affect ozone through both dynamics and chemistry. The changes in circulation, however, do not affect the distribution of the speci£ed species. If the Brewer-Dobson circulation were to speed up, as suggested by Butchart *et al.* (2000), the distribution of long lived species, such as N_2O and CH_4, would be altered, leading to changes in the production of NO_x and HO_x. If chlorine species were included and advected in the model they may be removed from the stratosphere more quickly by this mechanism, hastening ozone recovery (Butchart *et al.*, 2000). These feedbacks would not be simulated by this model. The advantage of this method is that it is computationally ef£cient as fewer species need to be calculated and advected. Similarly, changes in stratospheric water vapour and aerosol loading may be simulated, but the advection of these is not included. Thus, for example, the location of a volcanic eruption is not taken into account. Source gases also have an indirect radiative impact on ozone by chang-

*Available from the British Atmospheric Data Centre, http://www.badc/rl.ac.uk/data/slimcat/slimutils/metadata.html

ing temperature, and this will also be captured by the model. Ozone perturbations can also feed back onto the temperature and on the ozone below by absorbing UV and slowing the photolysis of oxygen below.

5.2.1 A Modelling Problem

A serious problem was found with the initial con£guration of the model. At about 2mb at high latitudes during autumn FASTOC calculated a massive unrealistic increase in O_x and HNO_3 and a corresponding fall in NO_x. The ozone problem is shown in £gure 5.2. Although the effect on the ozone column was initially small due to the low pressure, it was advected downwards and poleward leading to errors in this important region. This problem is almost certainly due to the importance of high order interactions here. As noted in chapter 3, the FEOM method assumes that only low order correlations between variables are important. Here, more than three variables are strongly coupled, leading to a poor simulation be FASTOC.

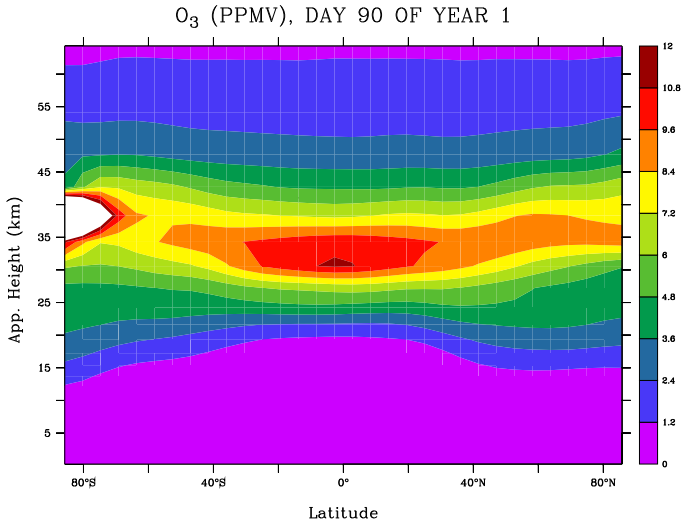

Figure 5.2: *Latitude height plot showing unrealistic ozone production in the upper stratosphere. during autumn. High values of ozone above 2mb are advected downwards and polewards.*

The £rst simulations reproted here, therefore, use chemistry from pole to pole and from the tropopause to 4mb. From 4mb to the model top at around 0.1mb the chemical species are relaxed towards climatological values with a timescale of 1 day. This method re¤ects the fast

chemistry at this level and avoids the problems mentioned in above. The drawback of this is that it constrains the model and does not allow the simulation of ozone trends above this. It is worth noting that all but about 97% of the ozone column is below 4mb, so the model is calculating the majority of that total column. The method used is not dissimilar to that used in UMETRAC (Austin, personal communication). In that model the chemistry is used up to 0.3mb, above which the family assumptions used (see section 1.4.5) are invalid. Above this level the mixing ratios are varied from the highest calculated mixing ratio to a £xed value at the model top using a prede£ned function. Note also that the ECHAM/CHEM (Schnadt *et al.*, 2002) model has a model top at 10mb, so is not capable of simulating anything above the middle stratosphere.

5.3 First Multi-Year Integrations

In this section a series of preliminary experiments using the IGCM-FASTOC model are described. Fifteen year timeslice experiments were performed for 1979 and for 2060 conditions under the WMO A2 scenario (WMO, 1999). These runs illustrate the performance of the model and its application in examining the future of the stratospheric ozone layer. As 1979 had, and 2060 is predicted to have, low anthropogenic halogen loading they are suitable for comparison with a non-halogenated model. A transient run would not be appropriate as the dip in global ozone during the 20th and 21st centuries due to halogens would be missing. Such a run would be a hypothetical case examining what might have happened if CFCs had not been emitted. Additionally a run was performed where changes in atmospheric gases in 2060 were only allowed to affect the chemical calculations. The radiation scheme used the same N_2O, CH_4 and CO_2 as the 1979 run, but did use the calculated 2060 ozone. Annually repeating, zonally and monthly averaged, conditions were used for greenhouse and source gases. The initial mixing ratios of chemical species used in these experiments are zonal averages (provided by M. Bourqui). Table 5.1 shows the mixing ratios of the well-mixed species and the source of the other climatological species used in the 1979 and 2060 experiments.

All simulations began with a three-year spin-up period using £xed chemical species. The following years had chemistry coupled to dynamics through the use of the calculated ozone in the radiative scheme and in the chemical calculations. Long experiments are needed for timeslice studies in order to determine whether changes are signi£cant. This is particularly important for highly variable regions such as the northern high latitudes.

Species	**1979**	**2060**
CO_2	335.8ppm	580.0ppm
CFC11	152.4ppb	101.0ppb
CFC12	271.8ppb	328.0ppb
CH_4	UARS	1979$\times$1.8
N_2O	UARS	1979$\times$1.3
CO	SLIMCAT	1979$\times$1.8
H_2O	UARS	1979$\times$1.0

Table 5.1: *Climatological species in 1979 and 2060 runs.* CO_2 *and the CFCs are considered to be well mixed with a £xed value everywhere. Note that the CFCs are used only in the radiation scheme. Other species have monthly varying climatologies (see text) and are multiplied by a given factor for the 2060 runs.*

5.3.1 1979 Interactive Experiment

Figure 5.3 shows the IGCM-FASTOC ozone column for £fteen years. It is clear that the model is stable and shows no signi£cant drift. This is vitally important if the model is to be used for simulations lasting many decades. Furthermore, it is a major achievement that the the coupled model maintains a realistic atmosphere throughout the simulation. Steil *et al.* (1998) state that a coupled model may not have a "stable tracer distribution" or produce "physically reasonable results", yet this model achieves both of these things.

An average of the £fteen year ozone column is given in £gure 5.4. For comparison, £gure 5.5 shows climatological values for the same year (Li and Shine, 1995), and the relative difference is given in £gure 5.6. The ozone column is generally realistic at all latitudes. Polar ozone is greatest in winter and spring with more ozone in the north than in the south. Also the southern hemisphere has a winter polar minimum, while the northern does not. The low ozone columns in the tropics are clearly seen and the annual cycle is correct.

There are, however, differences between the model ozone and observations. There is typically up to 10% too much ozone over most of the globe, except in the northern hemisphere polewards of about 30°N. This is partly due to the model's cold bias and partly due to the effect of halogen species in the observations, not captured by this version of the model. In the northern spring the maximum ozone column is displaced away from the pole at around 60°N, rather than at the pole as in the observations. The maximum column obtained is also lower in the model by about 20% or 50 DU. This suggests that the polar vortex is too strong, leading to descent away from the pole, as occurs in the southern hemisphere in observations. This is associated with polar temperatures which are too cold, which is a common problem in GCMs. In the southern hemisphere the spring maximum ozone column near the pole is of the correct magnitude, but the high values form a more elongated feature than in observations. Additionally, the vortex forms and breaks up too early compared to observations. The winter southern polar minimum is present, but not low enough, suggesting that too much descent is occuring here. The autumn minima are also not as deep in the simulation as in the observations, the ozone being 25-30% too high here.

Another important test is to compare this model to other similar models. The ozone climatology produced by IGCM-FASTOC is very good compared to other, more complex and costly, CGCMs. The problems in the pattern of the ozone column in the zonal average are typical of such models. The displacement of the northern hemisphere maximum is seen in ECHAM3/CHEM (Steil *et al.*, 1998), the CCSR/NIES model (Takigawa *et al.*, 1999) and CMAM (de Grandpré

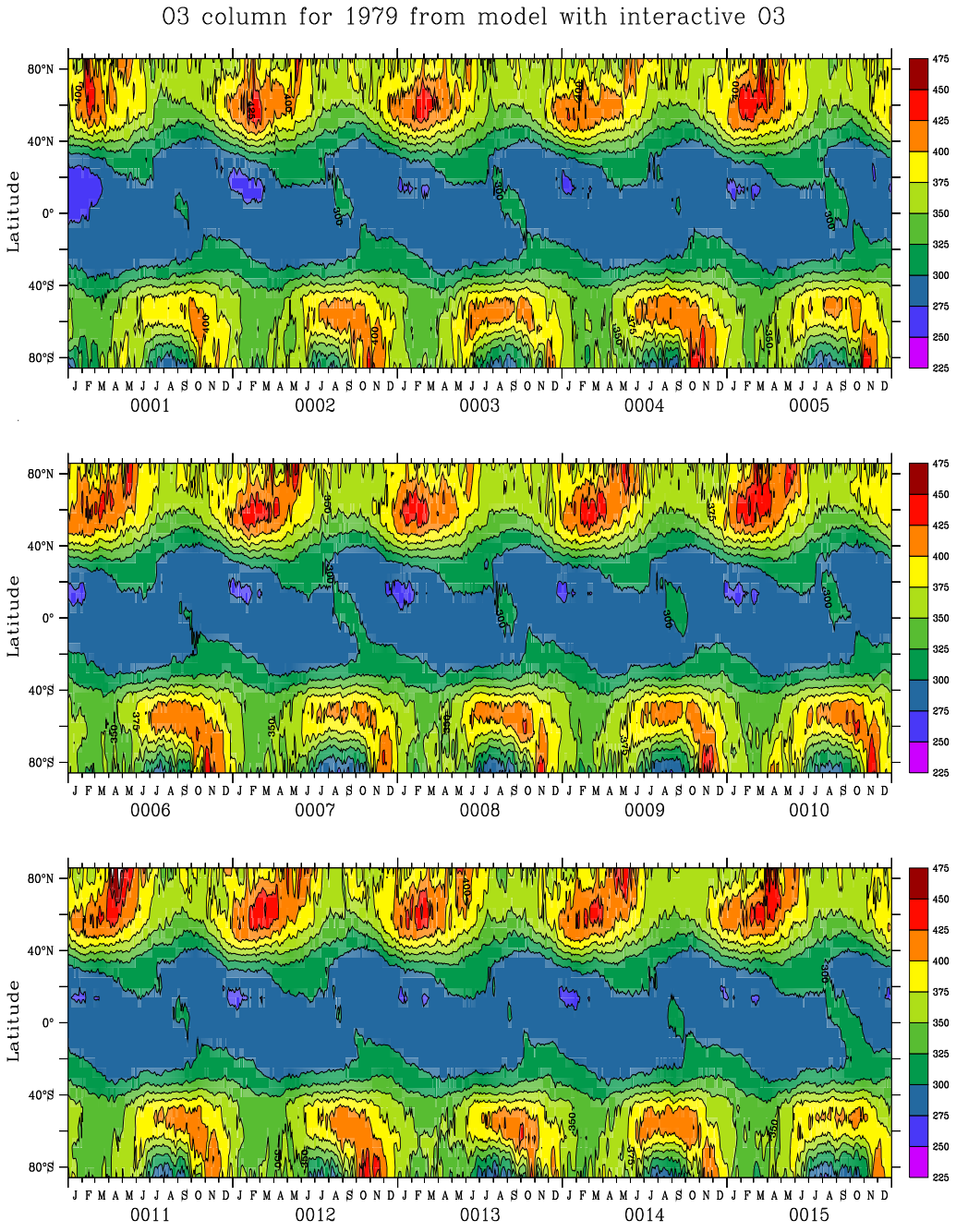

Figure 5.3: *Latitude time plot of the ozone column in Dobson Units for the 1979 run.*

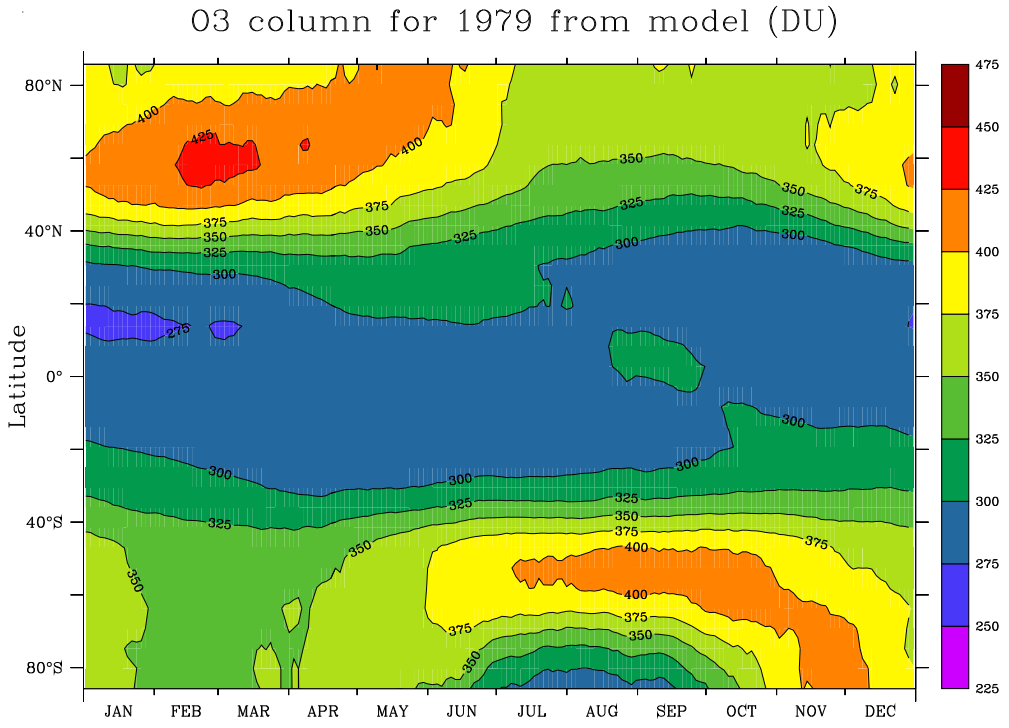

Figure 5.4: *Latitude time plot of the average annual cycle of ozone column in Dobson Units for the 1979 model run.*

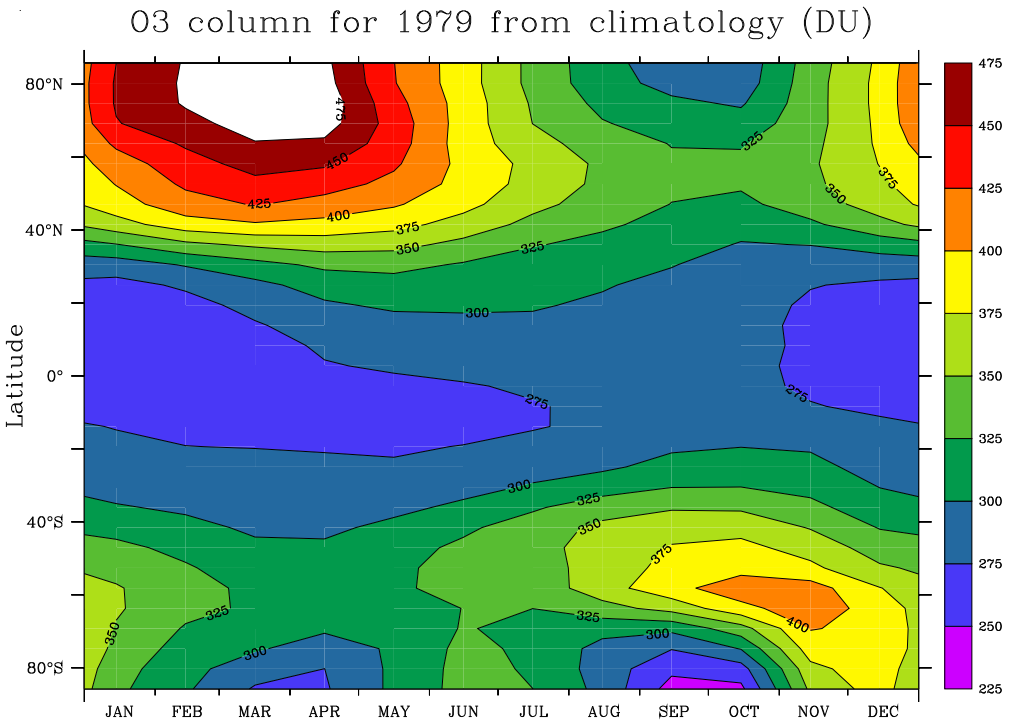

Figure 5.5: *Latitude time plot of the average annual cycle of ozone column in Dobson Units for the 1979 model run (top) and climatology (bottom).*

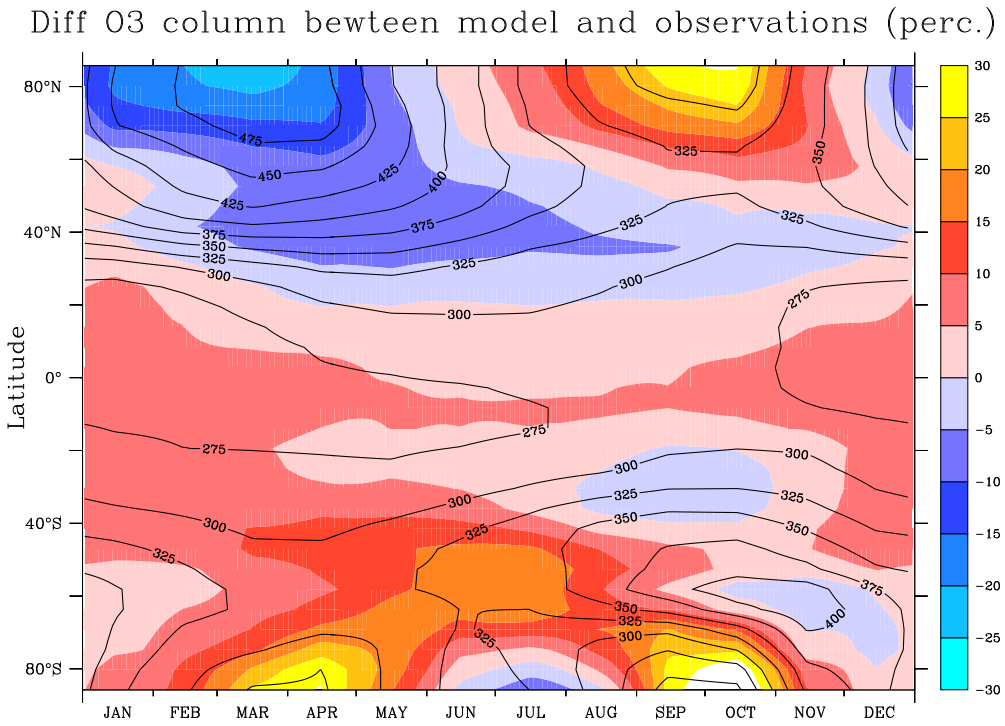

Figure 5.6: *Latitude time plot of the difference between model simulation of 1979 ozone column and observations in percent (bottom).*

et al., 2000). All of these models also have stretched southern hemisphere spring maxima, and only CMAM simulates the autumn polar minima. CMAM also has the correct tropical column, while that of ECHAM3/CHEM is about 25 DU too high and that of CCSR/NIES is about 25DU too low.

When using a three dimensional model, the zonal assymetries also need to be considered. Figure 5.7 shows total ozone over the northern hemisphere in observations and in some chemistry climate GCMs, including IGCM-FASTOC. It should be noted that, although the time period of the observations and individual model runs varies, all except IGCM-FASTOC include halogen chemistry and periods of high halogen loading. These means the observations and other models should have slightly more ozone than does IGCM-FASTOC. UMETRAC, CCSR/NIES, CMAM and IGCM-FASTOC simulate the correct maximum column of about 450 DU, although it is not positioned correctly in CMAM. MAECHAM/CHEM have over 500 DU and ULAQ has only just over 400 DU. It is clear that the pattern of northern hemisphere ozone in IGCM-FASTOC is very realistic, and is better than many other models. This excellent result for IGCM-FASTOC lends con£dence to model predictions of northern hemisphere ozone change.

The southern hemisphere total ozone cannot be compared to the models in Austin (2002) because it does not include halogens, so does not simulate an ozone hole. For information, it is shown for October in £gure 5.8. As noted earlier, there is too much ozone in the southern hemisphere at this time.

Another measure of the model performance compared to other models is the hemispheric mean total ozone. This is shown for observations, IGCM-FASTOC and other models in tables 5.2 and 5.3. In common with other models, IGCM-FASTOC has too much ozone in both hemispheres. Some of this is attributed to dynamical and chemical problems, and some to the neglect of halogen chemistry. IGCM-FASTOC is, however, one of the better models despite its relatively low resolution and parameterised chemical scheme. Overall, IGCM-FASTOC compares very well with both observations and other models by this metric.

Finally, the zonal mean ozone mixing ratios are also quite realistic. Figures 5.9 and 5.10 show the calculated and observed ozone mixing ratios respectively. The shape of the cross section is broadly correct, with a maximum of 10-11ppm, compared to 9-10ppm in observations. These maximum values occur at the correct altitude, between 30 and 35km. The high ozone mixing ratios, however, spread to the midlatitudes, whereas in reality they are con£ned to the tropics. The IGCM-FASTOC results also look good compared to the results of Takigawa *et al.* (1999).

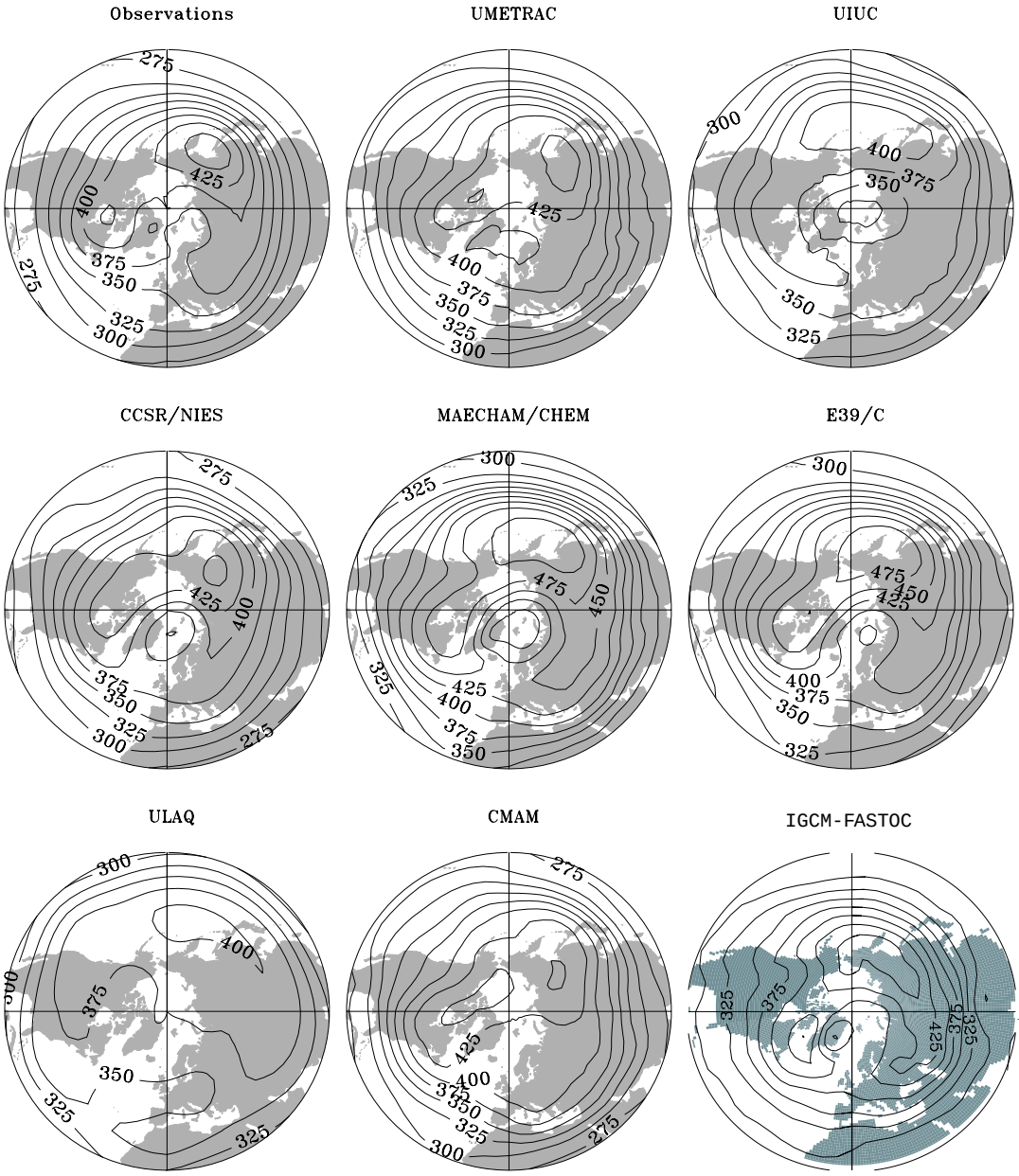

Figure 5.7: *Total ozone over the northern hemisphere in March in observations and a selection of CGCMs. Figure taken from Austin (2002) and IGCM-FASTOC £gure in bottom right position added. For further details of the observations and model runs, see Austin (2002)*

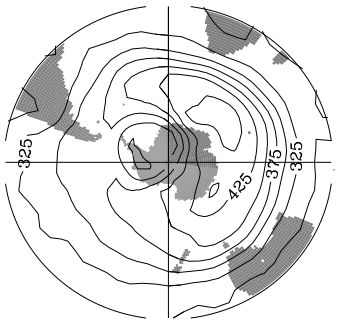

Figure 5.8: *Total ozone over the southern hemisphere in October in IGCM-FASTOC.*

March, NH	**Total Ozone/DU**	**△(%)**
Observations	318.0	-
IGCM-FASTOC	334.8	+5.0
UMETRAC	339.9	+6.9
CMAM	338.0	+6.3
MAECHEM/CHEM	371.8	+16.9
ECHEM4/CHEM	351.2	+10.4
UIUC	322.6	+1.4
CCSR/NIES	326.1	+2.5
ULAQ	337.6	+6.2

Table 5.2: *Area weighted monthly mean total ozone for observations, IGCM-FASTOC and other models for the northern hemisphere in March, and percentage difference between models and observations. Data for observations and models taken from Austin (2002). The observations were taken from satellite data for the period 1993-2000. As halogens are not included in IGCM-FASTOC the ozone should be higher in that model than in observations.*

October, SH	Total Ozone/DU	△(%)
Observations	291.0	-
IGCM-FASTOC	340.0	+16.8
UMETRAC	337.8	+16.0
CMAM	324.3	+11.4
MAECHEM/CHEM	349.0	+19.9
ECHEM4/CHEM	301.7	+3.6
UIUC	277.2	-4.8
CCSR/NIES	318.2	+9.3
ULAQ	314.8	+8.1

Table 5.3: *As for table 5.2, but for the southern hemisphere in October.*

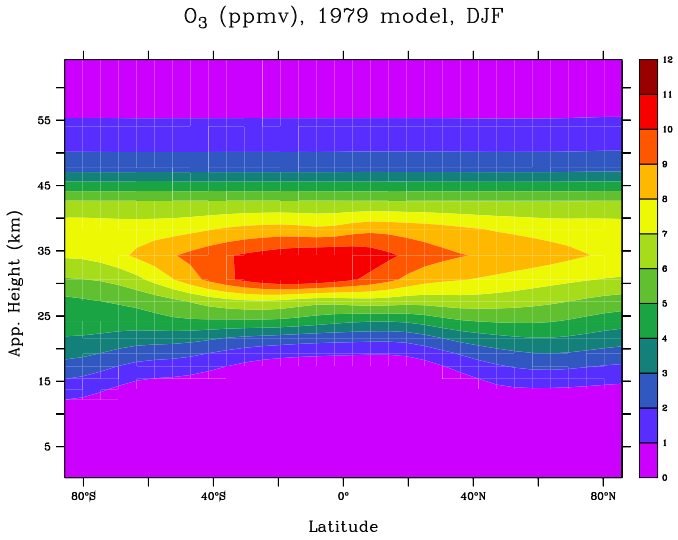

Figure 5.9: *Latitude height plot of ozone mixing ratio in ppm for DJF in 1979 from IGCM-FASTOC.*

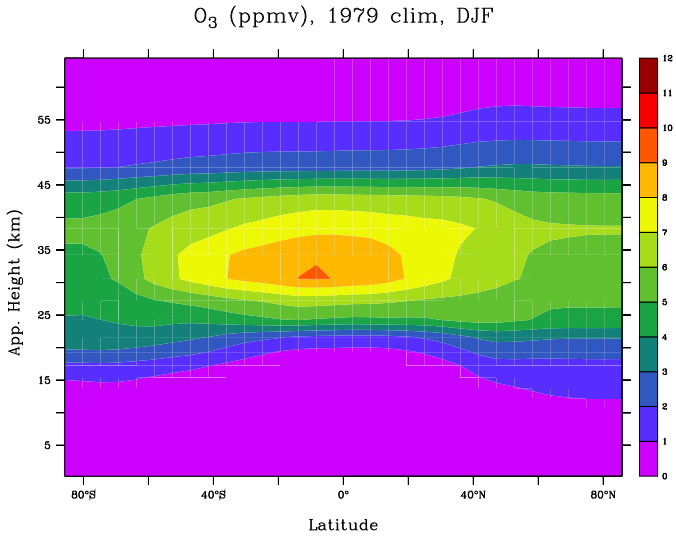

Figure 5.10: *Latitude height plot of ozone mixing ratio in ppm for DJF in 1979 from observations*

The ozone maximum in their CCSR/NIES model is at the correct altitude and is con£ned to the tropics, but reaches values of greater than 12ppm. As noted earlier, too high ozone values in IGCM-FASTOC should be expected due to the neglect of halogens in this version of the model. It is likely, however, that the model is generally overestimating ozone production.

Overall, IGCM-FASTOC produces a good ozone climatology that compares well with observations and other models. In addition, it is stable over long integrations which is crucial for climate change experiments.

5.3.2 2060 Experiments

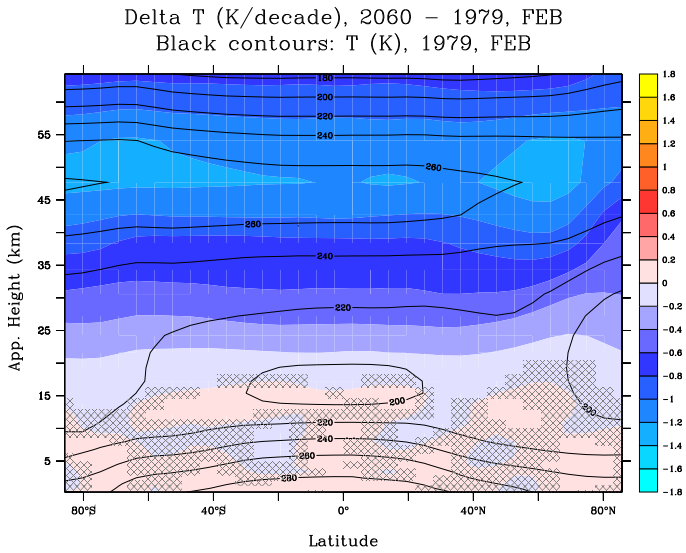

Figure 5.11: *Temperature difference between 1979 and 2060 simulations (colours) in K/decade for February. The temperature in 1979 is also shown (black contours). Shading signi£es regions that are not signi£cant to the 95% con£dence level.*

These model integrations used the A2 scenario for atmospheric gases from WMO (1999). This scenario has increased CO_2, N_2O, CH_4 and CO, as shown in table 5.1. H_2O was kept constant. Increasing N_2O will increase NO_x, enhancing ozone depletion particularly in the upper stratosphere. The extra methane will provide additional HO_x but will also be a source of O_x in the lower stratosphere. Increasing CO_2 will have a cooling effect, reducing the rate of ozone loss, while increases in ozone lead to localised heating. The net effect on temperature, shown in £gure

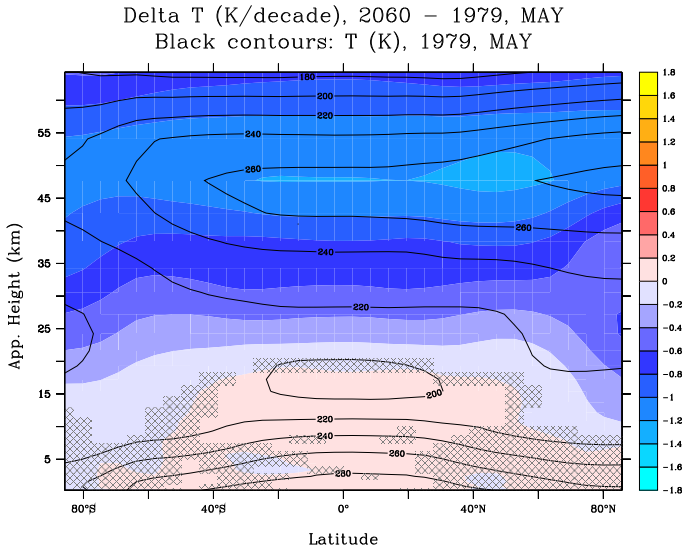

Figure 5.12: *Temperature difference between 1979 and 2060 simulations (colours) in K/decade for May. The temperature in 1979 is also shown (black contours). Shading signi£es regions that are not signi£cant to the 95% con£dence level.*

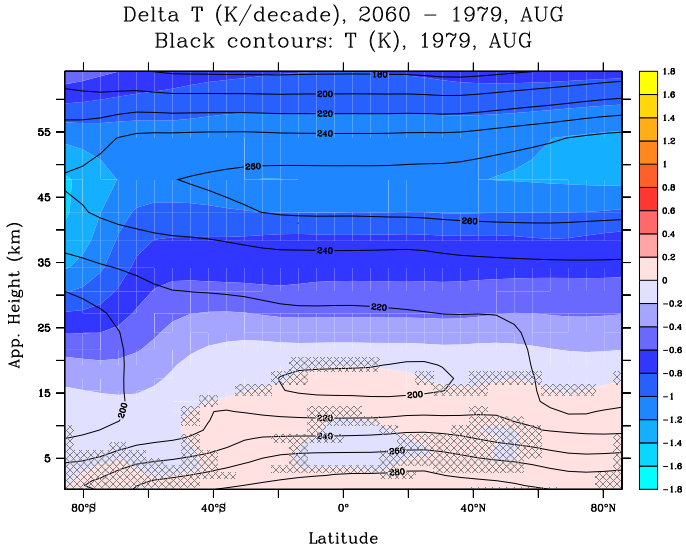

Figure 5.13: *Temperature difference between 1979 and 2060 simulations (colours) in K/decade for August. The temperature in 1979 is also shown (black contours). Shading signi£es regions that are not signi£cant to the 95% con£dence level.*

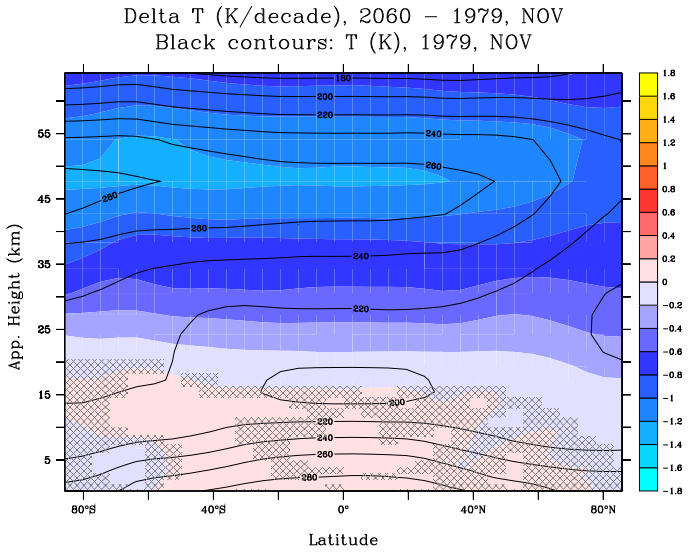

Figure 5.14: *Temperature difference between 1979 and 2060 simulations (colours) in K/decade for November. The temperature in 1979 is also shown (black contours). Shading signi£es regions that are not signi£cant to the 95% con£dence level.*

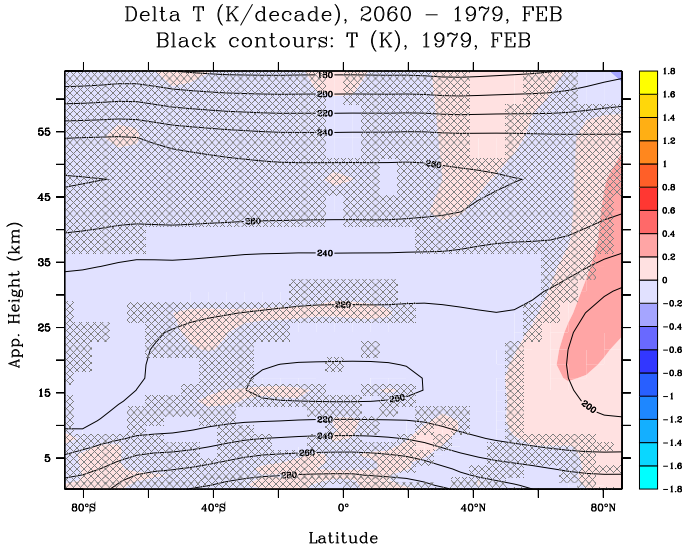

Figure 5.15: *Temperature difference between 1979 and 2060 "chemistry only" simulations (colours) in K/decade for February. The temperature in 1979 is also shown (black contours). Shading signi£es regions that are not signi£cant to the 95% con£dence level.*

5.11,5.12,5.13 and 5.14, is a signi£cant cooling throughout the stratosphere, with a maximum of greater than 1.2K/decade near 50km in the winter hemisphere. Note that above about 35km ozone is £xed so the change is mainly due to CO_2. Cooling in the region where chemistry is calculated, below 4mb, is generally less than 0.8K/decade. This gives a maximum change of about -6.5K between 1979 and 2060. The changing pattern of heating caused by ozone and greenhouse gas perturbations leads to changes in latitudinal temperature gradients, which cause changes in the zonal wind. Although the effect of CO_2 on temperature is much bigger than that of ozone, these zonal mean zonal wind changes are mainly due to the ozone perturbations. Temperature changes in the "chemistry only" run are small (see £gure 5.15), but the changes in latitudinal gradient and therefore zonal winds are similar to the "full" run.

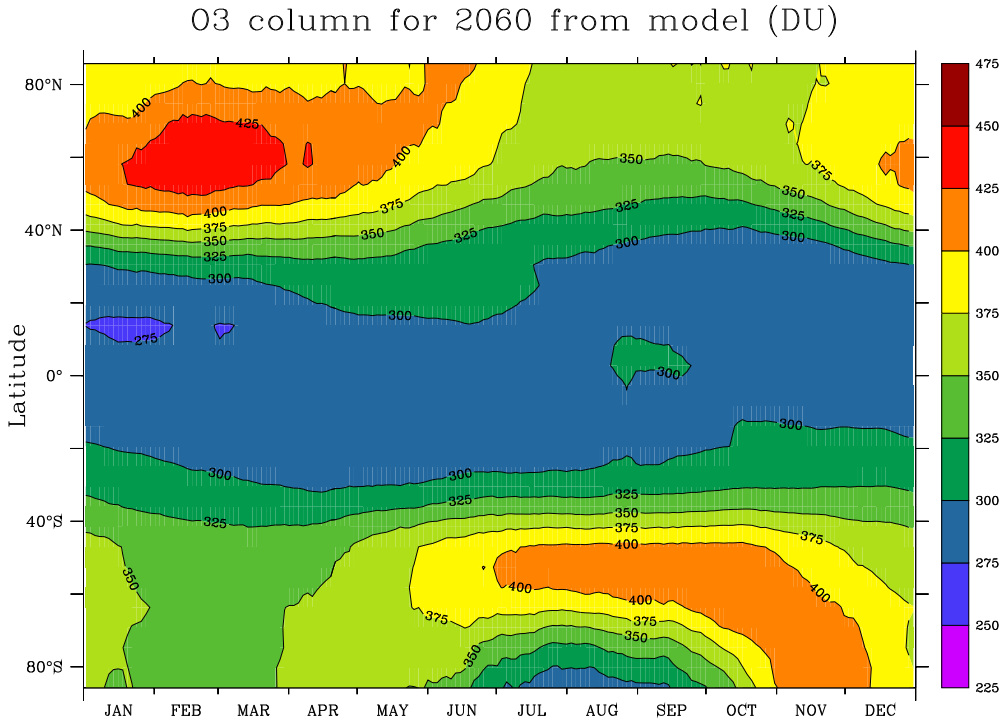

Figure 5.16: *Latitude time plot of average 2060 ozone column in DU*

The mean ozone column for £fteen years is shown in £gure 5.16. Figure 5.17 shows the 2060-1979 column and indicates that the ozone column in the tropics has decreased, but only by less than 0.5 DU/decade. In both hemispheres the ozone column has increased in the midlatitudes in winter and spring. There are maxima of greater than 2 DU/decade in February and November in the northern and southern hemispheres respectively. In terms of mixing ratio (see £gure 5.18) the changes occur mainly between 30 and 40km. A clearer picture, however, is given when the number density of ozone in considered, as will be done in the remainder of this discussion, as the

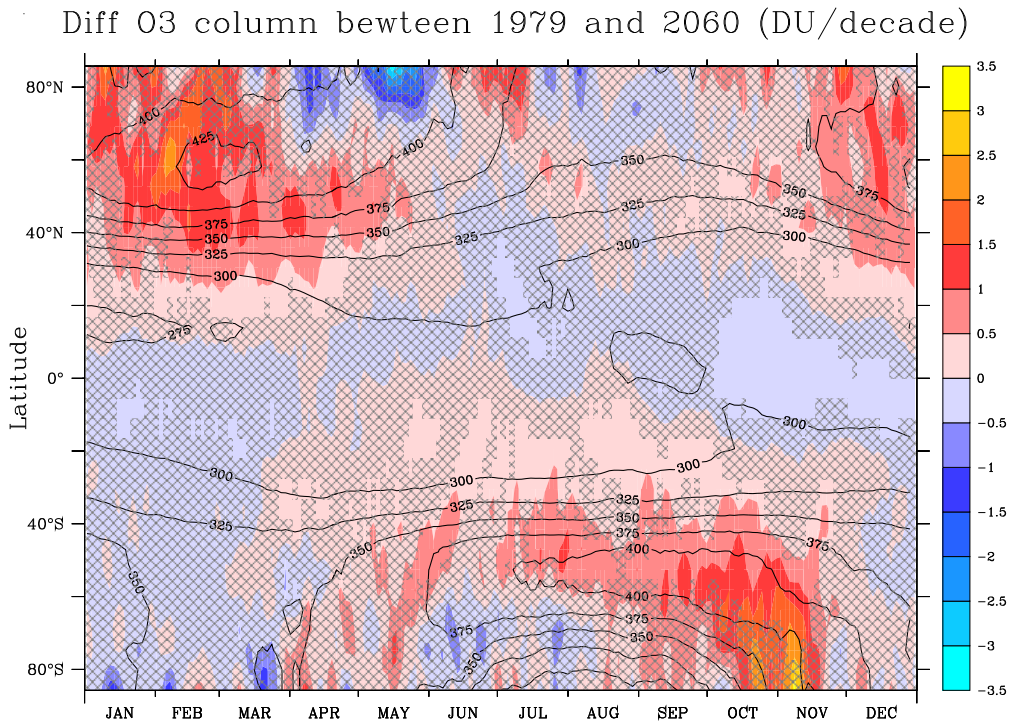

Figure 5.17: *Latitude time plot of the difference in ozone column between the 1979 and 2060 experiments in DU/decade (colours) and the 1979 ozone column (black contours). Shading indicates changes that are not signi£cant to the 95% con£dence level.*

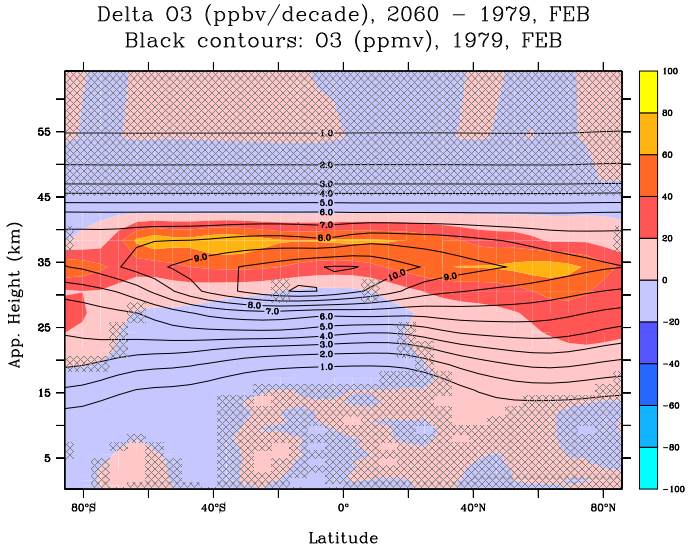

Figure 5.18: *Ozone mixing ratio difference between 1979 and 2060 simulations in ppb/decade (colours) for February. The mixing ratio in ppm for 1979 is also shown (black contours). Shading signi£es regions that are not signi£cant to the 95% con£dence level.*

vertical integral of this gives the total ozone column. An ozone increase above about 30km is the net effect of increasing NO_x and cooler temperatures. The idealised study in chapter 4 predicted a 6% increase in ozone for a 6K temperature decrease and a 6% decrease in ozone for a 30% NO_x increase. The overall increase in ozone seen in the CGCM experiments may be due to the increase in methane in this run. Randeniya *et al.* (2002) found that methane was an important source of O_x in the lower stratosphere of their model. Below this, a net ozone decrease results from increasing NO_x and reverse "self-healing". Ozone loss is also increased in the polar lower stratosphere. This, however, is ameliorated by dynamical changes and the fact that the air descending is more ozone rich than that in 1979. The hemispheric and global average total ozone columns are shown in table 5.4. There is a small increase in the 2060 run in both hemispheres, and a large decrease in the "chemistry only" run. The difference between the two 2060 simulations is caused by the effect of the cooler temperatures in the full run. The effects of increasing NO_x and decreasing temperature are not additive, as calculated in the simple experiments in chapter 4, when a global calculation is made. As noted in chapter 4, when the total column is considered there is a negative feedback on any upper stratospheric change due to "self-healing".

Experiment	**Global/DU**	**△(%)**	**NH/DU**	**△(%)**	**SH/DU**	**△(%)**
1979	323.9	-	323.0	-	324.7	-
2060	325.4	+0.5	324.8	+0.6	326.0	+0.4
2060 "chem. only"	319.9	-1.2	319.2	-1.2	320.6	-1.3

Table 5.4: *Area weighted mean total ozone for IGCM-FASTOC in 1979 and 2060 experiments. Also shown is the percentage change from the 1970 experiment.*

The high latitude changes are now examined in more detail for February, May, August and November.

In February the temperature gradient from equator to pole decreases in the north (see £gure 5.11), weakening the polar vortex (see £gure 5.19). The rate of descent, therefore, increases as the barrier to mixing is reduced. Ozone rich air is then brought downwards and polewards, as shown in £gure 5.20. This can also be seen in the total column, as shown in £gure 5.21. In the southern hemisphere, ozone loss is increased in the lower stratosphere. This is also seen in the "chemistry only" experiment (£gure 5.22), showing this lower stratospheric change to be chemical. As the temperature change in the lower stratosphere in both experiments is small, the depletion must be due to the increase in NO_x.

In May the change in zonal mean zonal wind in the northern hemisphere (see £gure 5.23)

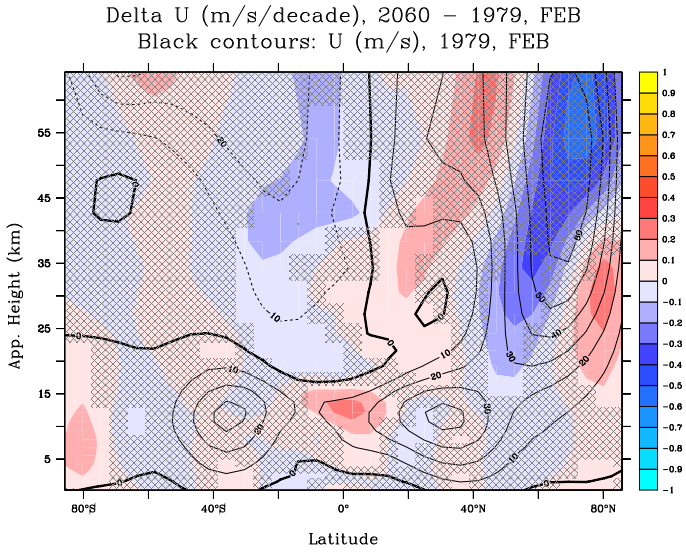

Figure 5.19: *Latitude height plot of the change in February mean zonal mean zonal wind from 1979 to 2060 (colours) in m/s/decade. Also shown is the zonal mean zonal wind in 1979 (black contours) in m/s.*

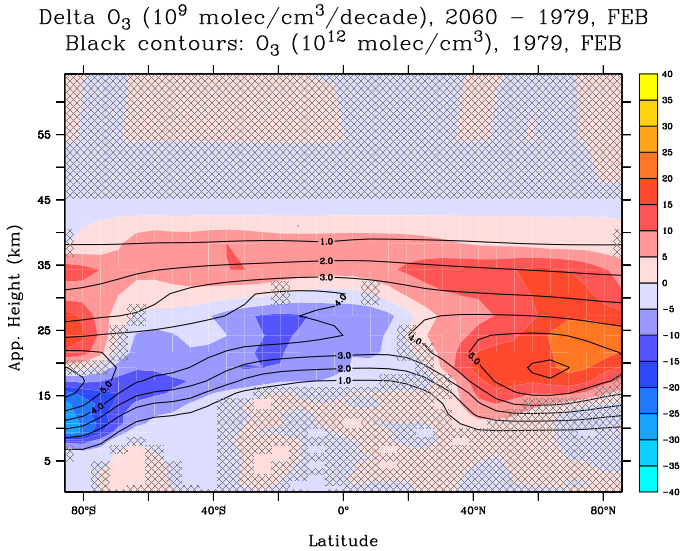

Figure 5.20: *Ozone concentration difference between 1979 and 2060 simulations in 10^9 molecules/cm^{-3}/decade (colours) for February. The concentration in 1979 is also shown (black contours). Shading signi£es regions that are not signi£cant to the 95% con£dence level.*

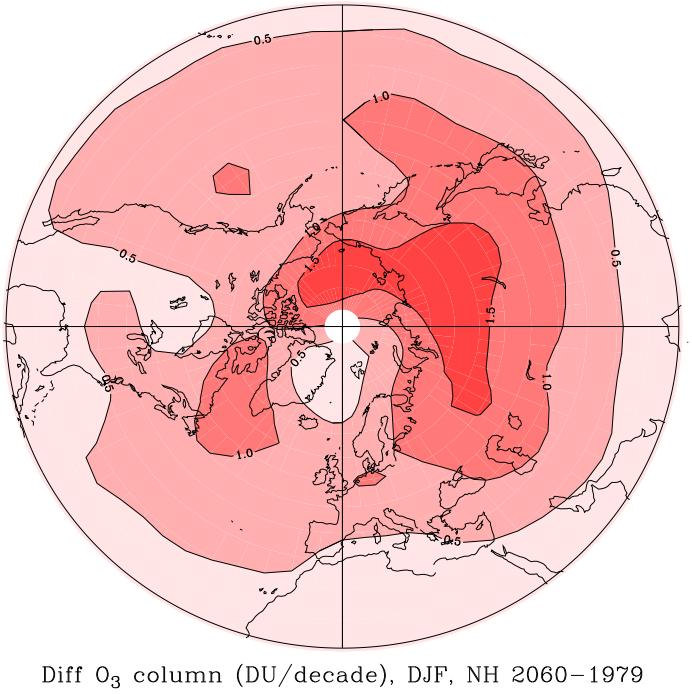

Figure 5.21: *Change on ozone column in DJF from 1979 to 2060 over the northern hemisphere.*

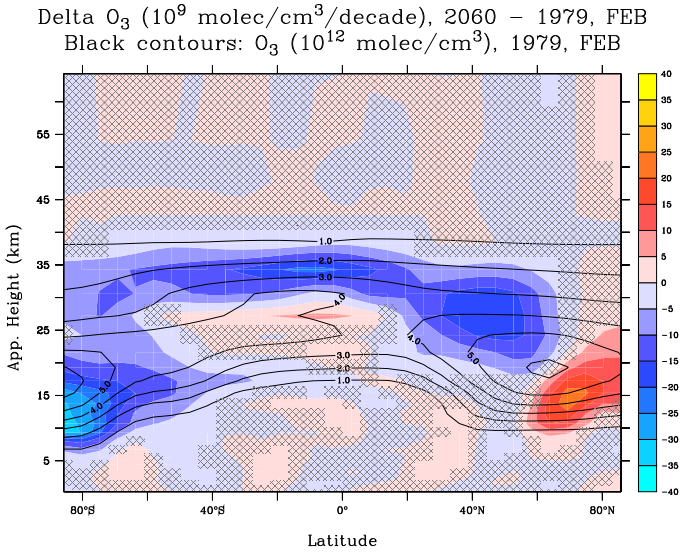

Figure 5.22: *Ozone concentration difference between 1979 and 2060 "chemistry only" simulations in 10^9 molecules/cm^{-3}/decade (colours) for February. The concentration in 1979 is also shown (black contours). Shading signi£es regions that are not signi£cant to the 95% con£dence level.*

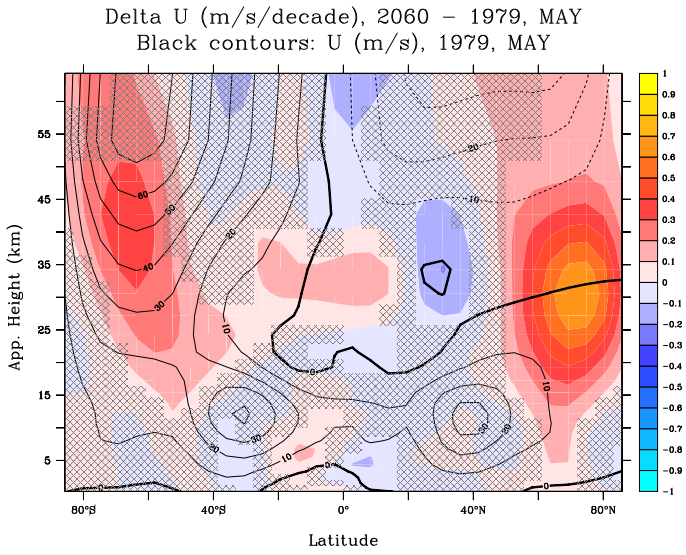

Figure 5.23: *Latitude height plot of the change in May mean zonal mean zonal wind from 1979 to 2060 (colours) in m/s/decade. Also shown is the zonal mean zonal wind in 1979 (black contours) in m/s.*

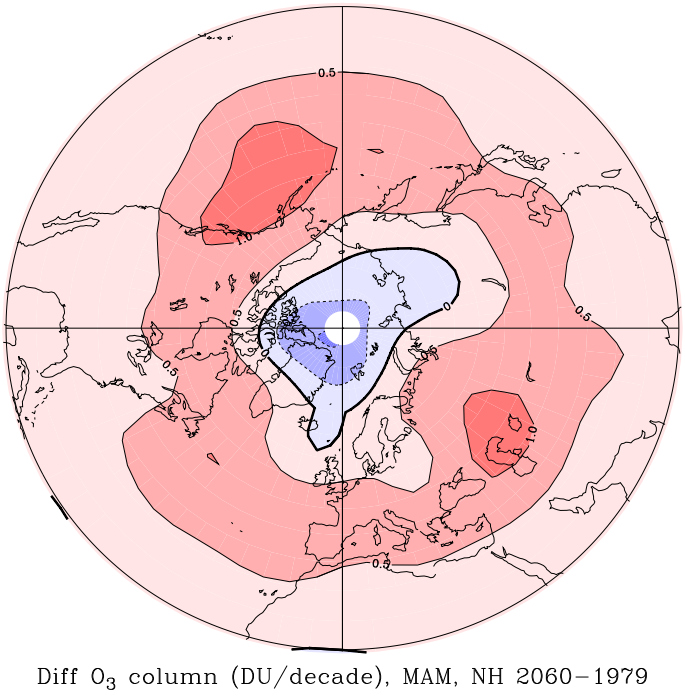

Figure 5.24: *Change on ozone column in MAM from 1979 to 2060 over the northern hemisphere.*

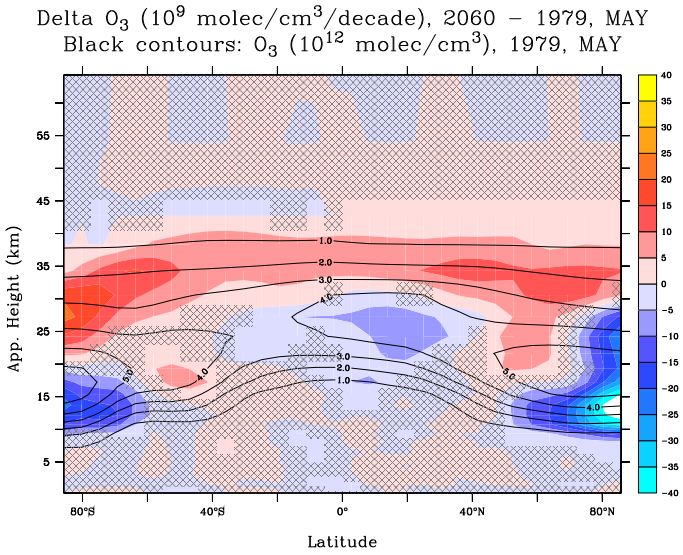

Figure 5.25: *Ozone concentration difference between 1979 and 2060 simulations in 10^9 molecules/cm^{-3}/decade (colours) for May. The concentration in 1979 is also shown (black contours). Shading signi£es regions that are not signi£cant to the 95% con£dence level.*

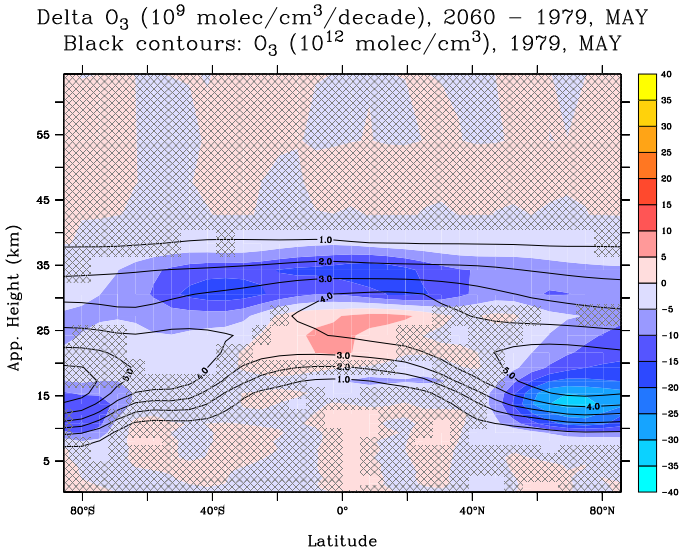

Figure 5.26: *Ozone concentration difference between 1979 and 2060 "chemistry only" simulations in 10^9 molecules/cm^{-3}/decade (colours) for May. The concentration in 1979 is also shown (black contours). Shading signi£es regions that are not signi£cant to the 95% con£dence level.*

resembles a vortex structure, suggesting that the vortex is frequently more persistent at this time. This is con£rmed by the change in northern hemisphere ozone column (see £gure 5.24), where the pole has become more isolated. This also isolates the additional ozone loss caused by increased NO_x. Similarly, in the southern hemisphere the vortex is stronger, associated with a reduced amount of descent and allowing chemical ozone loss to persist in the lower polar stratosphere (£gure 5.25). The chemical nature of the change is con£rmed by the same feature in the "chemistry only" run, shown in £gure 5.26

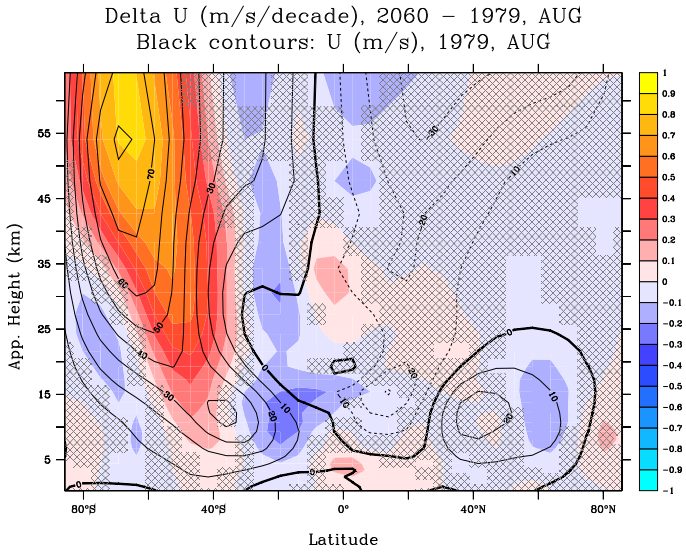

Figure 5.27: *Latitude height plot of the change in August mean zonal mean zonal wind from 1979 to 2060 (colours) in m/s/decade. Also shown is the zonal mean zonal wind in 1979 (black contours) in m/s.*

In August, in the northern hemisphere the zonal mean zonal winds are virtually unchanged in 2060 (£gure 5.27) so the upper stratospheric ozone increase and the lower stratospheric ozone decrease (£gure 5.28) are predominately chemical changes. The southern hemisphere vortex is a few metres per second stronger. This inhibits the descent of ozone rich air, leading to the low ozone values in the polar lower stratosphere shown in £gure 5.28 and smaller column shown in £gure 5.29.

In the northern hemisphere in November (see £gure 5.30) the vortex is shifted slightly polewards, but the increase is ozone seen in £gure 5.31 in the upper stratosphere is caused by the cooling. The southern hemisphere vortex is gone by this time (see £gure 5.30), but winds are

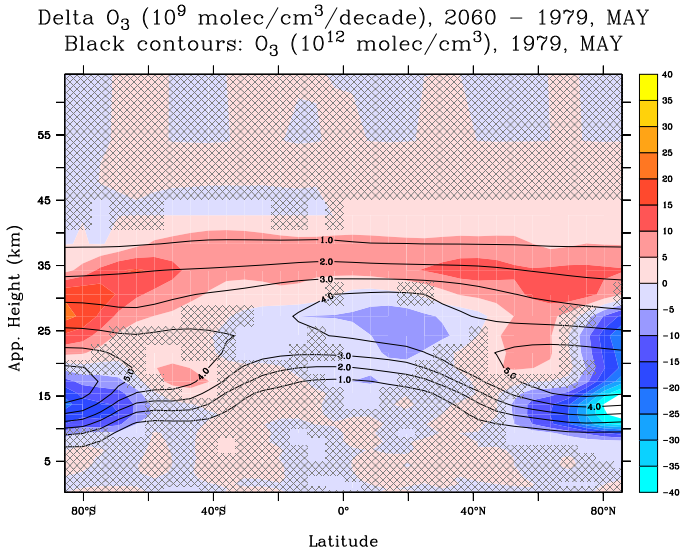

Figure 5.28: *Ozone concentration difference between 1979 and 2060 simulations in 10^9 molecules/cm^{-3}/decade (colours) for August. The concentration in 1979 is also shown (black contours). Shading signi£es regions that are not signi£cant to the 95% con£dence level.*

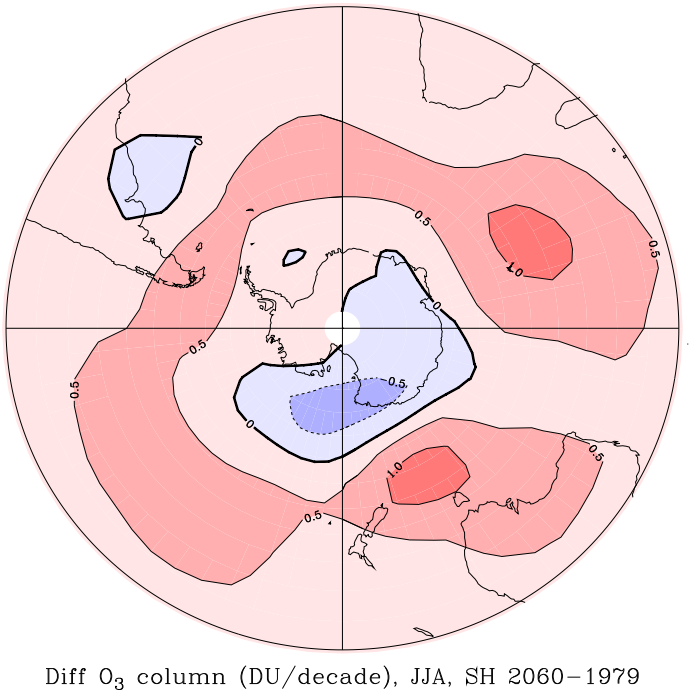

Figure 5.29: *Change on ozone column in JJA from 1979 to 2060 over the southern hemisphere.*

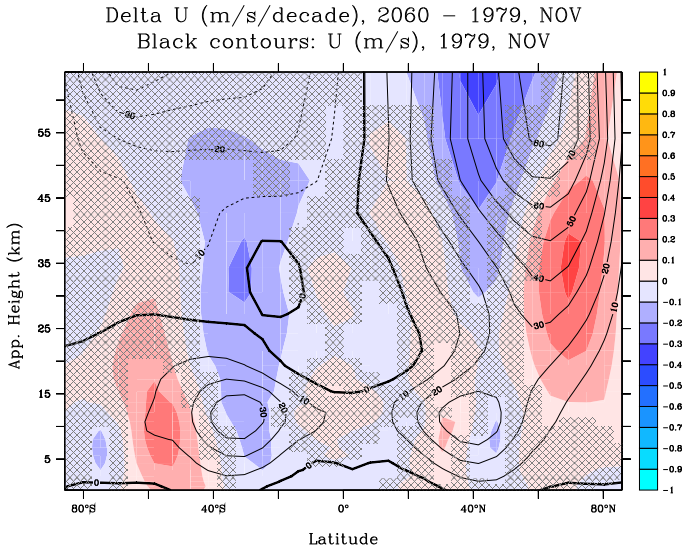

Figure 5.30: *Latitude height plot of the change in November mean zonal mean zonal wind from 1979 to 2060 (colours) in m/s/decade. Also shown is the zonal mean zonal wind in 1979 (black contours) in m/s.*

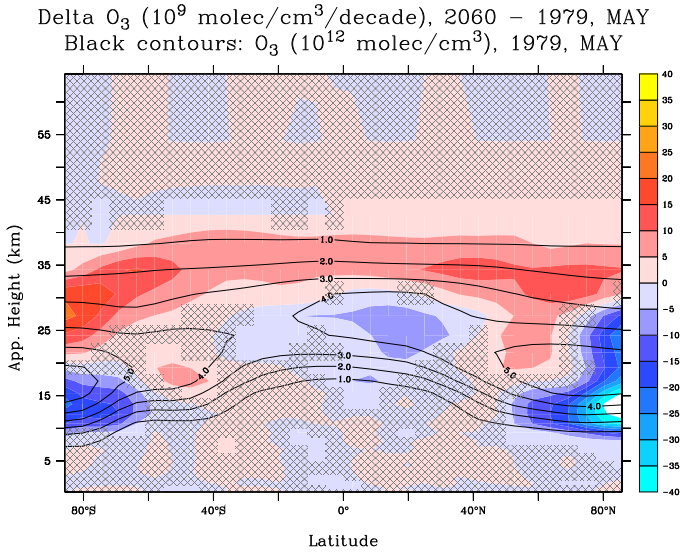

Figure 5.31: *Ozone concentration difference between 1979 and 2060 simulations in 10^9 molecules/cm^{-3}/decade (colours) for November. The concentration in 1979 is also shown (black contours). Shading signi£es regions that are not signi£cant to the 95% con£dence level.*

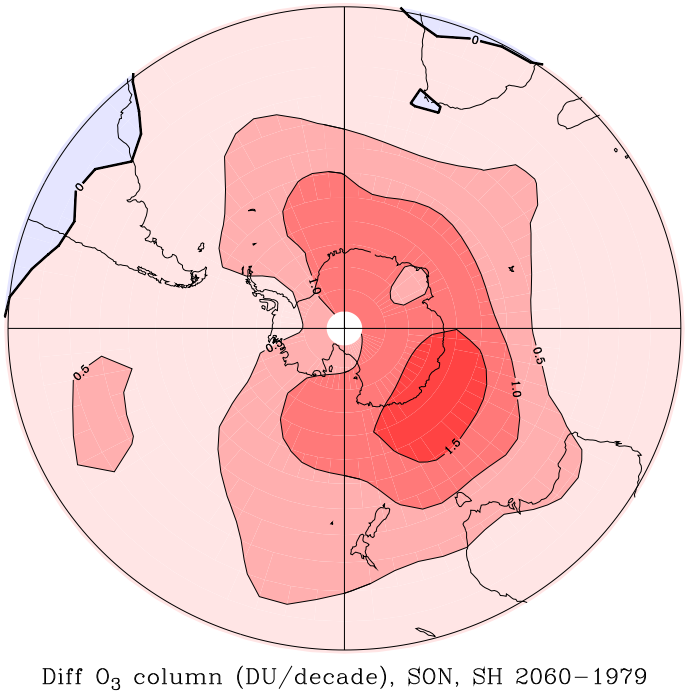

Figure 5.32: *Change on ozone column in SON from 1979 to 2060 over the southern hemisphere.*

signi£cantly more easterly. It appears that more descent is occurring, causing increased ozone concentrations in the lower stratosphere and a larger ozone column, shown in £gure 5.32.

5.3.3 Conclusions

In 2060 , if the A2 scenario were to be followed, the recovery of the ozone layer would be strongly affected by changes in atmospheric gases. The strongest effects are caused by carbon dioxide and nitrous oxide, causing an increase in upper stratospheric and decrease in lower stratospheric ozone respectively. The modest changes in ozone column re¤ect the cancellation of these two effects. The "chemistry only" experiment shows that, if temperature changes did not take place in the upper stratosphere, a global decline in ozone should be expected.

Although much of the discussion of ozone recovery has focused on globally averaged ozone column, this is certainly too simplistic. Firstly, these experiments show that the vertical pro£le of the ozone column is likely to change. An increase in upper stratospheric ozone and a decrease in ozone below could decrease the vertical stability of the stratosphere compared to a £xed ozone scenario. Secondly the spatial pattern of total ozone column recovery will be affected. The tropics may not ever see full ozone recovery as increased NO_x leads to enhanced ozone depletion. The mid and high latitudes, however, may experience a signi£cant super-recovery caused by stratospheric cooling and an increase in extra-tropical descent.

5.4 Chapter Summary

The formulation of a new coupled chemistry general circulation model has been described. The FASTOC chemical parameterisation was coupled to the Reading Intermediate General Circulation Model to create a model that is fast enough to perform many long model integrations but simulates a realistic three-dimensional atmosphere. O_x, NO_x, N_2O_5 and HNO_3 are calculated by the chemical scheme, while CO_2, N_2O, H_2O and CO were £xed at climatological values. Various aerosol climatologies were also made available for the model.

A model problem of ozone overproduction in the upper stratosphere was identi£ed. To allow realistic simulations for this thesis FASTOC was only used up to 4mb. Above this level ozone was relaxed toward climatological values.

The £rst coupled chemistry-climate experiments were performed. The £rst of these was a £fteen year timeslice experiment, simulating 1979 conditions. Crucially, the model was stable,

showing no drift over that time. Additionally, the model produced an ozone climatology that compared well to observations and to other CGCMs. This is the most important result of this thesis as it proves the potential of the model to be used for investigations into the long term development of the stratospheric ozone layer. Some differences were caused by problems with the IGCM temperatures and dynamics. For example, a too strong northern polar vortex led to ozone columns that were too small and with a maximum displaced from the pole. The too cold temperatures also caused there to be generally too much ozone. This was enhanced by the neglect of halogen species in these experiments. The biggest differences between simulation and observations were found at the summer poles, where the model had more than 25% too much ozone.

To illustrate the potential of the new model, two further 15 year timeslice experiments were performed, representing 2060 conditions. This year was chosen as atmospheric halogen concentrations are expected to decrease to values similar to those in 1979 by this time, making the comparison using a non-halogenated model fair. One run was fully interactive and the other only allowed trace gas changes to affect the chemical scheme. Both 2060 experiments used the WMO (1999) A2 scenario. This had increased CO_2, N_2O, CH_4 and CO, but constant H_2O. The CO_2 induced cooling in the “full” run caused a ozone increase in the tropical and midlatitude upper stratosphere, but reverse ”self-healing” and NO_x increases caused an ozone decrease in the middle stratosphere. The net effect in the topical ozone column was a small decrease that was only significant in a few months of the year. High latitude changes were attributed to either ozone destruction by NO_x or dynamical changes. The “chemistry only” run helped to distinguish between chemical and dynamical in¤uences on ozone, and also showed that small, localised temperature changes caused by ozone perturbations led to most of the changes in zonal mean zonal wind.

A number of further experiments would help to isolate the effect of each change in a long-lived gas. These experiments, for example, have not determined whether the £nding of Randeniya *et al.* (2002), that methane help to mitigate the ozone destruction from NO_x, is reproduced in a more complex model. Although these experiments could not be completed in the time available for this thesis, they are planned for the time following its submission.

CHAPTER SIX

Conclusions

This chapter will summarise the work of this thesis and discuss this work in the wider context of atmospheric chemical modelling. It will also suggest aspects of related research that merit further investigation due to current uncertainty.

This thesis has shown the development of a new fast stratospheric chemical scheme, FASTOC, for general circulation models (GCMs). Although other coupled chemistry general circulation models have been developed, they are either simple parameterisations or complex models that are too computationally expensive to perform many long simulations. FASTOC is an intermediate scheme that has the bene£ts of both approaches, complementing other research. It is ef£cient enough to carry out many runs without the use of supercomputers when coupled to a GCM, yet complex enough to capture the non-linear chemistry-climate interactions which make the stratospheric system so complex. This new model is a useful tool that may be used to investigate the future development of the ozone layer under different emission scenarios and provide a measure of the natural variability. This would be far too costly to do using other existing models, so FASTOC provides a unique solution to this problem.

This thesis also describes some experiments which investigate the future development of the ozone layer, using both simple and complex tools. These experiments follow from the work of others including Shindell *et al.* (1998b) and Randeniya *et al.* (2002).

6.1 Thesis Summary

Chapter 1 of this thesis provided an introduction to the chemistry and dynamics of the stratosphere and to the modelling of those processes

Chapter 2 described the development of a stratospheric chemical box model. Firstly, an

introduction to ordinary differential equation solvers used to calculate chemical systems was given, along with methods of increasing computational ef£ciency.

The Stratospheric Ozone Reduced Model (STORM), a stratospheric chemical box model based on that described by Fish and Burton (1997), was described. Details of the integration, heterogeneous and photolysis schemes were given. Kinetic data, updated from previous versions of the model, were taken from Jet Propulsion Laboratory reports (DeMore *et al.*, 1997; Sander *et al.*, 2000). STORM was compared to the ASAD (A Self-contained Atmospheric chemistry coDe) model (Carver *et al.*, 1997a,b). Details of the ASAD model were given and differences between the models discussed. Four comparison experiments were carried out, covering the lower, middle and upper stratosphere, and polar ozone loss conditions. The models were generally in good agreement. Some differences were attributed to different calculations of photolysis rates and some to the use of updated kinetic data in STORM.

In chapter 3 the development of the FAst STratospheric Ozone Chemistry (FASTOC) model was described. It began by discussing input-output models and their advantages and disadvantages. The biggest problem was said to be the cost of sampling the input space of a high-dimensional system. The Fully Equivalent Operational Model (FEOM) technique of Rabitz *et al.* (1999) was described. This method decomposes the relationship between input and output into a sum of correlated functions of increasing order. By assuming that only low order correlations are signi£cant the sampling cost is reduced to a feasible task.

FASTOC, a FEOM initialised by STORM, was then described. The choice of input variables was important, particularly in the representation of photolytic reactions. Several input variables were trialed, and a combination of day length and noon solar zenith angle provided the best results. These variables describe a unique diurnal cycle and are only weakly coupled. An additional term must be added to account for regions of twenty-four hour sunlight.

The model functions were analysed to £nd the most signi£cant variables and correlations in the system. As well as providing an insight into the controlling processes this allows a reduction in computational cost as insigni£cant functions may be ignored. This was shown to offer a typical saving of about 30%. It was found that a single set of functions was unable to accurately represent stratospheric chemistry at all altitudes and in polar day, polar night and the midlatitudes. A large error was found when comparing with STORM, giving unacceptable results. Following the approach of Wang *et al.* (1999) a number of function sets were generated and used in different regions, based on pressure and day length. This gave satisfactory results at all latitudes.

FASTOC was compared to the stratospheric chemistry FEOM of Shorter *et al.* (1999). The Shorter *et al.* (1999) model was based on a scheme with a highly parameterised photolysis scheme, making it easy to parameterise but less accurate. It also had many unnecessary functions which added to its cost. Additionally the Shorter *et al.* (1999) model was only tested in midlatitudes and its performance in polar regions was not shown. It was not, therefore, shown to be suitable for GCMs. FASTOC was validated by comparing it to STORM, the model used to initialise it. It was tested under a variety of conditions and found to be typically within 10% and often within 5% for all chemical species.

Chapter 4 presented some idealised climate change experiments using a simple perturbation method. The £nal response of a system is estimated from its initial response and the timescale of the system. This timescale is calculated and assumed to remain constant, but in reality will vary as the composition of the atmosphere changes.

Some zero-dimensional experiments were performed for the upper stratosphere using STORM. This region is most likely to respond to changes in species involved in catalytic ozone loss. An increase in chlorine caused the largest ozone loss. This was followed by an increase in ozone caused by a fall in temperature due to CO_2 increases, and a decrease in ozone due to an increase in NO_x. Experiments simulating the atmosphere in the year 2100 were performed using STORM to examine some possible recovery scenarios. Various combinations of perturbations were made to NO_x and temperature. It was found that either ozone levels in 2100 may be either higher or lower than before the increase in CFCs depending in the exact scenario.

Chapter 5 presented the details of a new chemistry-climate general circulation model and the £rst experiments performed using it. IGCM-FASTOC, composed of the Reading Intermediate General Circulation Model and the FASTOC chemical parameterisation, calculated and advected O_x, NO_x, N_2O_5 and HNO_3. It was made interactive by the inclusion of the calculated ozone in the radiative and chemical schemes.

To demonstrate the potential of the new model a £fteen year timeslice experiments of 1979 conditions was performed. The results compared well with observations. The annual cycle in total ozone column was good at all latitudes, though there were dissimilararities, particularly at high latitudes. These were, however, mainly caused by the imperfect dynamics of the IGCM. A second £fteen year experiment used the WMO (1999) A2 scenario for the year 2060. This predicted a net decrease in the tropical ozone column and an increase in high latitude ozone in winter and spring. The small tropical change resulted from an increase in upper stratospheric ozone due to

cooling and from a larger decrease below caused by increasing NO_x and reverse "self-healing". The high latitude increases were mainly caused by dynamical changes forced by the midlatitude ozone perturbations.

6.2 Future Work

6.2.1 Developments and Applications of IGCM-FASTOC

Although the fast chemical scheme presented in this thesis will allow many long integrations it is limited by the omission of halogen chemistry. The inclusion of chlorine and bromine will allow the realistic simulation of the past and present day atmosphere, including a polar ozone hole. The halogenated model may then be used to perform ensembles of transient runs simulating past and possible future trends. These simulations should include scenarios for N_2O, CO, CH_4, H_2O and the halogens. These ensembles will aid the understanding of what the stratospheric system may or may not do, and the range of uncertainty in those estimates. These numerical experiments will give information about the possible future climate that may not be obtainable using other models and current computing power. An additional improvement that could be made is the calculation and advection of species that are currently £xed. Natural and anthropogenic emissions would then need to be estimated, and could be varied to examine more subtle changes in scenarios. This would also allow changes in circulation to be fully coupled to chemical changes. For example, the current model could not simulate the hastened ozone recovery predicted by Butchart *et al.* (2000), as the mechanism was an increase in the Brewer-Dobson circulation and subsequent faster removal of halogen species. This would, however, increase the computational cost of the model.

Improvements may also be made to the High Dimensional Model Representation (HDMR) algorithm used in FASTOC. The method used in this thesis is known as a cut-HDMR as the functions take the form of cuts or sub-volumes through the input space. Higher order terms are assumed to be small and not used. This, however, introduces error so any poor performance of the model may be attributed to the presence of signi£cant high order terms. The cost of calculating the functions increases exponentially with the highest order functions used, so including higher order terms is undesirable from this point of view. An alternative method of approximating these high order terms has been proposed by Li *et al.* (2001). This method is called monomial based preconditioned cut-HDMR, or mp-cut-HMDR. This approximation is made by multiplying additional n dimensional terms by a known monomial to create $n+1$ dimensional terms. Thus a third

order cut-HDMR is approximated by just second and £rst order tables. It is written as

$$\begin{aligned} f_{ijk}(x_i,x_j,x_k) \approx \quad & \varphi_{ijk}(x_i,x_j,x_k)\overline{f}_0 + \varphi_{ij}(x_i,x_j)\overline{f}_k(x_k) \\ & +\varphi_{ik}(x_i,x_k)\overline{f}_j(x_j) + \varphi_{jk}(x_j,x_k)\overline{f}_k(x_i) \\ & +\varphi_i(x_i)\overline{f}_{jk}(x_j,x_k) + \varphi_j(x_j)\overline{f}_{ik}(x_i,x_k) \\ & +\varphi_k(x_k)\overline{f}_{ij}(x_i,x_j). \end{aligned} \tag{6.1}$$

where φ_{ij} is a precomputed factor depending on i and j. Li *et al.* (2001) added fourth order mp-cut-HDMR functions to a third order cut-HDMR for a tropospheric chemical model with just £ve input variables. This increased the percentage of data with a relative error less than 1% from 55% to 75% and was just $\sim$11% more costly to generate and use. This method, therefore, could offer increased accuracy with only a minimal increase in cost.

There are also limitations in current parameterisations of the microphysics of solid and liquid particles and their sedimentation used in this model and others.. For example, the formation of so-called *NAT rocks* (see section 1.2.4) is not fully understood and is not included in current CGCMs. In fact, many CGCMs, including IGCM-FASTOC do not account for denitri£cation and dehydration caused by the sedimentation of ice particles whose existence has been known for many years (Austin, 2002). This process may be important in predictions of the future of ozone depletion in the northern hemisphere vortex if stratospheric cooling continues. In the future atmosphere, when chlorine loading is low, denitri£cation may reduce ozone loss if NO_x is the dominant ozone destruction catalyst.

Another issue that may need attention is the coupling of tropospheric and stratospheric processes. Most chemical schemes, including FASTOC, are only used for either tropospheric or stratospheric chemistry. Although the same physical processes take place either side of the tropopause, only the dominant processes of one region are included in any one model. This gives a computational saving, but ideally a scheme would account for the chemistry in all areas of the atmosphere. For example, stratospheric chemistry affects the troposphere by regulating the solar ¤ux, so controlling the production of the oxidant OH. Tropospheric chemistry determines which surface emissions cross the tropopause and which are oxidised or rained out. The FEOM technique could easily be applied to this problem. In fact, a simple four species scheme has been presented by Wang *et al.* (1999). Du to the cost of calculating extra species, a more complex hydrocarbon oxidation scheme could only be included if third order interactions were not used. The same

model could be applied from the surface to the upper atmosphere. Function analysis would allow the insigni£cant functions to be removed at each level. Additional processes, such as aqueous chemistry in the troposphere and ion chemistry in the mesosphere would need to be added to the box model in order to extend the boundaries of the model.

There are other possible applications that the current, or future halogenated, model could be put to. Chemical forecasting and data assimilation both require fast chemical schemes. The Cariolle and Déqué (1986) scheme is often used for these applications, but this scheme is simplistic and the linearised functions that it uses should be recalculated when trace gas concentrations change. FASTOC functions would not need to be recalculated and it would respond to changes in water vapour, methane or other gases and their non-linear interactions. A GCM with fully coupled stratospheric chemistry may also allow better prediction of weather patterns. There is growing evidence that the state of the stratosphere in¤uences the troposphere.

6.2.2 Stratospheric Ozone and Climate

Although the Montreal Protocol and its subsequent amendments have prevented the rapid destruction of the ozone layer by halogen compounds, there remain uncertainties in how the ozone layer will respond to future climate change. The work of Randeniya *et al.* (2002) has shown that the recovery of the ozone layer is by no means certain. These experiments should be repeated and expanded using more complex models to determine whether they are robust. This work has shown that recovery may be localised, with some areas failing to fully recover and other experiencing a super-recovery. Randeniya *et al.* (2002) also showed that the exact scenario followed will be extremely important. It will be necessary for many models to examine a range of scenarios as it must be determined whether any future emissions will have a detrimental effect on the biosphere. For example, if CO_2 emissions are not controlled the possible effects of increasing ozone on biota will have to be assessed. It may also be necessary to classify N_2O as an ozone depleting substance and control its emission as such.

Measurement of trace gases is also an important part of understanding ongoing chemical changes in the atmosphere. Satellite measurements with good vertical resolution must play a role if a global view is to be obtained.

In order for policy makers to have con£dence in the model results the models themselves will need improvement. This may include improved dynamics, more complete chemical schemes or improved ef£ciency to allow ensembles of runs to be performed. Additional process, such as

biospheric or ocean models, should also be coupled to the CGCMs. This would allow a more complete prediction of how the Earth system will respond to anthropogenic forcings.

6.3 Concluding Remarks

This thesis has presented the development and testing of a new chemical model for GCMs. It is both accurate and ef£cient, making it highly suitable for its intended purpose. The experiments performed illustrate its potential for performing ensembles of coupled chemistry climate runs and contributing greatly to our understand of the future development of the ozone layer.

Appendix
Derivation of Photolysis Parameters

Solar Zenith Angle Calculations

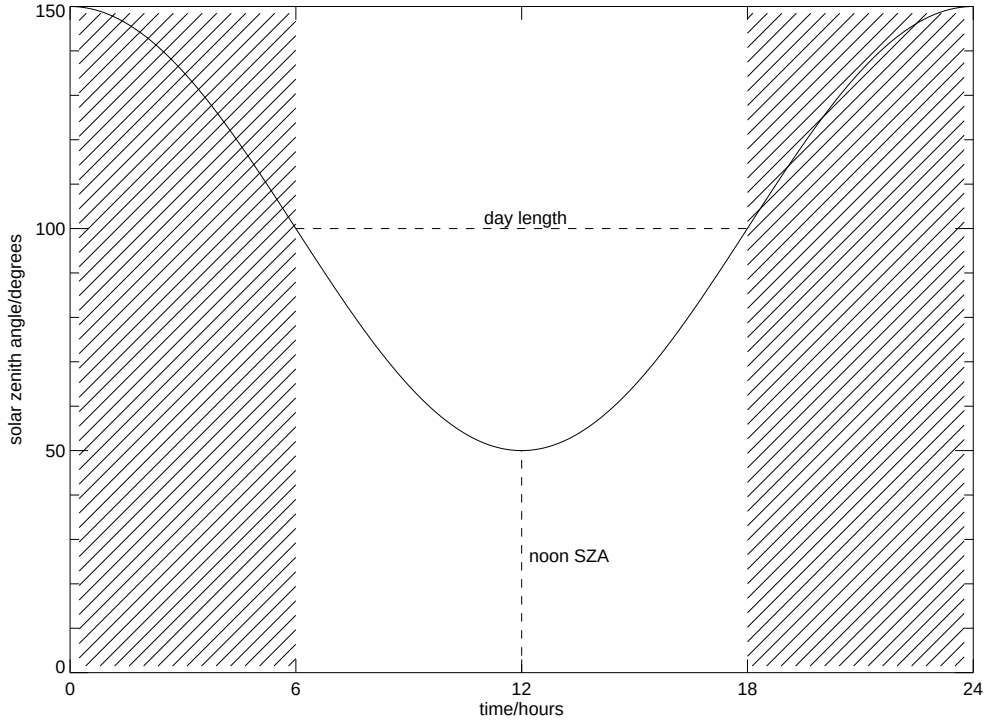

Figure 1: *Diurnal cycle produced by £xing day length and noon solar zenith angle. The day length is 12 hours and the noon solar zenith angle is 50°. The local sunrise angle here is set to 100°*

The solar zenith angle may be approximated as

$$\theta = a.cos(t_h - \pi) + b. \tag{2}$$

a and b may be calculated from the noon solar zenith angle, θ_n, and the the sunrise time, t_{ss}. The sunrise time is calculated using

$$cos(\theta) = sin(\phi)sin(\delta) + cos(\phi)cos(\delta)cos(t_h), \tag{3}$$

as

$$t_{ss} = cos^{-1}\left(\frac{cos\theta_{ss} - sin\phi sin\delta}{cos\phi cos\delta}\right) \tag{4}$$

where θ_{ss} is the local sunrise angle, which depends on alitude. At sunrise,

$$a.cos(t_{ss}) + b = \theta_{ss}, \tag{5}$$

and at noon,

$$a.cos(\pi) + b = \theta_n. \tag{6}$$

Rearranging equation 6 and substituting into equation 5 gives

$$a = \frac{\theta_{ss} - \theta_n}{cos(t_{ss}) + 1}. \tag{7}$$

Substituting back into equation 6 gives

$$b = \frac{\theta_n cos(t_{ss}) + \theta_{ss}}{cos(t_{ss}) + 1}. \tag{8}$$

Noon Zenith Angle and Day Length Calculations

The noon solar zenith angle is given by

$$cos(\theta_n) = sin(\phi)sin(\delta) + cos(\phi)cos(\delta)) \tag{9}$$

as $cos(t_h) = 0$. This can be simpli£ed to

$$cos(\theta_n) = cos(\phi - \delta) \tag{10}$$

So,

$$\theta_n = \phi - \delta. \tag{11}$$

The day length is twice the time from sunrise to noon. Using equation 4 and converting to hours gives:

$$\Lambda = \frac{24}{\pi} cos^{-1}\left(\frac{cos(\theta_{ss}) - sin(\phi)sin(\delta)}{cos(\delta)cos(\phi)}\right). \tag{12}$$

Glossary

Notation

Symbol	Description	Value or Units
[A]	concentration of A	molecules cm^{-3}
χ_A	mixing ratio of A by volume	dimensionless
k	rate constant - unimolecular	s^{-1}
	- bimolecular	$cm^3 molecule^{-1} s^{-1}$
	- termolecular	$cm^6 molecule^{-2} s^{-1}$
J	photolysis rate	s^{-1}
τ_A	lifetime of A	s
ϕ_{diss}	quantum yield of dissociation	dimensionless
γ	reactive uptake coef£cient	dimensionless
ν	frequency	s^{-1}
h	Planck constant	6.626×10^{-34} Js
θ	solar zenith angle	degrees
δ	solar declination angle	degrees
ϕ	latitude	degrees
DU	Dobson unit	2.687×10^{16} molecules cm^{-2}
P	pressure	Pa
T	temperature	K
Λ	day length	hours

Acronyms

Acronym	Meaning
CGCM	chemistry-general circulation model
CPU	central processing unit
CTM	chemical transport model
GCM	general circulation model
IPCC	Intergovernmental Panel on Climate Change
NAT	nitric acid trihydrate
LTS	liquid ternary solution
PSC	polar stratospheric cloud
UV	ultra-violet
WMO	World Meteorological Organisation

References

Aliş, O. F. and Rabitz, H. (2001). Ef£cient implementation of high dimensional model representations. *Journal of Mathematical Chemistry*, **29**(2), 127–142.

Anderson, D. E. (1983). The troposphere to stratosphere radiation £eld at twilight: a spherical model. *Planetary Space Science*, **31**(12), 1517–1523.

Atkins, P. W. (1994). *Physical Chemistry*. Oxford University Press, £fth edition.

Austin, J. (1991). On the explicit versus family solution of the fully diurnal photochemical equations of the stratosphere. *Journal of Geophysical Research*, **96**(D7), 12941–12974.

Austin, J. (2002). A three-dimensional coupled chemistry-climate model simulation of past stratospheric trends. *Journal of the Atmospheric Sciences*, **59**(2), 218–232.

Austin, J. and Butchart, N. (1994). The in¤uence of climate change and the timing of stratospheric warmings on arctic ozone depletion. *Journal of Geophysical Research*, **99**(D1), 1127–1145.

Austin, J., Butchart, N., and Shine, K. P. (1992). Possibility of an arctic ozone hole in a doubled co_2 climate. *Nature*, **360**, 221–225.

Austin, J., Butchart, N., and Swinbank, R. (1997). Sensitivity of ozone and temperature to vertical resolution in a GCM with coupled stratospheric chemistry. *Quarterly Journal of the Royal Meteorological Society*, **123**, 1405–1431.

Austin, J., Knight, J., and Butchart, N. (2000). Three-dimensional chemical model simulations of the ozone layer: 1979-2015. *Quarterly Journal of the Royal Meteorological Society*, **126**, 1533–1556.

Austin, J., Butchart, N., and Knight, J. (2001). Three-dimensional chemical model simulations of the ozone layer: 2015-2055. *Quarterly Journal of the Royal Meteorological Society*, **127**, 959–974.

Austin, J., Shindell, D., beagley, S. R., Brühl, C., Dameris, M., Mazini, E., Nagashima, T., Newman, P., Pawson, S., Pitari, G., Rosonov, E., Schnadt, C., and Shepherd, T. G. (2002). Assessments of chemistry-climate models of the stratosphere. *submitted to Atmospheric Chemistry Physics (Discussions)*.

Bell, J. B., Brown, N. J., Day, M. S., Frenklach, M., Grcar, J. F., Propp, R. M., Tonse, S. R., and Wagner, A. (2000). Scaling and ef£ciency of PRISM in adaptive simulations of turbulent premixed ¤ames. *Proceedings of the Combustion Institute*, **28**, 107–113.

Blasco, J. A., Fueyo, N., Dopazo, C., and Chen, J. Y. (2000). A self-organizing map approach to chemistry representation in combustion applications. *Combustion Theory and Modelling*, **4**(1), 61–76.

Borrmann, S., Solomon, S., Avallone, L., Toohey, D., and Baumgardner, D. (1996). On the occurrence of ClO in cirrus clouds and volcanic aerosol in the tropopause region. *Geophysical Research Letters*, **24**(16), 2011–2014.

Brasseur, G. P., Orlando, J. J., and Tyndall, G. S., editors (1999). *Atmospheric Chemistry and Global Change*. Oxford University Press.

Brown, P. N., Byrne, G. D., and Hindmarsh, A. C. (1989). VODE: a variable coef£cient ODE solver. *SIAM Journal of Scienti£c Statistical Computing*, **10**, 1038–1051.

Butchart, N. and Austin, J. (1996). On the relationship between the quasi-biennial oscillation, total chlorine and the severity of the antarctic ozone hole. *Quarterly Journal of the Royal Meteorological Society*, **122**, 183–217.

Butchart, N., Austin, J., Knight, J. R., Scaife, A. A., and Gallani, M. L. (2000). The response of the stratospheric climate to pojected changes in the conentrations of well-mixed greenhouse gases from 1992 to 2051. *Journal of Climate*, **13**, 2142–2159.

Cariolle, D. and Déqué, M. (1986). Southern hemisphere medium-scale waves and total ozone disturbances in a spectral general circulation model. *Journal of Geophysical Research*, **91**(D10), 10825–10846.

Carslaw, K., Peter, T., Bacmeister, J., and Eckermann, S. (1999). Widespread solid particle formation by mountain waves in the arctic stratosphere. *Journal of Geophysical Research*, **104**(D1), 1827–1836.

Carver, G. D. and Stott, P. A. (2000). IMPACT: an implicit time integration cheme for chemical species and families. *Annales Geophysicae - Atmospheres, hydrospheres and space sciences*, **18**(3), 337–346.

Carver, G. D., Brown, P. D., and Wild, O. (1997a). The ASAD atmospheric chemistry integration package and chemical reaction database. *Computer Physics Communications*, **105**(2-3), 197–215.

Carver, G. D., Brown, P. D., and Wild, O. (1997b). The ASAD atmospheric chemistry integration package and chemical reaction database, User Guide. http://www.atm.ch.cam.ac.uk/acmsu/asad/.

Chapman, S. (1930). A theory of upper-atmospheric ozone. *Mem. Royal Meteorological Society*, **3**, 103–125.

Chen, J. Y., Blasco, J. A., Fueyo, N., Dopazo, C., Pope, S. B., and Masri, A. R. (2000). An economical strategy for storage of chemical kinetics: Fitting in situ adaptive tabulation with arti£cial neural networks. *Proceedings of the Combustion Institute*, **28**, 115–121.

Chipper£eld, M. (1993). Intercomparison of stratospheric chemistry schemes of three-dimensional models. Technical Report 34, UGAMP, Centre for Global Atmospheric Modelling, Department of Meteorology, University of Reading, PO Box 243, Reading, RG6 6BB, UK.

Chipper£eld, M. P. and Pyle, J. A. (1998). Model sensitivity studies of arctic ozone depletion. *Journal of Geophysical Research*, **103**(D21), 28389–28403.

Chipper£eld, M. P., Lee, A. M., and Pyle, J. A. (1996). Model calculations of ozone depletion in the Arctic polar vortex for 1991/92 to 1994/95. *Geophysical Research Letters*, **23**, 559–562.

Daniel, J. S., Solomon, S., Portmann, R. W., and Garcia, R. R. (1999). Stratospheric ozone destruction: The importance of bromine relative to chlorine. *Journal of Geophysical Research*, **104**(D19), 23871–23880.

Danilin, M. Y., Sze, N. D., Ko, M. K. W., Rodriguez, J. M., and Prather, M. J. (1996). Bromine-chlorine coupling in the Antarctic ozone hole. *Geophysical Research Letters*, **23**(2), 153–156.

de Grandpré, J., Sandilands, J. W., McConnell, J. C., Beagley, S. R., Croteau, P. C., and Danilin, M. Y. (1997). Canadian Middle Atmosphere Model: preliminary results from the chemical transport module. *Atmosphere-Ocean*, **35**, 385–431.

de Grandpré, J., Beagley, S. R., Formichev, V. I., Griffoen, E., McConnell, J. C., and Medvedev, A. S. (2000). Ozone climatology using interactive chemistry: results from the Canadian Middle Atmosphere Model. *Journal of Geophysical Research*, **105**(D21), 26475–26491.

Delgado, J. and Liao, J. C. (1995). Control of metabolic pathways by time-scale separation. *Biosystems*, **36**(1), 55–70.

DeMore, W. B., Golden, D. M., Hampson, R. F., Howard, C. J., Kurylo, M. J., Molina, M. J., Ravishankara, A. R., and Sander, S. P. (1992). *Chemical kinetics and photochemical data for use in stratospheric modeling, JPL publication 92-20*. Jet Propulsion Laboratory, California Institute of Technology, Pasadena, CA.

DeMore, W. B., Sander, S. P., Golden, D. M., Hampson, R. F., Howard, M. J. K. C. J., Ravishankara, A. R., Kolb, C. E., and Molina, M. J. (1994). *Chemical kinetics and photochemical data for use in stratospheric modeling, JPL publication 94-26*. Jet Propulsion Laboratory, California Institute of Technology, Pasadena, CA.

DeMore, W. B., Sander, S. P., Golden, D. M., Hampson, R. F., Kurylo, M. J., Howard, C. J., Ravishankara, A. R., Kolb, C. E., and Molina, M. J. (1997). *Chemical kinetics and photochemical data for use in stratospheric modeling, JPL publication 97-4*. Jet Propulsion Laboratory, California Institute of Technology, Pasadena, CA.

Dessler, A. (2000). *The chemistry and physics of stratospheric ozone*, volume 74 of *International Geophysics Series*. Academic Press.

Donaldson, D. J., Tuck, A. F., and Vaida, V. (2000). Enhancement of HOx at high solar zenith angles by overtone-induced dissociation of HNO3 and HNO4. *Physics and Chemistry of the Earth Part C - Solar-Terrestrial and Planetary Science*, **25**(3), 223–227.

Dornbrack, A., Leutbecher, M., Reichardt, J., Behrendt, A., Muller, K. P., and Baumgarten, G. (2001). Relevance of mountain wave cooling for the formation of polar stratospheric clouds over Scandinavia: Mesoscale dynamics and observations for January 1997. *Journal of Geophysical Research*, **106**(D2), 1569–1581.

Dvortsov, V. L. and Solomon, S. (2001). Response of the stratospheric temperatures and ozone to past and future increases in stratospheric humidity. *Journal of Geophysical Research*, **106**(D7), 7505–7514.

Ehhalt, D. and Prather, M. (2001). *Climate Change 2001: The Scienti£c Basis*, chapter 4, Atmospheric Chemistry and Greenhouse Gases. Cambridge University Press, Cambridge.

Evans, S. J., Toumi, J., Harries, J. E., Chipper£eld, M. P., and Russel III, J. M. (1998). Trends in stratospheric humidity and the sensitivity of ozone to these trends. *Journal of Geophysical Research*, **103**, 8715–8725.

Fahey, D. W., Gao, R. S., KS, K. S. C., Kettleborough, J., Popp, P. J., Northway, M. J., Holecek, J. C., Ciciora, S. C., McLaughlin, R. J., Thompson, T. L., Winkler, R. H., Baumgardner, D. G., Gandrud, B., Wennberg, P. O., Dhaniyala, S., McKinney, K., Peter, T., Salawitch, R. J., Bui, T. P., Elkins, J. W., Webster, C. R., Atlas, E. L., Jost, H., Wilson, J. C., Herman, R. L., Kleinbohl, A., and von Konig, M. (2001). The detection of large HNO_3-containing particles in the winter arctic stratosphere. *Science*, **291**(5506), 1026–1031.

Farman, J. C., Gardiner, B. G., and Shanklin, J. D. (1985). Large losses of total ozone in Antarctica reveal seasonal ClO_x/NO_x interaction. *Nature*, **315**, 207–210.

Finlayson-Pitts, B. J. and Pitts Jr., J. N. (2000). *Chemistry of the Upper and Lower Atmosphere*. Academic Press.

Fish, D. J. and Burton, M. R. (1997). The effect of uncertainties in kinetic and photochemical data on model predictions of stratospheric ozone depletions. *Journal of Geophysical Research*, **102**, 25537–25542.

Fish, D. J., Shallcross, D. E., and Jones, R. L. (1999). The vertical distribution of NO_3 in the atmospheric boundary layer. *Atmospheric Environment*, **33**(5), 687–691.

Fish, D. J., Roscoe, H. K., and Johnston, P. V. (2000). Possible causes of stratospheric NO_2 trends observed at Lauder, New Zealand. *Geophysical Research Letters*, **27**(20), 3313–3316.

Flentje, H., Renger, W., and M, M. W. (2000). Validation of Contour Advection simulations with airborne lidar measurements of £laments during the Second European Stratospheric Arctic and Midlatitude Experiment (SESAME). *Journal of Geophysical Research*, **105**(D2).

Forster, P. M. d. F., Blackburn, M., Glover, R., and Shine, K. P. (2000). An examionation of climate sensitivity for idealised climate change experiments in an intermediate general circulation model. *Climate Dynamics*, **16**, 833–849.

Forster, P. M. F. and Shine, K. P. (1999). Stratospheric water vapour changes as a possible contributor to observed stratospheric cooling. *Journal of Geophysical Research*, **26**(21), 3309–3312.

Forster, P. M. F. and Shine, K. P. (2002). Assessing the climate impact of trends in stratospheric water vapor. *Geophysical Research Letters*, **29**(6), 10–1 – 10–4.

Fueglistaler, S., Luo, B. P., Voigt, C., Carslaw, K. S., and Peter, T. (2002). NAT-rock formation by mother clouds: a microphysical model study. *Atmospheric Chemistry Physics*, **2**, 93–98.

Gao, R. S., Richard, E. C., Popp, P. J., Toon, G. C., Hurst, D. F., Newman, P. A., Holecek, J. C., Northway, M. J., Fahey, D. W., Danilin, M. Y., Sen, B., Aikin, K., Romashkin, P. A., Elkins, J. W., Webster, C. R., Schauf¤er, S. M., Greenblatt, J. B., McElroy, C. T., Lait, L. R., Bui, T. P., and D, D. B. (2001). Observational evidence for the role of denitri£cation in Arctic stratospheric ozone loss. *Geophysical Research Letters*, **28**(15), 2879–2882.

Gear, C. W. (1967). The numerical integration of ordinary differential equations. *Mathematical Computing*, **21**, 146–156.

Gil, M., Puentedura, O., Yela, M., and Cuevas, E. (2000). Behavior of NO_2 and O_3 columns during the eclipse of February 26, 1998, as measured by visible spectroscopy. *Journal of Geophysical Research*, **105**(D3), 2583–3593.

Graf, H.-F., Kirchner, I., and Perlwitz, J. (1998). Changing lower stratosphere circulation: the role of ozone and greenhouse gases. *Journal of Geophysical Research*, **103**(D10), 11251–11261.

Hadjinicolaou, P., Pyle, J. A., Chipper£eld, M. P., and Kettleborough, J. A. (1997). Effect of interannual meteorological variability on mid-latitude O_3. *Geophysical Research Letters*, **24**(23), 2993–2996.

Hadjinicolaou, P., Jrrar, A., Pyle, J. A., and Bishop, L. (2002). The dynamically driven long-term trend in stratospheric ozone over northern middle latitudes. *Quarterly Journal of the Royal Meteorological Society*, **128**(583), 1393–1412.

Haigh, J. D. (1985). A fast method for calculating scale-dependent photochemical acceleration in dynamical models of the stratosphere. *Quarterly Journal of the Royal Meteorological Society*, **111**, 1027–1038.

Haigh, J. D. and Pyle, J. A. (1982). Ozone perturbation experiments in a two-dimensional model. *Quarterly Journal of the Royal Meteorological Society*, **108**, 551–574.

Hanson, D. R., Ravishankara, A. R., and Solomon, S. (1994). Heterogeneous reactions in sulfuric acid aerosols: A framework for model calculations. *Journal of Geophysical Research*, **99**(D2), 3615–3629.

Hein, R., Dameris, M., Schnadt, C., Land, C., Grewe, V., Köhler, I., Ponater, M., Sausen, R., Steil, B., Landgraf, J., and Brühl, C. (2001). Results of an interactively coupled atmospheric chemistry - general circulation model: Comparison with observations. *Annales Geophysicae*, **19**, 435–457.

Hoskins, B. J. and Simmons, A. J. (1975). A multi-layer spectral model and the semi-implicit method. *Quarterly Journal of the Royal Meteorological Society*, **101**, 637–655.

IPCC (2001). *Climate Change 2001, The Scienti£c Basis, Contribution of Working Group I to the Third Assessment Report of the Intergovernmental panel on Climate Change*. Cambridge Univerity Press.

Jacobson, M. Z. (1999). *Fundamentals of Atmospheric Modeling*, chapter 4. Cambridge University Press.

Jacobson, M. Z. and Turco, R. P. (1994). SMVGEAR a sparse-matrix vectorised Gear code for atmospheric models. *Atmospheric Environment*, **28**, 273–284.

James, I. N. (1995). *Introduction to Circulating Atmospheres*. Cambridge atmospheric and space science series. Cambridge University Press.

Kirchhoff, V. W. J. H., Schuch, N. J., Pinheiro, D. K., and Harris, J. M. (1996). Evidence for an ozone hole perturbation at 30 degrees south. *Atmospheric Environment*, **30**(9), 1481.

Kirk-Davidoff, D., Hinsta, E. J., and Anderson, J. G. (1999). The effect of climate change on ozone depletion through changes in stratospheric water vapour. *Nature*, **402**, 399–401.

Knudsen, B. M. and Grooß, J. U. (2000). Northern midlatitude stratospheric ozone dilution in spring modeled with simulated mixing. *Journal of Geophysical Research*, **105**(D5), 6885–6890.

Lary, D. J. (1996). Gas phase atmospheric bromine photochemistry. *Journal of Geophysical Research*, **101**, 1505–1516.

Lary, D. J. (1997). Catalytic destruction of stratospheric ozone. *Journal of Geophysical Research*, **102**(D17), 21515–21526.

Lary, D. J. and Pyle, J. A. (1992a). Diffuse radiation, twilight and photochemistry - I. *Journal of Atmospheric Chemistry*, **13**, 373–392.

Lary, D. J. and Pyle, J. A. (1992b). Diffuse radiation, twilight and photochemistry - II. *Journal of Atmospheric Chemistry*, **13**, 393–406.

Lelieveld, J., Bregman, A., Scheeren, H. A., Strom, J., Carslaw, K. S., Fischer, H., Siegmund, P. C., and Arnold, F. (1999). Chlorine activation and ozone destruction in the northern lowermost stratosphere. *Journal of Geophysical Research*, **104**(D7), 8201–8213.

Li, D. and Shine, K. P. (1995). A 4-dimensional ozone climatology for UGAMP models. Technical Report 35, UGAMP, Centre for Global Atmospheric Modelling, Department of Meteorology, University of Reading, PO Box 243, Reading, RG6 6BB, UK.

Li, G., Wang, S. W., Rosenthal, C., and Rabitz, H. (2001). High dimensional model representations generated from low dimensional data samples. I. mp-Cut-HMDR. *Journal of Mathematical Chemistry*, **30**(1), 1–30.

Liou, K.-N. (1980). *An Introduction to Atmospheric Radiation*, volume 26 of *International Geophysical Series*. Academic Press.

Lowe, R. and Tomlin, A. (2000a). Low-dimensional manifolds and reduced chemical models for tropospheric chemistry simulations. *Atmospheric Environment*, **34**, 2425–2436.

Lowe, R. M. and Tomlin, A. (2000b). The application of repro-modelling to a tropospheric chemical model. *Environmental Modelling and Software*, **15**, 611–618.

Mahlman, J. D., Pinto, J. P., and Umscheid, L. J. (1994). Transport, radiative, and dynamical effects of the antarctic ozone hole: a GFDL 'SKYHI' model experiment. *Journal of the Atmospheric Sciences*, **51**(4), 489–508.

Manney, G. L., Zurek, R. W., O'Neil, A., and Swinbank, R. (1994). On the motion of air through the stratospheric polar vortex. *Journal of the Atmospheric Sciences*, **51**(20), 2973–2994.

Massie, S. T., Tie, X., Brasseur, G. P., Bevilacque, R. M., Fromm, M. D., and Santee, M. L. (2000). Chlorine activation during the early 1995-1996 arctic winter. *Journal of Geophysical Research*, **105**(D6), 7111–7131.

McElroy, M. B., Salawitch, R. J., Wofsy, S. C., and Logan, J. A. (1986). Reductions in antartic ozone due to synergistic interactions of chlorine and bromine. *Nature*, **321**, 759–762.

McIntyre, M. E. (1995). The stratospheric polar vortex and sub-vortex - ¤uid-dynamics and mid-latitude ozone loss. *Philisophical transactions of the Royal Society of London Series A - Mathematical Physical and engineering sciences*, **352**(1699), 227–240.

Meier, R. R., Anderson, D. E., and Nicolet, M. (1982). Radiation £eld in the troposphere and stratosphere from 240-1000 nm-i. general analysis. *Planetary Space Science*, **30**(9), 923–933.

Millard, G. A., Lee, A. M., and Pyle, J. A. (2002). A moel study of the connection between polar and mid-latitude ozone loss in the northern hemisphere and lower stratosphere. *Journal of Geophysical Research*, **in press**.

Mo, R. P., Buhler, O., and McIntyre, M. E. (1998). Permeability of the stratospheric vortex edge: On the mean mass ¤ux due to thermally dissipating, steady, non-breaking Rossby waves. *Quarterly Journal of the Royal Meteorological Society*, **124**(550), 2129–2148.

Molina, M. J. and Rowland, F. S. (1974). Stratospheric sink for chloro¤uoromethanes: chlorine atom catalysed destruction of ozone. *Nature*, **249**, 820–822.

Morcrette, J.-J. (1991). Radiation and cloud radiative properties in the ECMWF forecasting system. *Journal of Geophysical Research*, **96**, 9121–9132.

Nagashima, T., Takahashi, M., Takigawa, M., and Akiyoshi, H. (2002). Future development of the ozone layer calculated by a general circulation model with fully interactive chemistry. *Geophysical Research Letters*, **29**(8), 3.

Nedoluha, G. E., Bevilacqua, R. M., Gomez, R. M., Siskind, D. E., Hicks, B. C., Russel III, J. M., and Conner, B. J. (1998). Increases in middle atmospheric water vapour as observed by the halogen occultation experiment and the ground based water vapor millimeter-wave spectrometer from 1991-1997. *Journal of Geophysical Research*, **103**, 3531–3543.

Nicolet, M., Meier, R. R., and Anderson, D. E. (1982). The radiation £eld in the troposphere and stratosphere from 240nm to 1000nm: general analysis. *Planetary Space Science*, **30**(9), 935–983.

Okino, M. S. and Mavrovouniotis, M. L. (1999). Simpli£cation of chemical reaction systems by time-scale analysis. *chemical engineering communications*, **176**, 115–131.

Orsolini, Y. J. (1995). On the formation of ozone laminae at the edge of the Arctic polar vortex. *Quarterly Journal of the Royal Meteorological Society*, **128**(528), 1923–1941.

Panegrossi, G., Fuá, D., and Fiocco, G. (1996). A 1-D model of the formation and evolution of polar stratospheric clouds. *Journal of the Atmospheric Sciences*, **23**, 5–35.

Pawson, S. *et al.* (2000). The GCM-Reality Intercomparison Project for SPARC (GRIPS): Scienti£c Issues and Initial Results. *Bulletin of the Americal Meteorological Society*, **81**(4).

Pitari, G., Palermi, S., Visconti, G., and Prinn, R. G. (1992). Ozone response to a CO_2 doubling - results from a stratospheric circulation model with heterogeneous chemistry. *Journal of Geophysical Research*, **97**(D5).

Pitari, G., Mancini, E., Rizi, V., and Shindell, D. T. (2002). Impact of future climate and emission changes on stratospheric aerosols and ozone. *Journal of the Atmospheric Sciences*, **59**(3), 414–440.

Plumb, R. A. and Ko, M. K. W. (1992). Interrelationships between mixing ratios of long-lived stratospheric constituents. *Journal of Geophysical Research*, **97**(D9), 10145–10156.

Popp, P. J., Northway, M. J., Holecek, J. C., Gao, R. S., Fahey, D. W., Elkins, J. W., Hurst, D. F., Romashkin, P. A., Toon, G. C., Sen, B., Schauf¤er, S. M., Salawitch, R. J., Webster, C. R., Herman, R. L., Jost, H., Bui, T. P., Newman, P. A., and Lait, L. R. (2001). Severe and extensive denitri£cation in the 1999-2000 Arctic winter stratosphere. *Geophysical Research Letters*, **28**(15), 2875–2878.

Portmann, R. W., Brown, S. S., Gierczak, T., Talukdar, R. K., Burkholder, J. B., and Ravishankara, A. R. (1999). Role of nitrogen oxides in the stratosphere: A reevaluation based on laboratory studies. *Geophysical Research Letters*, **26**(15), 2387–2390.

Prather, M., Garcia, M. M., Suozzo, R., and Rind, D. (1990). Global impact of the antarctic ozone hole - dynamic dilution with a 3-dimensional chemical-transport model. *Journal of Geophysical Research*, **95**(D4), 3449–3471.

Press, W. H., Teukolsky, S. A., Vettering, W. T., and Flannery, B. P. (1992). *Numerical Recipes in FORTRAN*. Cambridge University Press, 2nd edition.

Pyle, J. A. (1995). Ozone loss in middle latitudes and the role of the arctic polar vortex. *Philisophical transactions of the Royal Society of London Series A - Mathematical Physical and engineering sciences*, **352**(1699), 241–245.

Quaite, F. E., Sutherland, B. M., and Sutherland, J. C. (1992). Action spectrum for DNA damage in alfalfa lowers predicted impact of ozone depletion. *Nature*, **358**, 576–578.

Rabitz, H. A. and Aliş, O. F. (1999). General foundations of high-dimensional model representations. *Journal of Mathematical Chemistry*, **25**, 197–233.

Rabitz, H. A., Aliş, O. F., Shorter, J., and Shim, K. (1999). Ef£cient input-output model representations. *Computer Physics Communications*, **117**, 11–20.

Ramaroson, R., Pirre, M., and Cariolle, D. (1992). A box model for on-line computations of diurnal variations in a 1-D model: potential for application in multidimensional cases. *Annales Geophysicae*, **10**, 416–428.

Ramaswamy, V., Chanin, M. L., Angell, J., Barnett, J., Gaffen, D., Gelman, M., Keckhut, P., Koshelkov, Y., Labitzke, K., Lin, J. J. R., O'Neill, A., Nash, J., Randel, W., Rood, R., Shine, K., Shiotani, M., and Swinbank, R. (2001). Stratospheric temperature trends: Observations and model simulations. *Reviews of Geophysics*, **39**(1), 71–122.

Randel, W. J. and Wu, F. (1995). TOMS total ozone trends in potential vorticity coordinates. *Geophysical Research Letters*, **22**(6), 683–686.

Randel, W. J., Wu, F., Russell, J. M., Roche, A., and W, W. J. (1998). Seasonal cycles and QBO variations in stratospheric CH_4 and H_2O observed in UARS HALOE data. *Journal of the Atmospheric Sciences*, **155**, 163–185.

Randell, W. J. and Wu, F. (1999). A stratospheric ozone trends data set for global modeling studies. *Geophysical Research Letters*, **26**, 3089–3092.

Randeniya, I. K., Vohralik, P. F., and Plumb, I. C. (2002). Stratospheric ozone depletion at northern mid latitudes in the 21st century: The importance of future concentrations of greenhouse gases, nitrous oxide and methane. *Geophysical Research Letters*, **29**(4), 10–1–10–4.

Rees, D., Barnett, J. J., and Labitzke, K., editors (1990). *COSPAR international reference atmosphere: 1986 Part II: Middle Atmosphere Models*, volume 10 of *Advances in Space Science*. Pergamon Press.

Roehl, C. M., Nizkorodov, S. A., Zhang, H., Blake, G. A., and Wennberg, P. O. (2002). Photodissociation of peroxynitric acid in the near-IR. *Journal of Physical Chemistry A*, **106**(15), 3766–3772.

Rosanov, E. V., Zubov, V. A., Schlesinger, M. E., Yang, F., and Andronova, N. G. (1999). The UIUC three-dimensional stratospheric chemical transport model: Description and evaluation of the simulated source gases and ozone. *Journal of Geophysical Research*, **104**(D9), 11755–11781.

Rosanov, E. V., Schlesinger, M. E., and Zubov, V. A. (2001). The University of Illinois, Urbana-Champaign three dimensional stratosphere-troposphere general circulation model with interactive ozone photochemistry: Fifteen-year control run climatology. *Journal of Geophysical Research*, **106**(D21), 27233–27254.

Rosen£eld, J. E., Douglass, A. R., and Considine, D. B. (2002). The impact of increasing carbon dioxide on ozone recovery. *Journal of Geophysical Research*, **107**(D6), ACH 7.

Rosier, S. M. and Shine, K. P. (2000). The effect of two decades of ozone change on stratospheric temperature as indicated by a general circulation model. *Geophysical Research Letters*, **27**(D17), 2617–2620.

Rosier, S. M., Shine, K. P., and Tourpali, K. (1999). An 'intermediate' general circulation model for ozone change studies. In *NATO ASI on Chemistry and Radiation Changes in the Ozone Layer*.

Roumeau, S., Bremaud, P., Riviere, E., Baldy, S., and Baray, J. L. (2000). Tropical cirrus clouds: a possible sink for ozone. *Geophysical Research Letters*, **27**(15), 2233–2236.

Sander, S. P., , Friedl, R. R., DeMore, W. B., Golden, D. M., Hampson, R. F., Kurylo, M. J., Huie, R. E., Moortgat, G. K., Ravishankara, A. R., Kolb, C. E., and Molina, M. J. (2000). *Chemical kinetics and photochemical data for use in stratospheric modeling, JPL publication 00-3*. Jet Propulsion Laboratory, California Institute of Technology, Pasadena, CA.

Sandilands, J. W. and McConnell, J. C. (1997). Evaluation of a reduced Jacobian chemical solver. *Journal of Geophysical Research*, **102**(D15), 19073–19087.

Schnadt, C., Dameris, M., Ponater, M., Hein, R., Grewe, V., and Steil, B. (2002). Interaction of atmospheric chemistry and climate and its impact of stratospheric ozone. *Climate Dynamics*, **18**(6), 501–518.

Shindell, D. T. (2001). Climate and ozone response to increased stratospheric water vapor. *Geophysical Research Letters*, **28**(8), 1551–1554.

Shindell, D. T. and de Zafra, R. L. (1996). Chlorine monoxide in the Antarctic spring vortex 2. A comparison of measured and modeled diurnal cycling over McMurdo Station. *Journal of Geophysical Research*, **101**, 1475–1487.

Shindell, D. T. and de Zafra, R. L. (1997). Limits on heterogeneous processing in the Antarctic spring vortex from a comparison of measured and modeled chlorine. *Journal of Geophysical Research*, pages 1441–1450.

Shindell, D. T. and Grewe, V. (2002). Separating the in¤uence of halogen and climate changes on ozone recovery in the upper stratosphere. *Journal of Geophysical Research*, **107**(D12), 3–1 – 3–10.

Shindell, D. T., Wong, S., and Rind, D. (1997). Interannual variability of the Antarctic ozone hole in a GCM. Part I: the in¤uence of tropospheric wave variability. *Journal of the Atmospheric Sciences*, **54**, 2308–2319.

Shindell, D. T., Rind, D., and Lonergan, P. (1998a). Climate change and the middle atmosphere. Part IV: ozone response to doubled CO_2. *Journal of Climate*, **11**, 895–918.

Shindell, D. T., Rind, D., and Lonergan, P. (1998b). Increased polar stratospheric ozone losses and delayed eventual recovery owing to increasing greenhouse-gas concentrations. *Nature*, **392**, 589–592.

Shorter, J., Ip, P., and Rabitz, H. (2000). Radiation transport simulation my means of a fully equivalent operational model. *Geophysical Research Letters*, **27**(D21), 3485–3488.

Shorter, J. A., Ip, P. C., and Rabitz, H. A. (1999). An ef£cient chemical kinetics solver using high dimensional model representation. *Journal of Physical Chemistry A*, **103**, 7192–7198.

Sinnhuber, B. M., Muller, R., Langer, J., Bovensmann, H., Eyring, V., Klein, U., Trentmann, J., Burrows, J. P., and Kunzi, K. F. (1999). Interpretation of mid-stratospheric Arctic ozone measurements using a photochemical box-model. *Journal of Atmospheric Chemistry*, **34**(3), 281–290.

Smith, A. K. (1995). Impact of averaged photolysis rates on stratospheric ozone. *Journal of Geophysical Research*, **100**(D6), 11173–11183.

Smith, J. B., Hintsa, E. J., Allen, N. T., Stimp¤e, R. M., and Anderson, J. G. (2001). Mechanisms

for midlatitude ozone loss: Heterogeneous chemistry in the lowermost stratosphere? *Journal of Geophysical Research*, **106**(D1), 1297–1309.

Solomon, R. W. P. S., Garcia, R. R., Poole, L. W. T. L. R., and McCormick, M. P. (1996a). Role of aerosol variations in anthropogenic ozone depletion in the polar regions. *Journal of Geophysical Research*, **101**(D17), 22991–23006.

Solomon, S. (1999). Stratospheric ozone depletion: a review of concepts and history. *Review of Geophysics*, **37**(3), 275–316.

Solomon, S., Portmann, R. W., Garcia, R. R., Thomason, L. W., Poole, L. R., Winker, D., and McCormick, M. P. (1996b). The role of aerosol variations in anthropogenic ozone depletion at northern midlatitudes. *Journal of Geophysical Research*, **101**(D3), 6713–6727.

Solomon, S., Borrmann, S., Garcia, R. R., Portmann, R., Thomason, L., Poole, L. R., Winker, D., and McCormick, M. P. (1997). Heterogeneous chlorine chemistry in the tropopause region. *Journal of Geophysical Research*, **102**(D17), 21411–21429.

Solomon, S., Portmann, R. W., Garcia, R. R., Randel, W., Wu, F., and McCormick, M. P. (1998). Ozone depletion at mid-latitudes: Coupling of volcanic aerosols and temperature variability to anthropogenic chlorine. *Geophysical Research Letters*, **25**(11), 1871–1874.

SORG (1999). *Stratospheric Ozone 1999*. UK Stratospheric Ozone Review Group. Department of the Environment, Transport and the Regions, DETR Free Literature, PO Box 236, Wetherby LS23 7NB. DETR ref. No. 99EP0458.

Spivakovsky, C. M., Wofsy, S. C., and Prather, M. J. (1990). A numerical method for parameterization of atmospheric chemistry - computation of tropospheric OH. *Journal of Geophysical Research*, **95**(D11), 18433–18439.

Sportisse, B. and Djouad, R. (2000). Reduction of chemical kinetics in air pollution modeling. *Journal of Computational Physics*, **164**, 354–376.

Steil, B., Dameris, M., Brühl, C., Crutzen, P. J., Grewe, V., Ponater, M., and Sausen, R. (1998). Development of a chemistry module for GCMs: £rst results of a multiannual integration. *Annales Geophysicae*, **16**, 205–228.

Stimp¤e, R. M., Koplow, J. P., Cohen, R. C., Kohn, D. W., Wennberg, P. O., Judah, D. M., Toohey, D. W., Avallone, L. M., Anderson, J. G., Salawitch, R. J., Woodbridge, E. L., Webster, C. R.,

May, R. D., Prof£tt, M. H., Aiken, K., Margitan, J., Lowenstein, M., Podolske, J. R., P£ster, L., and Chan, K. R. (1994). The response of ClO radical concentrations to variations in NO_2 radical concentrations on the lower stratosphere. *Geophysical Research Letters*, **21**(23), 2543–2546.

Stockwell, D. Z., Giannakopoulos, C., Plantevin, P. H., Carver, G. D., Chiper£eld, M. P., Law, K. S., Pyle, J. A., Shallcross, D. E., and Wang, K. Y. (1999). Modelling NO_x from lightning and its impact on global chemical £elds. *Atmospheric Environment*, **33**(27), 4477–4493.

Stolarski, R. S. and Cicerone, R. J. (1974). Stratospheric chlorine: a possible sink for ozone. *Canadian Journal of Chemistry*, **52**, 1610–1615.

Stott, P. A. and Harwood, R. S. (1993). An implicit time-stepping scheme for chemical species in a global atmospheric general circulation model. *Annales Geophysicae*, **11**, 377–388.

Sun, P., Chock, D. P., and Winkler, S. L. (1994). An impicit-explicit hybrid solver for a system of stiff kinetic equations. *Journal of Computational Physics*, **115**, 515–523.

Sze, N. D., Ko, M. K. W., Weisenstein, D. K., Rodriguez, J. M., Stolarski, R. S., and Schoeberl, M. R. (1989). Antarctic ozone hole - possible implications for ozone trends in the southern-hemisphere. *Journal of Geophysical Research*, **94**(D9), 11521–11528.

Takigawa, M., Takahashi, M., and Akiyoshi, H. (1999). Simulation of ozone and other chemical species using a Center for Climate System Research National Institute for Environmental Studies atmospheric GCM with coupled stratospheric chemistry. *Journal of Geophysical Research*, **104**(D11), 14003–14018.

Tomlin, A. S., Turányi, T., and Pilling, M. J. (1997). *Mathematical tools for the construction, investigation and reduction of combustion mechanisms*, volume 35 of *Comprehensive Chemical Kinetics*, chapter 4. Elsevier, Amsterdam.

Tourpali, K., Tie, X. X., Zerefos, C. S., and Brasseur, G. (1997). Decadal evolution of total ozone decline: observations and model results. *Journal of Geophysical Research*, **102**(D20), 23955–23962.

Toyota, K., Takahashi, M., and Akimoto, H. (2001). Modeling multi-phase halogen chemistry in the marine boundary layer with size-segregated aerosol module: implications for quasi-size-dependent approach. *Geophysical Research Letters*, **28**(15), 2899–2902.

Tuck, A. F., Russell, J. M., and Harries, J. E. (1993). Stratospheric dryness - Antiphased desiccation over Micronesia and Antarctica. *Geophysical Research Letters*, **20**(12), 1227–1230.

Turanyi, T. (1994). Parameterization of reaction-mechanisms using orthonormal polynomials. *Computers and Chemistry*, **18**(1), 45–54.

Ushimaru, S. and Tanaka, H. (1994). The role of planetary-waves in the formation of interhemispheric asymmetry in ozone distribution. *Journal of the Meteorological Society of Japan*, **72**(5), 653–670.

Vohralik, P. F. (2002). *manuscript in preparation*.

Vohralik, P. F., Randeniya, L. K., Plumb, I. C., and R., R. K. (1998). Use of correlations between long-lived atmospheric species in assessment studies. *Journal of Geophysical Research*, **103**(D3), 3611–3627.

Waibel, A. E., Peter, T., Carslaw, K. S., Oelhaf, H., Wetzel, G., Crutzen, P. J., öscl, U. P., Tsias, A., Reimer, E., and Fischer, H. (1999). Arctic ozone loss due to denitri£cation. *Science*, **283**, 2064–2068.

Wang, S. W., Levy, H., Li, G., and Rabitz, H. (1999). Fully equivalent operational models for atmospheric chemical kinetics within global chemistry-transport models. *Journal of Geophysical Research*, **104**(D23), 30417–30426.

Wayne, R. P. (2000). *Chemistry of Atmospheres*. Oxford University Press, third edition.

Webster, C. R., May, R. D., Toumi, R., and Pyle, J. A. (1990). Active nitrogen partitioning and the nightime formation of N_2O_5 in the stratosphere: Simultaneous in situ measurements of NO, NO_2, HNO_3, O_3 and N_2O using the bliss diode laser spectrometer. *Journal of Geophysical Research*, **95**(D9), 13,851–13,866.

Wennberg, P. O. (2001). Atmospheric and laboratory observations constraining the role of HO_2NO_2 in the stratosphere. Paper presented at 8th Scienti£c Assembly of IAMAS, Innsbrück.

Wild, O. and Prather, M. J. (2000). Excitation of the primary tropospheric mode in a global three-dimensional model. *Journal of Geophysical Research*, **105**(D20), 24647–24660.

Williamson, C. E., Neale, P. J., Grad, D., de Lange, H. J., and Hargreaves, B. R. (2001). Benifical and detrimental effects of UV on aquatic organisms: Implications of spectral variation. *Ecological Applications*, **11**(6), 1843–1857.

WMO (1999). *Scienti£c Assessment of Ozone Depletion: 1998*. Global Ozone Research and Monitoring Project - Report No. 44. World Meteorological Organization, Geneva. ISBN: 92-807-1722-7.

Xiong, F. S. and Day, T. A. (2001). Effect of solar ultraviolet-B radiation during springtime ozone depletion on photosynthesis and biomass production of Antarctic vascular plants. *Plant Physiology*, **125**(2), 738–751.

Yang, P. C. and Brasseur, G. P. (2001). The nonlinear response of stratospheric ozone to NOx and ClOx perturbations. *Geophysical Research Letters*, **28**(4), 717–720.

Zhou, X. L., Geller, M. A., and Zhang, M. H. (2001). Cooling trend of the tropical cold point tropopause temperatures and its implications. *Journal of Geophysical Research*, **106**(D2), 1511–1522.